NANYANG TECHNOLOGICAL UNIVERSITY

PHOTO-DRIVEN SMART POLYMERS AND THEIR MOLECULAR SELF-ASSEMBLY

HU JINHUA

SCHOOL OF MATERIALS SCIENCE AND ENGINEERING

2013

PHOTO-DRIVEN SMART POLYMERS AND THEIR MOLECULAR SELF-ASSEMBLY

HU JINHUA

School of Materials Science and Engineering

A thesis submitted to the Nanyang Technological University
in fulfillment of the requirement for the degree of
Doctor of Philosophy

2013

This thesis is dedicated to my parents:

Hu Churong & Xia Guizhen

ACKNOWLEDGEMENTS

The author would like to express her deepest gratitude to the following people, without whom the completion of this research work and thesis would not be possible.

Firstly, I gratefully express my sincere thanks to my supervisor, Professor Hu Xiao, for his great patience, thoughtful guidance and continuous support during my graduate study. In my pursuit of scientific research, he has offered me many invaluable opportunities which have molded not only my research mindset but also my personality.

Next, I would like to acknowledge Prof. Jiang Ming and Prof. Yaoping from the Department of Macromolecular Science, Fudan University, and Prof. Liang Li from the Department of Food Science and Technology, Jiangnan University. They advise me to adopt positive and pragmatic perspectives while facing a research challenge. I would also like to acknowledge Nanyang Assistant Professor Duan Hongwei, Professor Michael Kam Chiu Tam, and Professor Leong Huat Gan for allowing me to use the facilities in their laboratories. It is my pleasure to thank Dr. Yu Hui, Dr. Bao Hongqian and Dr. Lu Yong for their kind assistance in the experiments and valuable discussion. I would like to give my most sincere thanks and warmest appreciation to Dr. Liang Yen Nan, who always encourages me to keep fighting and help me with technical writing.

Last but not least, I need to extend my great gratitude to the encouragement and help from all my friends including: Song Jibin, Shen Wenming, Hou Xiaoya, Wang Xinghua, Ding Hui, Liu Ming, Li Bing, Lu Jie, Shen Yiqiang, Peng Yan, Ba Te, all my group members, and all the technical staff that provided advice and support to me in my research work. On this occasion, I would like to thank my parents for their constant support and encouragement. I sincerely dedicate this thesis to them.

ABSTRACT

The development of responsive biomimetic self-assembled polymeric materials constitutes an exciting research field. The focus of this research is to utilize photo-sensitive molecules to trigger polymeric self-assemblies. This objective is achieved through detailed studies in the following directions: (i) the preparation and characterization of amphiphilic azobenzene derivative functionalized polymers (azobenzene containing poly(ethylene glycol), azo-PEGs) having both linear shape and star shape, (ii) the construction of their self-assemblies in both mixed solvents and aqueous solutions, and (iii) the investigation of the photo-responsive properties of these self-assemblies, (iv) the insights to mechanisms.

Azobenzene is chosen as the photo-trigger in this study because it is an organic photo-chromic molecule that exhibits clear photo-isomerization mechanism. Its *trans*-state is hydrophobic and its *cis*-state is relatively hydrophilic. The synthesized azo-PEG polymers are lipid-like azobenzene-containing molecules. The simplistic and representative design of the azo-PEGs enables the in-depth studies of the self-assembly mechanism. For the water/THF mixed solvent system, investigations on the vesicle formation and its pulsation behaviour were carried out. A liquid-liquid phase separation accused owing to a partition of the solvents as the vesicles formed in the water/THF mixture. The hydrophobic and rigid azobenzene groups at chain ends aggregated in THF-rich phase, driven by the hydrophobic and π-π interactions. The hydrophilic PEG chains thus assembled in the water-rich phase forming the inner and outer layers of the membrane. The interfacial energy between the hydrophobic core-layer and the more polar solvent was one of the key factors that governed the vesicle formation. When the vesicles were exposed to UV light, the azobenzene terminal groups experienced *trans-to-cis* photo-isomerization. The rearrangement of the azobenzene molecules caused an increase in the surface tension. In

order to lower the surface energy, the vesicle shrank by expelling the *cis* isomers from the parallel *trans* isomers and corralling of the remaining *trans* isomers. Polymer concentrations and volume ratios of THF and water were identified as very important factors that influence the morphological properties of self-assemblies. The different photo-isomerization behaviours of the azobenzene derivatives were identified to have contributed to regulation of the pulsation behaviour. The extraordinarily large change in vesicle size was originated from an isomerization-driven molecular assembly upon UV-visible irradiation cycles, and was associated with substantial transmembrane solvent transport. For the aqueous system, self-assembly of azo-PEGs was achieved with a modified molecular design, eventually producing a pulsating vesicle that is promising for selective ion transport. Further study was carried out on the star shaped azo-PEGs that exhibit more interesting and complicated self-assembly behaviour.

Our main scientific contribution is the mechanism illustrating the extraordinarily large change in vesicle size originated from an isomerization-driven molecular assembly and the substantial transmembrane solvent transport.

The photo-driven pulsation of the vesicles described in the thesis is certainly most unusual, very interesting and potentially useful. This photo-driven vesicle is a typical example of pulsating self-assemblies reported for the first time. Other examples have been reported are pH-responsive[1] and thermo-responsive[2] pulsating vesicles, respectively. The further studies on the vesicles self-assembled in dilute solute solutions present the photo-driven ion transport selectivity. This photo-sensitive vehicle provides promising applications in areas such as bio-sensors, controlled drug release, and water treatment.

TABLE OF CONTENTS

LIST OF EQUATIONS

ABBREVIATIONS

AFM	Atomic absorption spectroscopy
AQP	Aquaporin
ATRP	Atom transfer radical polymerization
azo	Azobenzene
azo-PEGs	Azobenzene-poly(ethylene glycol)
BHT	6-di-tert-butyl-4-methylphenol
Br-PEG-Br	Bromine terminated poly(ethylene glycol)
CD	Cyclodextrin
$CDCl_3$	Deuterated chloroform
CH_2Cl_2	Methylene dichloride
CMC	Critical micelle concentration
CVD	Chemical vapor deposition
D_2O	Deuterated water
DI water	Deionized water
DLS	Dynamic light scattering
DMAEMA	2-(dimethylamino) ethyl methacrylate
DMAP	4-(dimethylamino)-pyridine
DMF	Dimethylformamide
DNA	Deoxyribonucleic acid
GPC	Gel permeation chromatography
HPMC	Hydroxypropyl methylcellulose
ITC	Isothermal titration calorimetry
KCl	potassium chloride
LB	Langmuir–Blodgett
LBL	Layer-by-layer
LCST	Lower critical solution temperature
LiCl	Lithium chloride
LLS	Laser light scattering
NaCl	Sodium chloride
NMR	Nuclear magnetic resonance
PAA	Poly(acrylic acid)
PCL	Poly(ε-capro-lactone)-block-poly(ethylene oxide)

PDI	Polydispersity index
PEG	Poly(ethylene glycol)
PEI	Poly(ethyleneimine)
PEL	Polyelectrolyte
PEO	Poly(ethylene oxide)
PGEA	Poly(2-glucosyl-oxyethyl acrylate)
PLA	Polylactide
PMMA	Poly(methyl methacrylate)
PNIPAm	Poly(N-isopropylacrylamide)
PtBA	Poly(tert-butyl acrylate)
QCM	Quartz crystal microbalance
RMS	Root meant square
SLS	Static light scattering
TEM	Transmission electron microscopy
THF	Tetrahydrofuran
THF-d_8	Deuterated tetrahydrofuran
UV-visible	Ultraviolet-visible absorption spectroscopy

NOMENCLATURE

[X]	Concentration of X
[*Trans*]	The concentration ratio of *trans*-state at a photo-stationary state of $\mathbf{S_{VIS}}$
[*Cis*]	The concentration ratio of *cis*-state at a photo-stationary state of $\mathbf{S_{UV}}$
$\mathbf{S_{VIS}}$	Photo-stationary state or dark-adapted state with all *trans*-isomers
$\mathbf{S_{UV}}$	Photo-stationary state with maximum *cis* fraction
A	Absorbance
A_0	The initial absorbance with all *trans*-isomers present at wavelength λ
A_t	The absorbance of the *trans*-isomers at time t
A_{Cis}	Optical density of a solution containing only *cis* isomers
A_{Trans}	Optical density of a solution containing only *trans* isomers
$\boldsymbol{f_z}(t)$	The fraction of *cis*-isomers at time t
Φ_{Trans}	The quantum yield of the *trans-to-cis* photo-isomerization upon UV irradiation
Φ_{Cis}	The quantum yield of the *cis-to-trans* isomerization upon visible light irradiation
ε_{Trans}	The extinction coefficients of the *trans*-azobenzene
ε_{Cis}	The extinction coefficients of the *cis*-azobenzene
$G^{(1)}(\theta)$	The normalized first-order autocorrelation function
$G^{(2)}(t, \theta)$	The normalized second-order autocorrelation function
t	The delay time
θ	The angle at which the detector is located with respect to the sample cell
Γ	Decay rates
$G(\Gamma)$	The distribution of decay rates Γ
q	The magnitude of the scattering wave-vector
D	The translation diffusion coefficient
D_0	The translation diffusion coefficient in a infinite dilute solution
K_b	The Boltzmann constant
T	The absolute temperature
n	the refractive index of the solution
D_h	Hydrodynamic diameter
R_h	Hydrodynamic radius (the apparent hydrodynamic radius)

R_g	The radius of gyration (the root mean square of the distance)
M_W	Weight-average molar mass
M^{x+}	Metallic ions
ΔH	Heat change
ΔS	Entropy change
α	Degree of deprotonation (page)
α	The concentration ratio of *tran*-state/*cis*-state at a photo-stationary state (page)
β	A parameter of the optical system (constant)
λ	The wavelength of the incident light
χ	Electronegativity

GLOSSARY OF TERMS

Miktoarm	Miktoarm star polymer is also called heteroarm star-branched polymer or mixed arm star polymer. Miktoarm star polymer is a special class of asymmetric star-branched polymer with various molecular weights or chemically different branch chains radiating from the same central core.
Isomer	The word 'isomer' was coined by Swedish chemist Jöns Jacob Berzelius in 1830.[3] In chemistry, isomers are compounds with the same molecular formula but different structural formulas. There are two main forms of isomerism: structural isomerism and stereoisomerism (spatial isomerism). The chart below summarizes different classes of isomers. 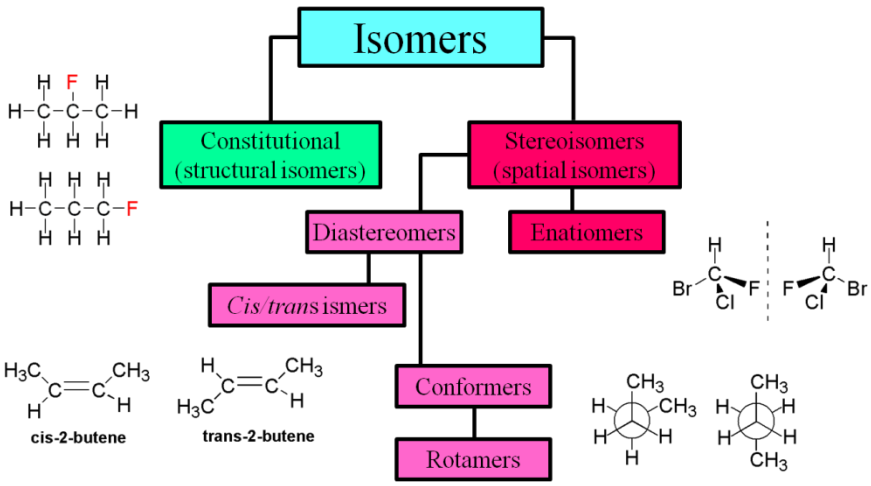 In structural isomers, sometimes referred to as constitutional isomers, the atoms and functional groups are joined together in different ways. The bond structure is the same in stereoisomers, but the

	geometrical positioning of atoms and functional groups in space differs. This class includes 'enantiomers' where different isomers are non-superimposable mirror-images of each other, and 'diastereomers' when they are not. Diastereomerism is again subdivided into '*cis-trans* isomers' and 'conformational isomers' (conformers). Conformers can rotate about one or more single bonds within the molecule.
Cis and *trans*	*Cis* and *trans* describe the relationship between two ligands attached to separate atoms that are connected by a double bond or are contained in a ring. The two ligands are said to be located *cis* to each other if they lie on the same side of a plane. If they are on opposite sides, their relative position is described as *trans*. [4]
	Cis-trans isomers have restricted rotation within the molecule (typically isomers containing a double bond). An obsolete term for '*cis-trans* isomerism' is 'geometric isomers'.[5]
Isomerization	Isomerization is the process by which one molecule is transformed into another molecule which has exactly the same atoms, but the atoms are rearranged.[6]
Lipid bilayer	The lipid bilayer is a thin polar membrane made of two layers of lipid molecules. Natural bilayers are usually composed of phospholipids, which have a hydrophilic head and two hydrophobic tails each. When phospholipids are exposed to water, they arrange themselves into a two-layered sheet (a bilayer) with

	all of their tails pointing toward the centre of the sheet. A bilayer structure from conventional lipids is drawn in the below picture. 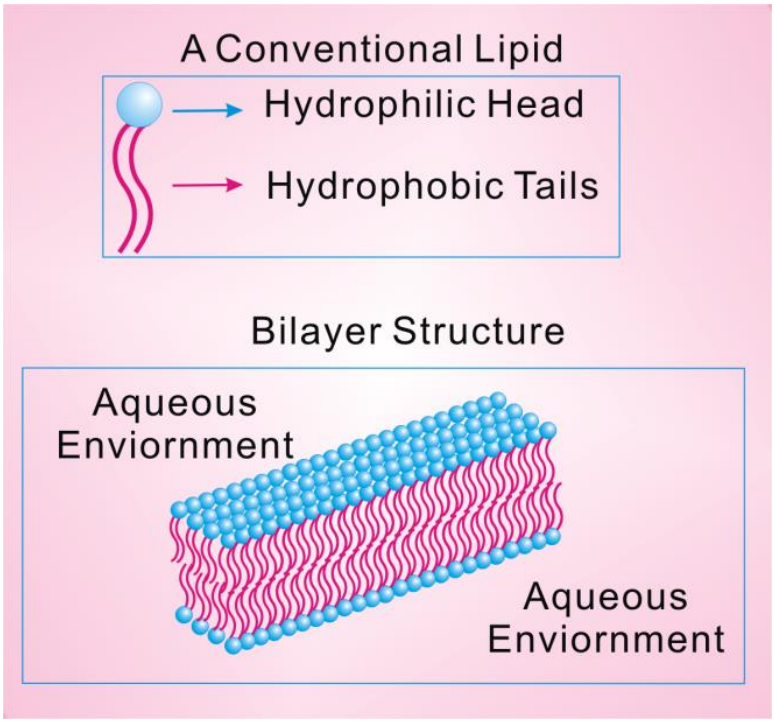
Vesicle and unilamellar vesicle	In cell biology, a vesicle is a small bubble within a cell, and thus a type of organelle. Vesicles can form naturally by enclosed lipid bilayer. If there is only one phospholipid bilayer, they are called unilamellar vesicles; otherwise they are called multi-lamellar. 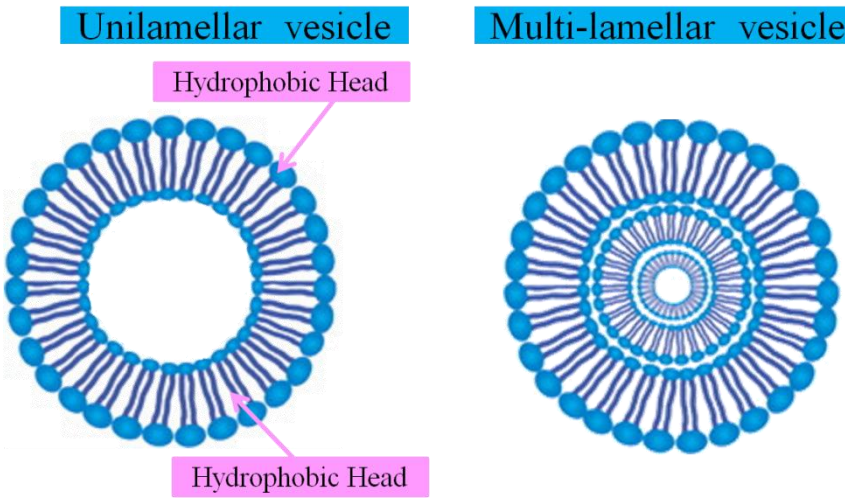

REPES	Regularized Positive Exponential Sum Program in the Gendist software.
CONTIN	A general-purpose constrained regularization method for continuous distributions, such as inverse Laplace transforms in relaxation studies and in dynamic light scattering.

LIST OF FIGURES

LIST OF TABLES

1 INTRODUCTION

1.1 Research Background

Artificial systems responsive to external stimuli, e.g., photo responsive artificial membranes, are currently drawing considerable attention as they can mimic the hierarchy structures and sophisticated functions of biological systems.[7] In nature, a class of integral membrane proteins is well-known for containing channels for ion transport from the cell interior to the exterior. For example, aquaporins can facilitate rapid and highly selective water transport.[8] Besides water channels, bacteriorhodopsin in purple membranes is proven to be able to pump protons out of cells upon visible light-irradiation, owing to the light-induced isomerization from the all-*trans* isomer to the 13-*cis* isomer of the protonated retinal.[9]

Amphiphilic block copolymers with characteristic microphase-separation structures have a strong tendency to undergo intra- and inter-molecular associations and can self-assemble to micellar aggregates with varied morphologies in selective solvents,[10] such as crew-cut micelles, star micelles, vesicles, and rods.[11] In addition, the perturbation of micellar segregates, by means of external stimuli such as the pH, ionic strength, and oxidation reactions, has attracted much interest due to the potential use for controlled cargo release.[11] It would thus be of great interest to explore the opportunity to introduce photo-isomerization as a light responsive trigger into the construction of polymeric self-assembly smart materials such as light-driven pulsating vesicles.

1.2 Objectives and Scope of this Research

The photochromic molecules introduced into the polymer can represent the photo-switches. When the modified amphiphilic polymers self-assemble into the hierarchical structures, the photo-switches are able to trigger cascading changes in achieved materials at the molecular, micro- to eventually macro-scopic scales. The photo-responsive molecules in the materials may resemble some biological photo-receptors, such as the bacteriorhodopsin in the purple membrane that is able to pump protons out of the cell membrane. The hypothesized biomimetic architectures may lead to applications in various separation processes using photo-energy. Based on the above hypothesis, this work aims to develop novel photo-responsive azobenzene-based polymers and construct photo-driven self-assemblies. The objectives can be achieved by chemically incorporating the azobenzene derivative on both chain ends of poly(ethylene glycol) (PEG). The azobenzene derivative acts as the hydrophobic end group as well as the photo-responsive trigger. The process of self-assembly, as induced by the amphiphilicity of azobenzene containing PEGs, is expected to be regulated by the photo-isomerization of azobenzene derivatives. Such photo-responsive self-assemblies would have great potential for applications in bio-sensors, and biomedical encapsulation and release carriers.

The objectives of this work include:

(1) Design and synthesize amphiphilic azobenzene derivatives functionalized PEG polymers (azo-PEGs).

(2) Construct and characterize the self-assembly process of azo-PEGs in mixed solvents or aqueous solutions.

(3) Study the *trans*-*cis* isomerization of azo-PEGs in different solvents.

(4) Investigate the photo-driven behaviour i.e., photo-pulsating size change, solvent transport, and ion selectivity of the azo-PEGs self-assemblies.

(5) Discuss the insights of mechanism.

1.3 Contributions of this study

This work involves a systematic study on the *trans-cis* photo-isomerization of lipid-like azo-PEGs polymers and their photo-responsive self-assembly behaviour in mixed solvents as well as aqueous solutions. The main contributions of this study are as follows:

1. Detailed studies have been carried out on a series of azo-PEGs with representative molecular design, including one-end capped linear azo-PEGs, two-end capped linear azo-PEGs, and four-end capped four-arm azo-PEGs. The *trans-cis* isomerization of synthesized azo-PEGs in different solvents has been investigated to provide important insight on the photo-driven self-assembly behaviour of azo-PEGs.

2. We have carried out the first systematic study on pulsating vesicles driven by UV-visible irradiation. Different azobenzene derivatives act as stimulus responsive triggers and control the pulsating behaviour to different extent.

3. The significance of the pulsating vesicles in this study is extended to the exploitation of biomimetic artificial membranes with water channels, which could be used for water treatment.

1.4 Thesis Organization

This thesis begins with an introduction to the research work, which is given in Chapter 1. Chapter 2 presents the literature review focusing on biomimetics, smart materials,

self-assembly and photo-responsive polymers self-assembly in different solvents. Chapter 3 provides the details of the research methodology and experimental procedures. Chapter 4 discusses linear azo-PEGs self-assembly in THF/water mixed solvents. Chapter 5 presents the self-assembly behaviour of linear azo-PEGs in aqueous solution with or without the presence of salts. Chapter 6 investigates star-shaped azo-PEGs self-assembly in aqueous solution. Lastly, Chapter 7 gives the conclusions together with recommendations for future works.

2 LITERATURE REVIEW

In this chapter, a literature review focusing on four main topics is carried out:

1. Biomimetics and bionics: from nature to technology
2. Self-assembly: learning from the nature
3. Smart materials and smart polymers: mimicking nature
4. Azobenzene based photo-sensitive polymers and their self-assembly behaviour in solution

2.1 Biomimetics and bionics: from nature to technology

In 1957, Otto Schmitt coined the word 'biomimetics',[12,13] which later appeared in the Webster dictionary in 1974. It is defined as 'the study of the formation, structure or function of biologically produced substances and materials (such as enzymes or silk) and biological mechanisms and processes (such as protein synthesis or photosynthesis) especially for the purpose of synthesizing similar products by artificial mechanisms which mimic natural ones'.[14] The related term 'biomimicry', which appeared as early as 1962,[12,15] was used as a book title: 'Biomimicry: Innovation Inspired by Nature' written by Janine Benyus in 1997.[16] She defined 'biomimicry' as a 'new science that studies nature's models and then imitates or takes inspiration from these designs and processes to solve human problems'. In 1958, Jack E. Steele first introduced the word 'bionic' which meant 'like life',[13] combining the 'bion' (meaning 'unit of life' in ancient Greek) and the suffix –'ic' (meaning 'like' or 'in the manner of'). He defined 'bionic' as 'the science of systems which have some functions copied from nature'. In 1960, the Webster dictionary explained 'bionics' as 'a science concerned with the application of data about the functioning of biological systems to the solution of engineering problems'.[14] Bionics was

in the centre-stage and developed as an independent discipline in 1960. The first bionics symposium 'Living Prototypes-the Key to New Technology' was organized by the U.S. Air Force at Wright-Patterson Air Force Base in Ohio, 13-15th September. In November 2005, ***Science*** magazine published a special issue named 'design for living'.[17]

Starting from the first biomimetic fiber i.e., 'nylon',[18] researchers moved into development of artificial organs. Tissue engineering,[19,20] aiming to develop artificial candidates, has hinted much promise in the past several decades. The biocompatible materials for eyes,[21] bone,[22] tooth,[23] cartilage,[24] vascular,[25] neural,[26] muscle[27] and skin tissue[28] have already been synthesized and demonstrated.

Besides investigating the mechanical properties (e.g., stiffness and toughness),[29,30,31,32] fascinating surface-enabled functions of the biological systems (**Figure 2-1**),[33,34] such as the self-cleaning effect of a lotus leaf[35] or cicada wing,[36] the anisotropic dewetting behaviour on a rice leaf,[37] super-hydrophobic force of a water strider's leg,[38] super-hydrophobic and antifogging coatings on mosquito eyes[39] have been observed. Borrowing the surface-related concepts, super-hydrophobicity,[40] super-hydrophilicity,[41] super-amphiphobicity,[42] super-amphiphilicity,[43] super-hydrophobicity/super-oleophilicity,[44] and reversible super-hydrophobicity and super-hydrophilicity,[45] have already been realized in practical applications. There are many more examples of research directions related to surface phenomena, e.g., self-healing,[46] structural color,[47] anti-reflection,[48] high/reversible adhesion,[49] energy conversion[50] and conservation.[51]

Table 2-1 Typical nature-inspired surface-related properties with the corresponding biological materials and research applications.

Surface with function	Biological materials and the functionality-related surface structure		Applications
Anisotropic wettability	Rice leaf	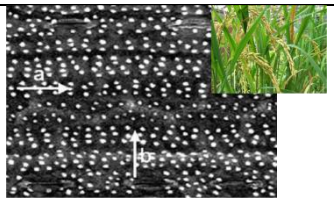 a	Anisotropic films, fluid micro-chips or micro-reactors, patterned surfaces
Anti-reflection	Mosquito eyes	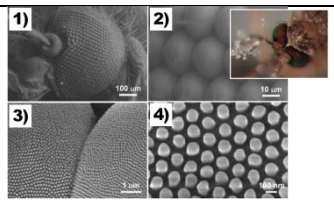 b	Anti-reflective coatings/films, anti-fogging coating, photonics materials
Fluid resistance	Sharkskin riblet	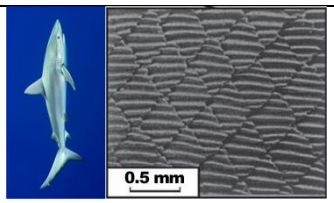 c	Anti-fouling coatings, drag reductive surface, paintings of ship bottom, swimwear (e.g., Sharklet^{TM})
High adhesion	Gecko's finger	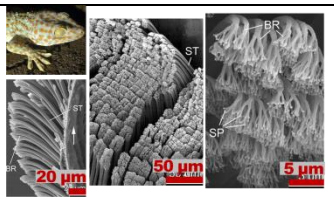 d	Adhesive materials
Structural color	Butterfly wing	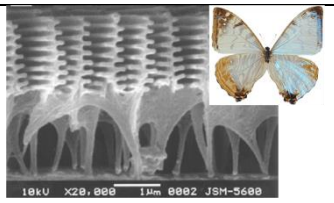 e	Paints, fibers
Super-hydrophobicity	Cicada wing	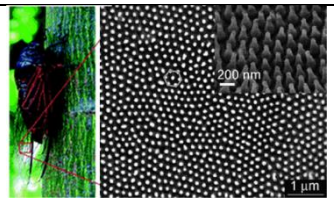 f	Super-hydrophobic surface/textiles, surface inhibiting snow sticking, contamination or oxidation, self-cleaning coatings/paints/fibres
	Lotus leaf	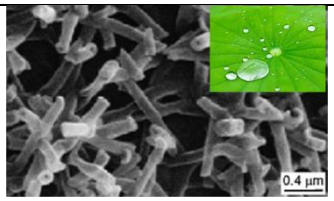 g	
	Water strider's leg	 h	

*a. Anisotropic arrangement of micropapilla on rice leaf (Oryza sativa).[52] (Inset) Rice leaf (Oryza sativa). b. SEM micrographs of 1) An SEM image of a single mosquito eye. 2) An hexagonally close-packed micro-

hemisphere (ommatidia). 3) Two neighbouring ommatidia. 4) Hexagonally non-close-packed nanonipples covering an ommatidial surface.[53] (Inset) Antifogging mosquito compound eyes that remains dry and clear when exposed to moisture. c. Scale pattern on Galapagos shark (Carcharhinus Galapagensis) (Right). (Left) Galapagos shark (Carcharhinus Galapagensis). d. SEM micrographs (shown at three magnifications) of the hierarchical adhesive structures of Gekko gecko, which consists hundreds of thousands of setae and each seta contains hundreds of spatulae.[54] ST: seta; SP: spatula; BR: branch. (Inset) Gekko gecko. e. SEM micrograph of scale surface of a butterfly (M. sulkowskyii) in which discrete 1D periodicity can be found.[55](Inset) Butterfly (M. sulkowskyii). f. SEM micrograph of a nanostructure on the superhydrophobic surface of cicada wings (Cryptympana atrata Fabricius) (Right). The image shows the space between each pillar is about 190 nm and the pillars are arranged in a hexagonal array.[36] (Left) Cicada (Cryptympana atrata Fabricius). g. SEM micrograph of tubular waxes on the Lotus (Nelumbo nucifera) leaf surface. [56] (Inset) Lotus (Nelumbo nucifera). h. SEM micrograph of the numerous oriented spindly micro-setae of a water strider leg.[38] (Inset) Water strider.

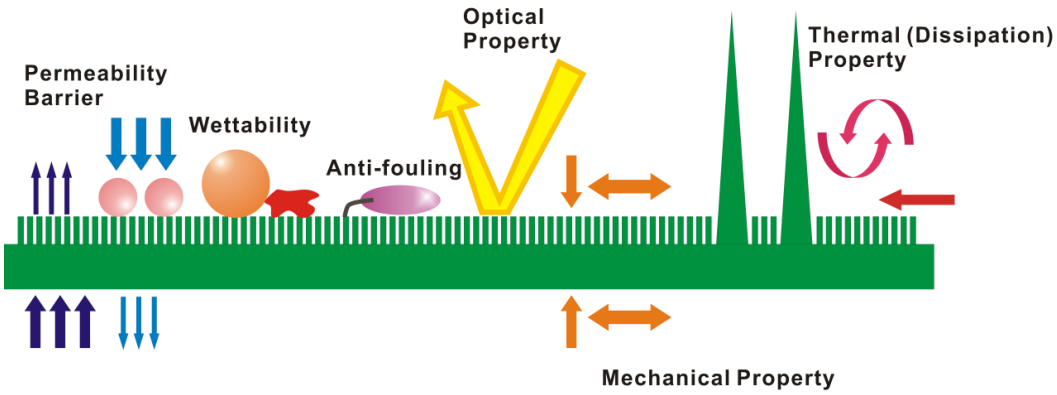

Figure 2-1 Illustration of multi-functionality of a biological surface.

'Biomimetic Chemistry' which studies the molecular-level emulation of enzymes and biomembranes has been studied since the 1970s.[57] In this field, scientists aim to imitate processes in nature[58] with control.[59]

2.2 Self-assembly: learning from the nature

Scientists have been learning from self-assembly phenomena in nature and making strides to uncover nature's mysteries of creating complex and hierarchical organisms. Self-assembly of artificially designed molecules (from both organic and inorganic entities) into highly hierarchical structures is a very exciting and important scientific research topic.[60-62]

2.2.1 'Self-assembly': definition and its driving force

Broadly speaking self-assembly is a self-governing conversion process from a disordered to an organized structure. In chemistry, self-assembly is governed by energetically favourable reactions, producing precise structure via 'like prefers like' routes and exhibiting novel geometries and functions.[63] George M. Whitesides defined 'self-assembly' as 'the autonomous organization of components into patterns or structures without human intervention'.[11] Self-assembly can be classified into two main categories. One is static self-assembly and the other is dynamic self-assembly. Two further variants were defined as templated self-assembly and biological self-assembly.[11] Various driving forces, such as hydrogen bonds, coordination bonds, π–π interactions, van der Waals forces, electrostatic and hydrophobic interactions, and host-guest interactions, drive small molecules to self-assemble into an organized hierarchy.[64]

2.2.2 Scientific research on self-assembly of materials

Self-assembly in living systems reveals on amazing correlation between hierarchical structures and specific multi-functionality in terms of mechanical properties and biological functions. In scientific research, the study of constructing hierarchical architecture via self-assembly of synthetic molecules (e.g., low molecular weight amphiphiles, super-amphiphiles and giant amphiphiles) has been carried out for over a hundred years.[65] Control over the functionality of self-assembled structures has been successfully demonstrated in different systems. For example, Bharat Bhushan and his group reported modification of micro-structured surfaces via the self-assembly of hydrophobic alkanes and plant wax. They have created functional surfaces (e.g., with super-hydrophobicity, self-cleaning and low adhesion functions) as well as lotus-like biomimetic structures.[56,66-69] Their studies indicated the feasibility of extracting self-

assembled design from nature to achieve smart materials from a structural aspect. Smart materials will be introduced and discussed in detail in section 2.3.

Certain applications rely on properties that are manifest only in nano-scale materials. Therefore, a major research effort has been put into fabrication of nano-materials. The traditional engineering approach to achieve nano-materials is the 'top-down' process used widely in the electronics industry through breaking down large-scale objects into nano-scale entities. The 'top-down' approach has its drawbacks in terms of the high energy consumption and high manufacturing cost.[70] The alternative approach i.e., 'bottom-up' approach, involves building up a structure from small building blocks, using many methods such as sol-gel processing, chemical vapor deposition (CVD), etc.[71] **Figure 2-2** shows a representative example using a block copolymer to fabricate nano-structured devices. Our interest is on the nano-structured biological membranes that give inspiration towards fabrication of self-assembled monolayer[72]/ bilayer membranes,[73] Langmuir-Blodgett films,[74] and layer-by-layer polyelectrolyte multi-layers (**Figure 2-3**).[75] Among the 'bottom-up' approaches, self-assembly is a practical, low-energy, and cheap strategy to create ensembles of nanostructures. It is an efficient way to produce nano-architectures with precisely controlled geometries and specific functions, replicating those found in nature.

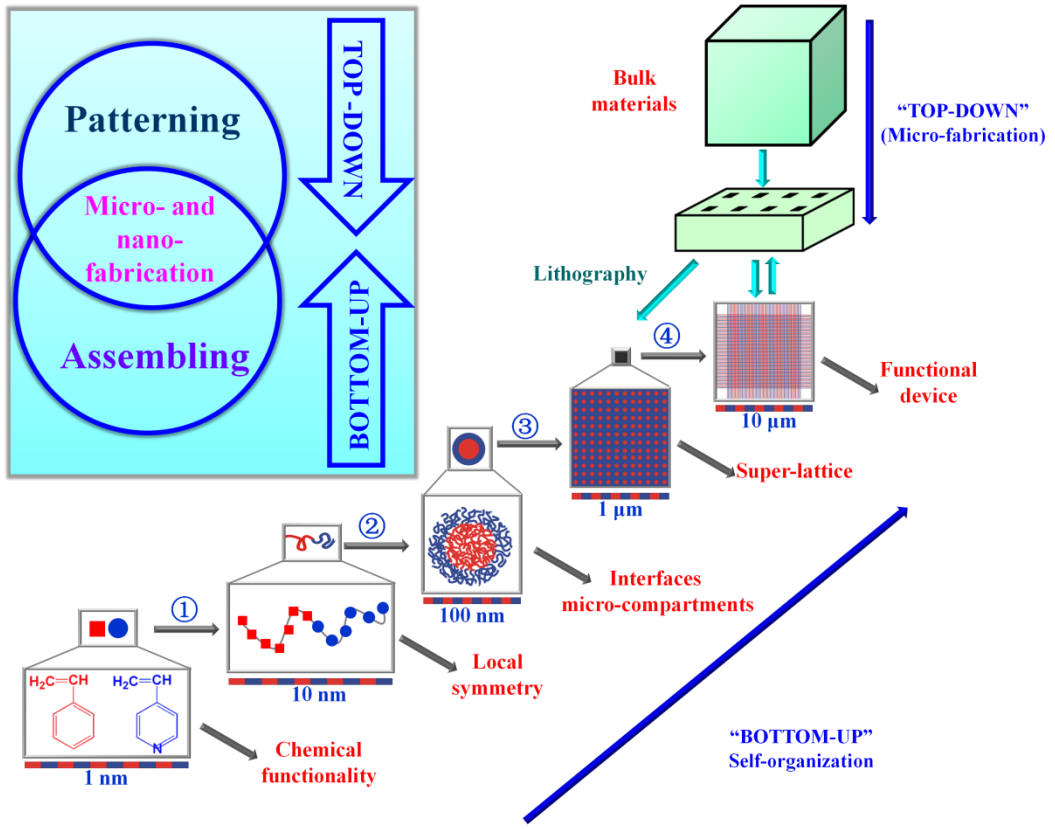

Figure 2-2 A representative example of 'bottom-up' versus 'top-down' strategies towards preparation of several hierarchy levels in block copolymer systems. The illustration takes poly (styrene-b-4-vinylpyridine) for example. The monomers defining the chemical functionality are on the smallest length scale (~1 nm). The length scale of the AB di-block copolymer is about 10 nm. The copolymer can self-assemble into a core-shell micelle with the diameter around 100 nm. The 'bottom-up' strategy shows that the superlattice with a scale length around 1 µm is self-assembled by the micelles. The 'top-down' strategy shows that the superlattice is generated in a litho-graphically produced structure. A functional device with a scale length of 10 µm is prepared with the help of self-organization processes. A picture describing the relationship between 'top-down' and 'bottom-up' is inserted in this figure.[70]

2.2.3 Self-assembly of Polymers

Controlled assembly of block polymers enables a broad variety of self-assembled structures from a simple structural regularity (e.g., spherical micelles, vesicles, simple lamella, and rods) to complex superstructures (e.g., hexagonally packed cylindrical micelles, Janus micelles, large polydisperse vesicles, onions, large compound micelles,

hollow concentric vesicles, entrapped vesicles, and vesicles with tubes in the wall).[76,77] For the block copolymers self-assembled in solution, one general and straightforward strategy is via the micellization in a selective solvent for one segment. At the molecular level, it simulates the formation of a conventional lipid bilayer with the hydrophobic tails corralling together and the hydrophilic heads facing out into the water. The variation of the selective solvent or its strength for the constituent blocks could tune the morphologies of self-assembled structures. The 'Crew-Cut micelles' from the Eisenberg group is one of the most classic studies.[78]

Another strategy to produce self-assemblies such as micelles is called 'non-covalently connected micelles (NCCM)' (**Figure 2-3**).[79-83] The strategy is a block copolymer-free strategy developed by the Jiang Ming research group. The NCCM strategy can produce self-assemblies using different polymers or small molecules as building blocks instead of conventional block copolymers. For example, the core and shell of the NCCM micelles can be non-covalently connected via hydrogen bonding rather than chemical bonds.[80] NCCM can be utilized to build polymeric micelles, hollow spheres, and structured assemblies with suitable functionalities via specific interactions (e.g., hydrophobic interaction), through using different building blocks such as homopolymers, random copolymers, graft copolymers, oligomers, and ionomers. Many more studies of self-assembly phenomena based on different driving forces have been carried out, which include pH-dependent micellization, temperature induced self-assembly, ion-ion interaction assisted self-assembly, and chemical cross-linking in producing concentrated micelles. Furthermore, host-guest coordination complexes and biological affinity could be utilized to direct molecular self-assembly. Photo-induced self-assembly as an important research direction will be discussed in detail in the next section.

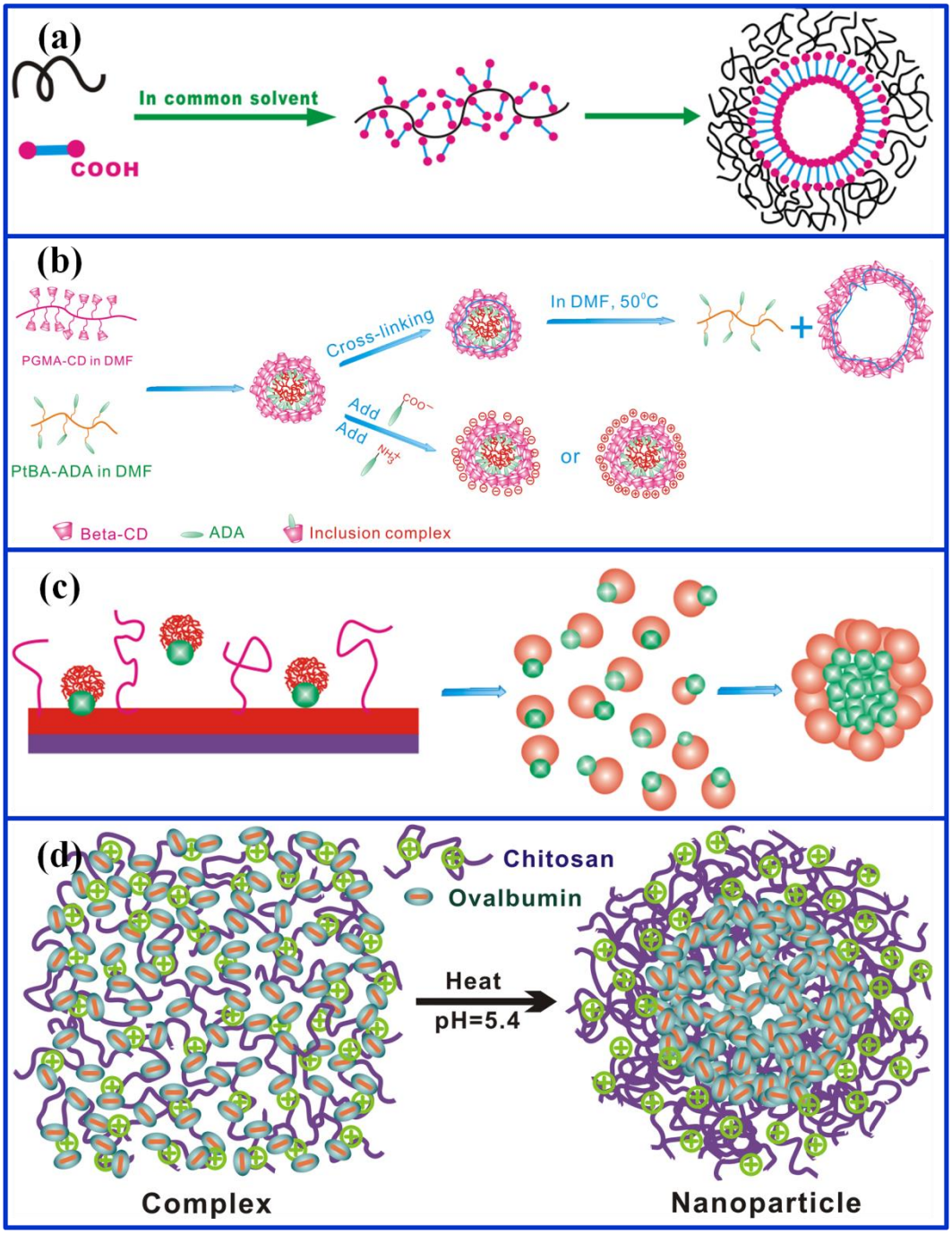

Figure 2-3 (a) A schematic illustration of a hollow sphere self-assembled via a rod-like polyimide with two carboxyl end groups and coil-like poly(4-vinyl pyridine) in chloroform.[80] (b) An illustration of fabrication of non-covalently connected micelles (NCCM) of poly(glycidyl methacrylate)-(β-cyclodextrin) (PGMA-CD)/poly(tert-butyl acrylate)-adamantyl (PtBA-ADA) micelles in aqueous media based on host guest interaction of β-CD and ADA. The hollow spheres can be obtained via shell cross-linking and core removal of the micelles.[81] (c) Illustration of the self-assembly of Janus particles into a flower-like super-micelle.[82] (d) Illustration of pH-sensitive nano-gel of chitosan and ovalbumin self-assembly.[83]

2.3 Smart materials and smart polymers: mimicking nature

2.3.1 Smart Materials and Systems

A ‘smart material’, also known as an ‘intelligent or responsive material’, changes or alters automatically one or more properties (e.g., shape, size, viscosity, colour, strength, and conductivity) in response to an external stimuli (e.g., humidity, temperature, moisture, light, stress, electric charge, or magnetic field).[84] The response is reversible when the external stimuli from the surrounding medium changes again. Smart material systems can be classified into three main types: (i) Smart Metal Materials, including shape memory alloys, (ii) Smart Inorganic Materials, including piezoelectric/magneto-rheostatic materials/electro-rheostatic materials, and (iii) Smart Polymeric Materials, including environmentally responsive hydrogels, reversible sol-gel materials, responsive polymer micelles, and smart coatings on a substrate.[85,86] We will focus on polymeric smart materials, which is the research in this work.

Biological systems can sense a whole range of signals through sight, taste, smell and touch. Researchers studied the creation of functional materials through mimicking biological intelligence, such as the detection and processing of information from mechanical, magnetic, electric, and optical sensors.[87] Current research interests on smart materials is focused on the construction of biosensors,[88] molecular recognition,[89] signal transduction,[89] as well as structural control systems.[90] Recently, an artificial muscle mimicking the chromatophores of biological cells has been reported.[91] These chromatophores, such as those found in squid and zebrafish, are responsible for colour-change upon any environmental changes (e.g., mood, temperature, stress). The artificial muscle is able to stretch and deform through emulating the biological muscles using voltage-sensitive and shape-changing dielectric elastomers.[91] Another ultimate goal in biomimetic materials is to create a bionic eye to reproduce human vision. The recent

breakthrough is the hemispherical electronic elastic membrane created by the team of Professor Yonggang Huang and Professor John Rogers from Northwestern University and University of Illinois at Urbana-Champaign.[92] It mimics the biological imaging device with wide field view and low aberrations. The design of the flexible hemispherical cameras includes a photo-detecting diode to provide local light detection and a *p-n* junction blocking diode. The unit cell has high-contrast response to light. This light-curving detection membrane is believed to open the door to transplanting it into a human eye in the future.

In the future, smart functional materials will be obtained with high reliability, lightweight, cost effective, and low power consumption. They provide the possibility of nano-scale smart design with varied and complex intelligence. Moreover they provide new functions that are presently unavailable, for example, artificial body parts.[93] Smart materials equipped with sensor arrays can one day help to detect drugs, toxic pollutants, and measure the level of electromagnetic radiation.

2.3.2 Smart Polymers

Peptides, proteins and polysaccharides, as the basic structural components of biological systems, have inspired synthetic polymer chemists to synthesize new biomimetic polymers. These types of new polymers that are responsive to environmental stimuli are defined as ‘smart polymers’ or ‘stimuli-responsive polymers’.[94,95]

Based on the types of external stimuli (e.g., pH, temperature, magnetic field, electric field, light, and biological molecules), smart polymers can be categorized into pH-sensitive polymers, thermo-responsive polymers, magnetically active polymers, electro-responsive polymers, photo-switchable polymers, and chemically activated polymers (**Table 2-2**).

The most widely investigated smart polymers are pH-sensitive and thermo-responsive polymers.[96] Polymers with pH-sensitivity are usually polyelectrolytes with attached ionizable weak acidic moieties or basic moieties. They are able to undergo ionization (accepting or releasing protons) in response to environmental pH changes. Typical examples of anionic polyelectrolytes are poly(acrylic acid), poly(2-ethylacrylic acid), poly(methacrylic acid), and poly(2-propylacrylic acid).[97] Their functional groups remain non-ionized at low pH and change into negatively charged polymers at increased pH. For the polybasic polymers, such as poly(ethylenimine) and poly(N,N-diakyl aminoethyl methacrylates), they become positive charged at decreased pH because of the ionization of the basic groups.

Thermo-responsive polymerscan either exhibit an upper critical solution temperature (UCST) or a lower critical solution temperature (LCST) behaviour. UCST polymers,turn bi-phasic below a specific temperature. Polymers with a LCST are monophasic below the critical temperature and phase separate above this temperature. The representative example is poly(N-isopropylacrylamide) whose LCST is 32 °C that is close to our body temperature,[98] making it a good candidate for drug-delivery.

Table 2-2 Representative examples of smart molecules, polymers and systems responsive to external stimuli.

Stimuli	Abbreviation	Molecules, polymers or systems	Structure	Ref.
pH	PAA	poly(acrylic acid)	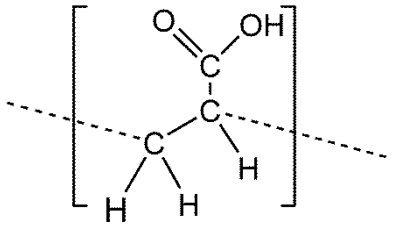	[99]
pH	PEI	poly(ethylenimine)	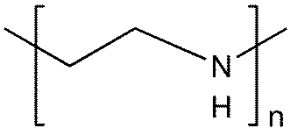	[100]
Temp.	PNIPA, PNIPAAm, PNIPAA or PNIPAm	poly(N-isopropylacrylamide)	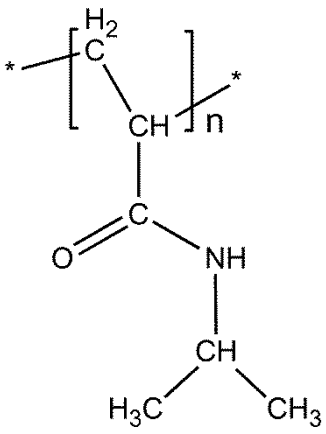	[101]
Temp.	HPMC	Hydroxypropyl methylcellulose	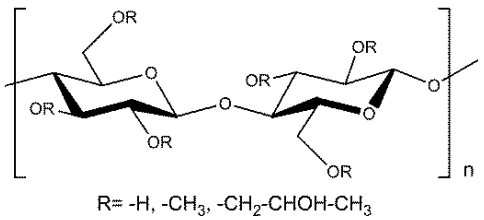 R= -H, $-CH_3$, $-CH_2$-CHOH-CH_3	[102]

Electric field	PDMAPAA	poly(dimethylami-nopropylacrylamide)	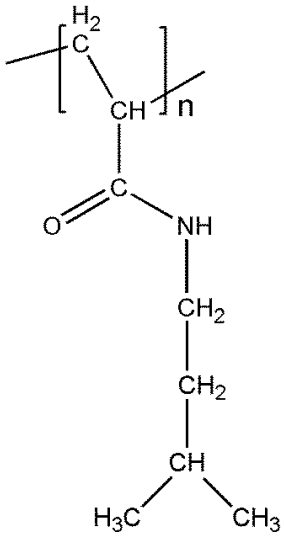	103
Electric field		corannulenes 3	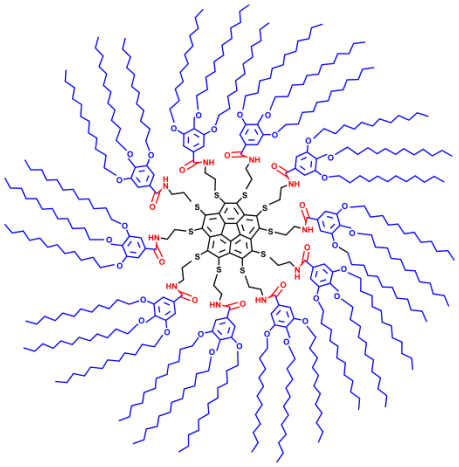	104
Magnetic field	SiO_2-Fe_3O_4-Au_{seeds}	Au nanoparticle seeds loaded silica-primed Fe_3O_4 nanoparticles	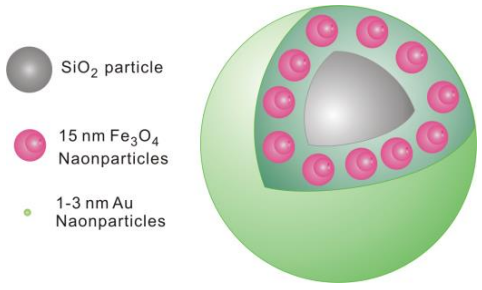	105
Glucose	PEO-b-PGEA	Poly(ethylene oxide) -block-poly(2-glucosyl-oxyethyl acrylate)	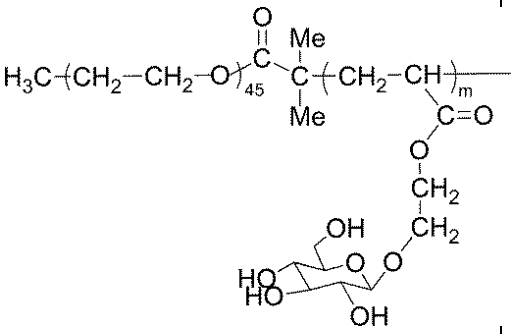	106

Light	Photo-reacting units	Stilbene/dihydrophenanthrene 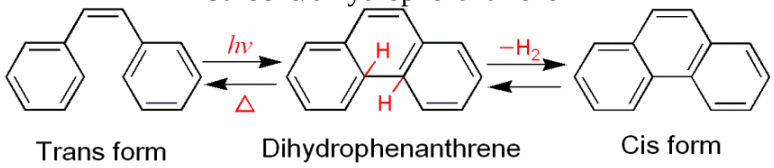 	107
		Azobenzene and three different types of azobenzene chromophores 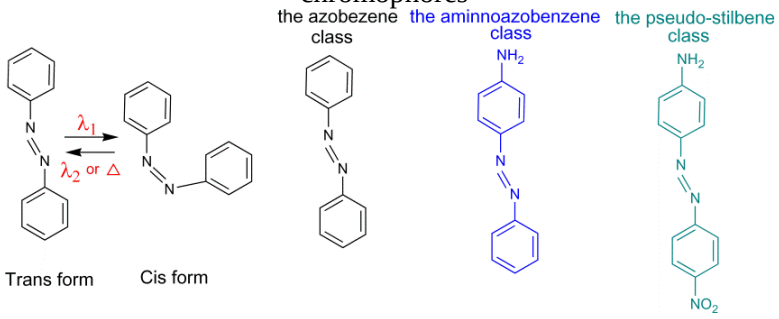 	108
		Spiropyran compounds 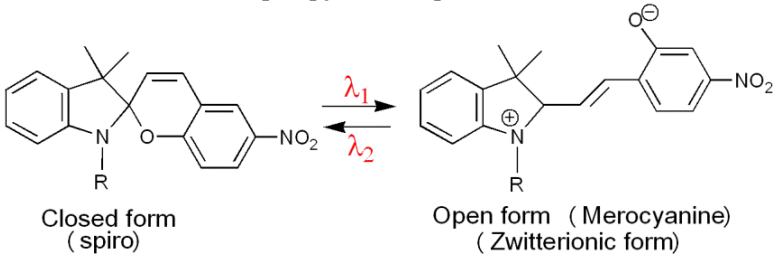 	109
		Fulgides 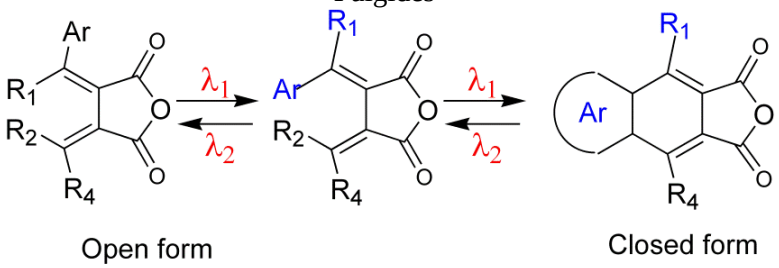 	110
		Triphenylmethane derivatives (photo-isomerization) 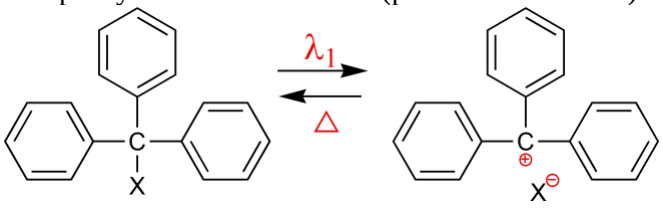 	111
		Coumarin (photocyclization/photodimerization) 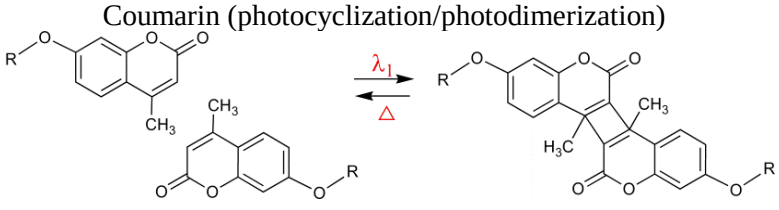 	112

	Photoresponsive amphiphiles	4,(4'-alkylphenylazo) phenyl derivatives 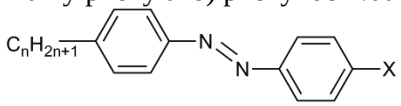	[113]
	Photoreacting unit in the main chain of the polymer	Poly (γ-methyl L-glutamate)-azobenzene- Poly (γ-methyl L-glutamate) (MAzoM) 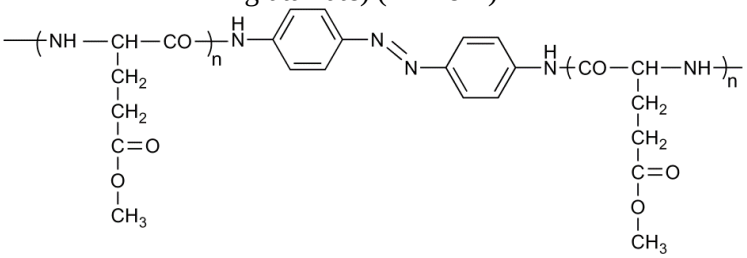	[114]
	Photoreacting unit endcapped the polymer chain	4-Dihydroxyethoxyazobenzene end-capped poly (N-isopropylacrylamide) 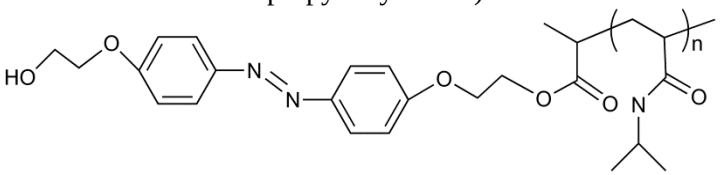	[115]
	Photoreacting unit in the side chains of the polymer	Poly (t-butyl acrylate-co-acrylic acid)-b-poly (methacrylate) (P (tBA-co-AA)-b-PMAz) 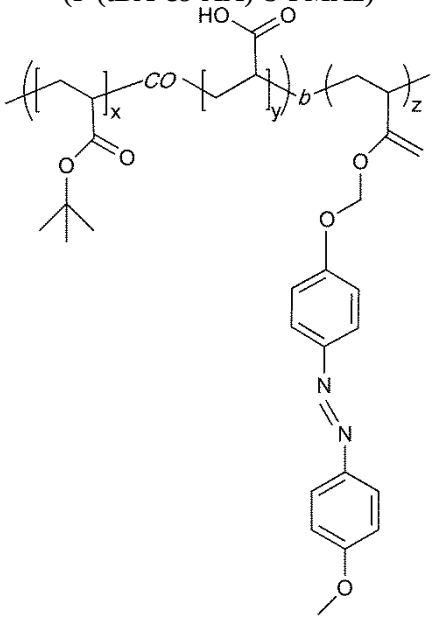	[116]

These smart polymers possess good potential for biological-related applications including drug delivery, gene delivery,[117,118] and metabolic control devices (e.g., glucose sensors).[119, 120] Among all these smart polymers, photo-switchable polymers are becoming more widely studied recently. In this type of smart polymer, light energy is

used to trigger conformational changes in the polymer structures. These photo-responsive polymers can also be used in devices with photo-controllable design, converting light energy into mechanical energy. These photo-responsive polymers will be discussed in details in a subsequent section.

2.4 Self assembly study of azobenzene-based polymers

2.4.1 Photo-responsive polymers

A photo-responsive polymer is a functional polymer with photo-receptor chromophores, which can convert light into a polymer conformational change. The light is stored as a chemical structural change of the chromophores initially, and then transferred to a reversible conformational change. The conformational change produces concomitant changes in the polymer physical and chemical properties inside the solution or melt states.[121] Utilizing the photo-responsive trigger molecules is the basic concept for controlling polymer properties by photo-irradiation. Such photo-responsive molecules including azobenzene,[108] spiropyran,[122] spirooxazines,[123] diarylethenes,[124] and fulgides,[125] could transform to the other isomeric form upon photo-irradiation. Furthermore, they could reversibly recover to the initial state thermally or photo-chemically. This type of isomerization is named photochromism.[126] Among the above mentioned molecules, azobenzene and its derivatives are highly attractive as their photochemical process is unique and comparatively clear.[108]

2.4.1.1 Photo-responsive behaviour of liquid crystals containing photo-chromic molecules

Liquid crystals (LCs) have an ordered arrangement and yet can still flow like a liquid. LCs are divided into different types of LC phases, which can be distinguished by their

different optical properties (such as birefringence). Most substances that exhibit the properties of LCs consist of long, rigid rod- or disk-shaped molecules that are easily polarizable and can orient themselves in one of three different ways, e.g., nematic, smectic, and cholesteric LC phases. LC molecules exhibit good cooperative motion; thus, if a small portion of the LC molecules change their alignment in response to an external stimulus, the alignment of other LC molecules also changes (domino effect). Some photo-chromic molecules can act as liquid-crystal mesogens. For example, the *trans*-azobenzene molecule is rod-like and the molecular core is rigid and anisotropic. Thereby the *trans*-azobenzene is an ideal liquid-crystal mesogen (**Figure 2-4a**). When the liquid-crystal photo-chromic molecules are introduced into the LCs, they can cause alignment modulation of LCs induced by photo-chemical reactions.

On illumination with linearly polarized light, the photo-chromic molecules exhibit photo-induced orientation. Taking azobenzene as an example, a polarized light will cause the azobenzene molecules to isomerize and relax in random positions. However, those relaxed molecules (*trans*-azobenzene) that fall perpendicular to the incoming light polarization will no longer be able to absorb, and will remain fixed (**Figure 2-4b**). The photo-induced orientation involves the *trans-cis* photo-isomerization and subsequent thermal and/or photochemical *cis*-trans back-isomerization. By repetition of these *trans-cis-trans* isomerization cycles, the optic axis of azobenzene groups becomes aligned perpendicular to the electric vector of the polarized actinic light (**Figure 2-5**).

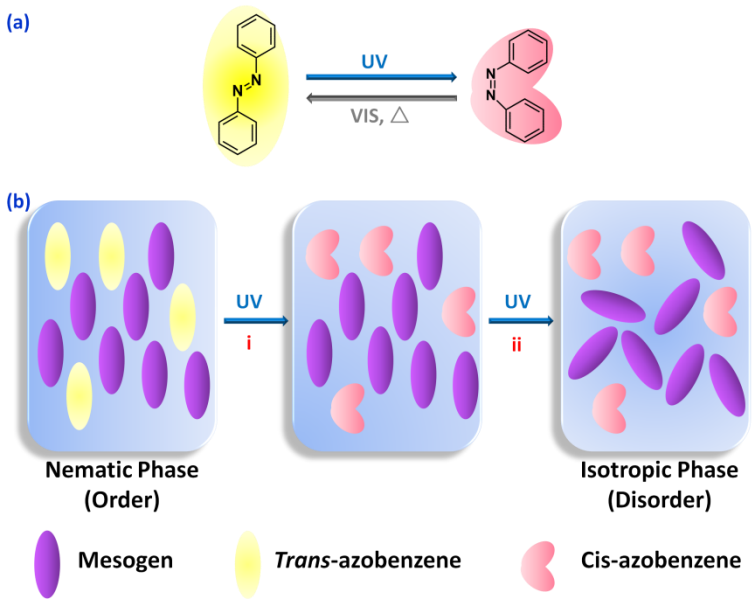

Figure 2-4 **(a) The photo-isomerization between the rod-like *trans*-azobenzene and the bent *cis*-azobenzene under UV-visible light irradiation. (b) The process of the photo-chemical phase transition of azobenzene/LC systems: (i) *trans–cis* photo-isomerization; (ii) orientational relaxation process; N, nematic; I, isotropic.**

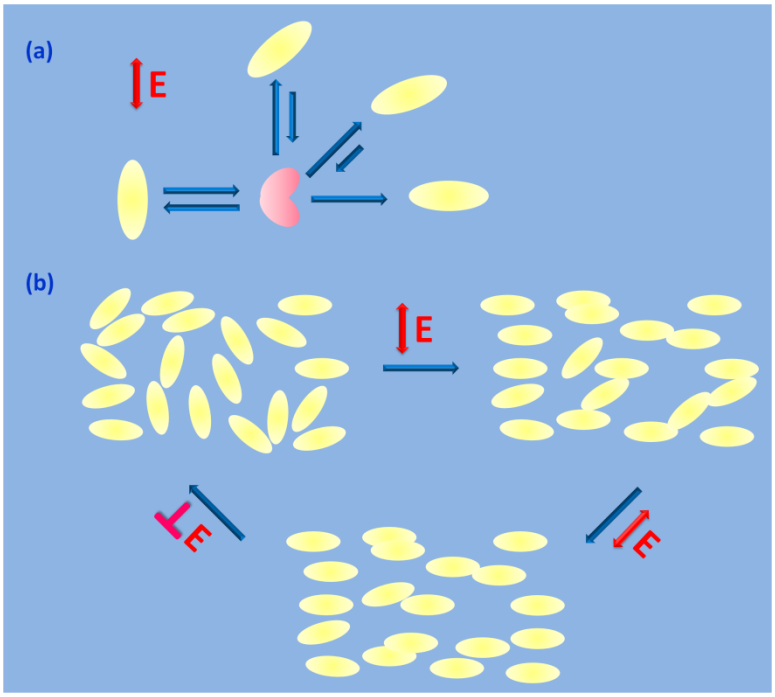

Figure 2-5 **Mechanisms of statistical photo-orientation of azobenzene molecules. (a) The molecules aligned along the polarization direction of the incident light will isomerize and take on a new random orientation. The molecules that lie perpendicular to the polarization of light cannot absorb a photon and remain fixed. (b) An initially isotropic distribution of chromophores will become progressively aligned with polarized irradiation. Irradiation with circularly polarized light can restore isotropy.[127]**

These photo-sensitive molecules can play roles as both mesogentic segments and photosensitive chromophores. They are present in the LCs as dopants, or incorporated into a polymer to fabricate a photo-sensitive LC polymer.

When a small portion of photo-chromic molecules such as an azobenzene, stilbene, spiropyran, or fulgide derivatives are incorporated into the LC molecules as the guest molecules, an LC-to-isotropic phase transition of the mixtures can be induced isothermally. For example, the rod-like *trans*-azobenzene molecules stabilize the phase structure of the LC phase, whereas the bent *cis*-azobenzene molecules tend to destabilize the phase structure of the mixture (illustrated in **Figure 2-4**). As a result, the LC–isotropic phase transition temperature (T_c) of the mixture with the *cis* form (T_{cc}) is much lower than that with the *trans* form (T_{ct}).

However, LCs possess a high viscosity so that the orientational relaxation of mesogens requires a relatively long time. New photo-responsive LC materials have been studied to improve the photo-induced phase transition efficiency. Every mesogen in these LCs or LC polymers is provided with a photosensitive moiety (illustrated in **Figure 2-6**). It is expected that photochemical phase transitions could be induced essentially on the same timescale as photochemical reactions of the photoactive moiety in each mesogen if the photochemical reactions of a large number of mesogens are induced simultaneously by means of a short laser pulse.

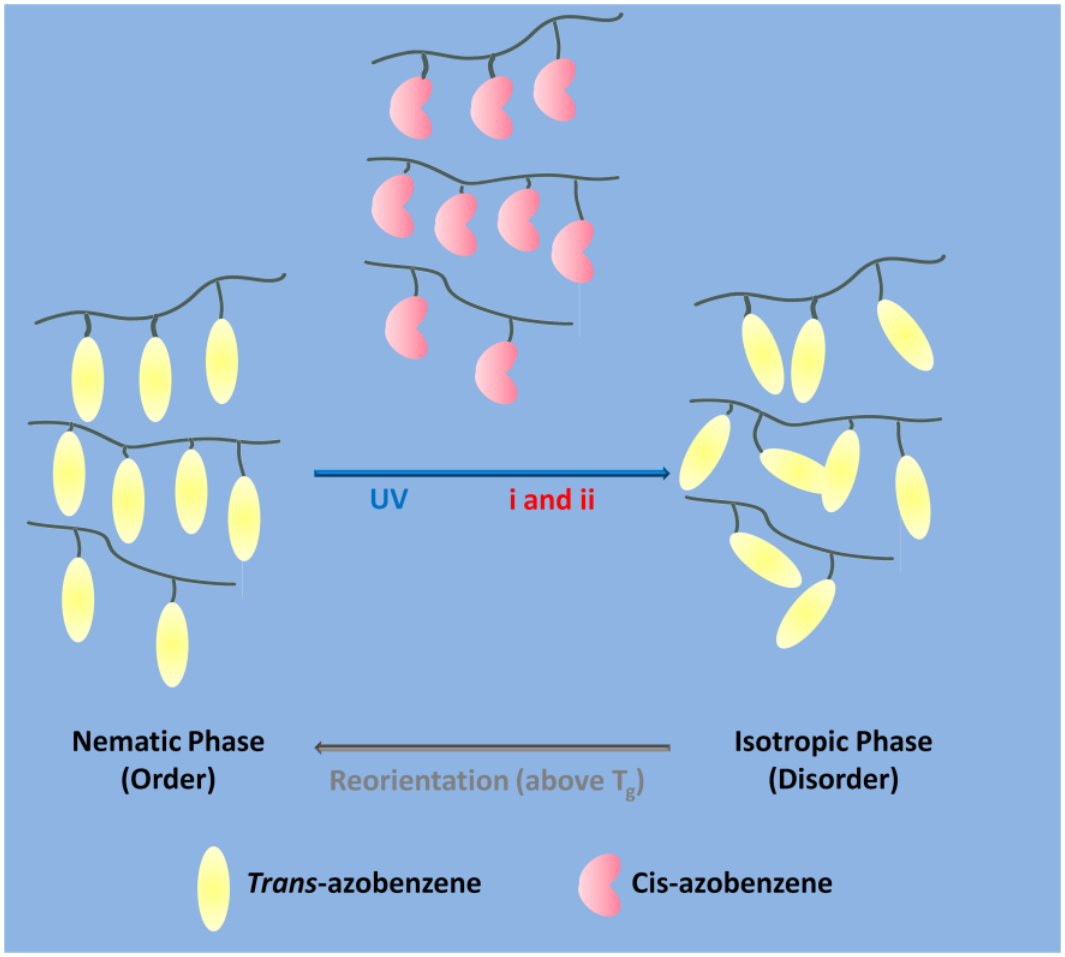

Figure 2-6 Fast response by means of azobenzene LCs with a photosensitive moiety in every mesogen: (i) *trans–cis* photo-isomerization; (ii) orientational relaxation process.

For example, azobenzene are also used to modify the chemical structure of LC elastomers (e.g., LC polymer films[128] or LC polymer gels), which exhibits the unique combination of the orientational order of the liquid crystal phase and the rubber elasticity of polymer networks. Photo-induced mechanical deformation is enabled when azobenzene megosens changing their macroscopic shape upon a linearly polarized light irradiation. These photo-responsive LC materials are promising for applications as photo-driving micro-/nano-machines, soft high-speed muscle-like actuators,[129] and non linear opticals.[130] A polydomain liquid-crystal film consists of many micro-sized domains of azobenzene liquid-crystal moieties which are aligned in one direction in each domain. However, the

macroscopically the direction of alignment is random. On irradiation of a linearly polarized light, the azobenzene mesogens aligned along the direction of light polarization selectively absorb the light. Dierected bending of the polydomain azobenzene-LCN film is achieved as a result of the cooperative movement of the liquid-crystal moieties and polymer segments.[128] Unlike polydomain azobenzene-LCNs, monodomain azobenzene-LCNs bend in only one direction. Timothy J. White, et al. reported a high frequency photo-driven polymer oscillator which is a monodomain azobenzene-LCN. The photomechanical deformation in the monodomain azobenzene-LCN cantilever was fast and large. The frequency of the oscillation was nearly 30 Hz and the displacement angle between the two extremes was greater than 170. The oscillation showed little fatigue over 250 000 cycles under a polarized argon-ion laser (Ar^+) laser beam, realizing the conversion of light input into mechanical output. The plausible mechanism of photo-induced bending behaviour in homogeneously or homeotropically aligned monodomain LC films is illustrated in **Figure 2-7**.

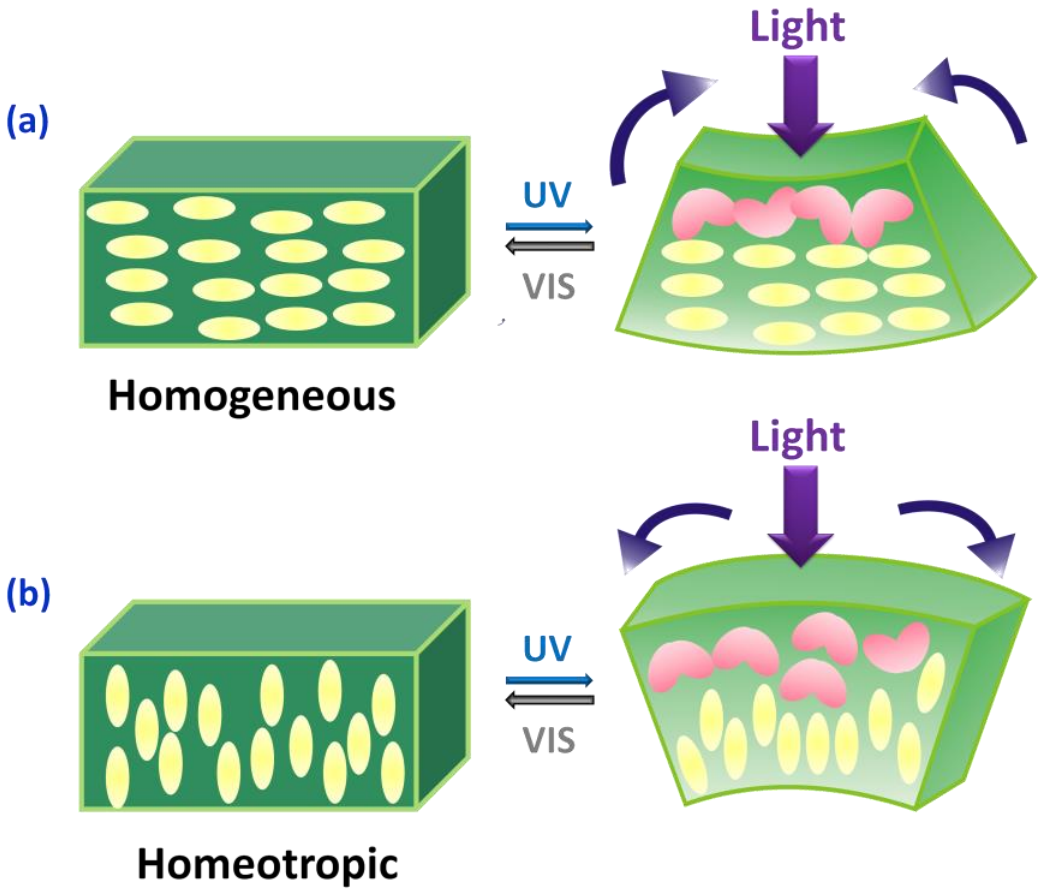

Figure 2-7 Schematic illustration of the three-dimensional bending mode in the homogeneous films (a) and the homeotropic films (b). (a) The monodomain LC film with in-plane alignment of mesogens bent along the alignment direction toward the irradiation source. (b) The homeotropically aligned monodomain LC films undergo the bending away from the irradiation direction of the actinic light. Because the alignment direction of the azobenzene mesogens in the homeotropic films is perpendicular to the film surface, exposure to UV light induces anisotropic expansion contributing to the bending in a completely opposite direction.

2.4.1.2 Photo-induced phase transition behaviour of photo-sensitive polymers

The photo-chemically induced phase transitions are interpreted in terms of a change in the phase-transition temperature of LC systems upon accumulation of one isomer of the photo-chromic guest molecule. The LC–isotropic phase transition temperature (T_c) of the mixture with the *cis* form (T_{cc}) is much lower than that with the *trans* form (T_{ct}). If the temperature of the sample (T) is set at a temperature between T_{ct} and T_{cc} and the sample

is irradiated to cause *trans–cis* photo-isomerization of the azobenzene guest molecules, T_c decreases with an accumulation of the *cis* form. When T_c becomes lower than the irradiation temperature T, an LC–isotropic phase transition of the sample is induced. The sample reverts to the initial LC phase through *cis–trans* back-isomerization. Thus, phase transitions of LC systems can be induced isothermally and reversibly by photochemical reactions of photo-responsive guest molecules.

Lately, it has been reported that localized photo-excited species can trigger the macroscopic phase transition in p-conjugated polymers, charge transfer complexes, organo-metal complexes and manganese oxide systems. In these systems, strong electron-electron and electron (spin)-lattice interactions play a key role in their optical, magnetic, dielectric and galvano-magnetic properties. In addition, these interactions also act as a driving force in the conversion process of the localized photo-excited species into the macroscopic phase domain. This photo-effect is specifically named as photo-induced phase transition (PIPT).

2.4.2 Utilization of azobenzene chromophores in polymers

Azobenzene and its derivatives are compounds that have the characteristic double bonded -N=N- functional group. The stereochemistry of the double bond generally has profound effects on the molecular physical and chemical properties. The bond provides rigidity to the molecule and imposes geometrical restrictions on the molecule, rendering the flatness or planar configuration.[108]

Azobenzene chromophores exist in two isomeric states: (i) the thermodynamically stable *trans*-state and (ii) the metastable *cis*-states. The energy difference between the ground states of the *trans* and *cis* isomers of azobenzene is about 50 kJ/mol. Efficient photo-

isomerization from the *trans* isomer to the *cis* isomer can be induced by UV irradiation. The metastable *cis*-state can be reversed to the *trans*-state either by a spontaneously thermal process or a reverse *cis*-*trans* photo-isomerization cycle. The *trans*-state is more stable. The *cis*-state can thermally isomerize to the *trans*-state even in the dark.

The actual mechanism of isomerization (including inversion, rotation, or hula-twist[131,132]) remains unclear and requires extensive experimental and computational work to ascertain the general principles governing this phenomenon. Three associated changes are known to take place in the photo-induced isomerization of azobenzene (**Figure 2-8**):

a) Change in the absorption profile. The *trans*-*cis* isomerization causes a decrease in the absorption at 320 nm owing to a π-π^* transition, and an increase in absorption at 440 nm owing to a n-π^* transition.

b) Change in the molecular dimension. The distance between the 4- and 4'-carbons is shortened from 9.0 Å to 5.5 Å by isomerization, changing from the *trans* isomer to the *cis* isomer, as shown in **Figure 2-8**.

c) Change in the dipole moment. The dipole moment changes from 0.5 Debye (*trans*-state) to 3.1 Debye (*cis*-state).[133]

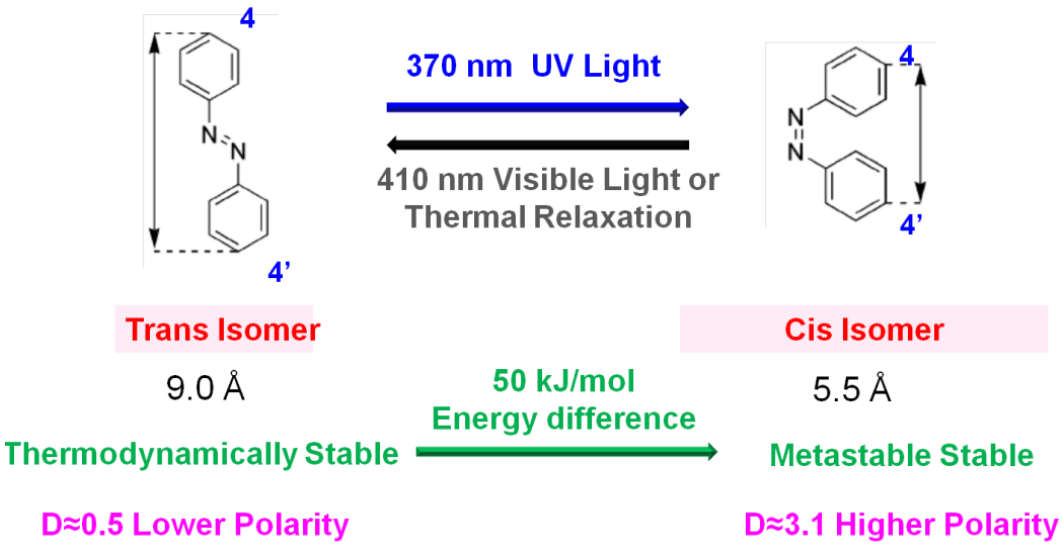

Figure 2-8 Isomerization changing from the *trans* isomer to the *cis* isomer of the azobenzene group as well as the associated properties change.

Azobenzene chromophores can be classified into three types based on the energetic ordering of the (n, π*) and (π, π*) states: (i) azobenzene type, (ii) amino-azobenzene type, and (iii) pseudo-stilbene type.[134] The azobenzene type molecules display a low intensity *n*-*π** band in the visible region of the spectrum and a high intensity *π*-*π** band in the UV region. The amino-azobenzene type molecules are characterized spectroscopically by a close or overlapping *n*-*π** and *π*-*π** band in the violet or near-visible UV region. The pseudo-stilbene type molecules, a type of the azobenzene molecules with electron-donor and electron-acceptor (pull/push) substituents at the 4 and 4' positions, have a long wavelength *π*-*π** band and the sequence of (n, π*) and (π, π*) states are reversed on the energy scale, which is similar to stilbene. The duration of the photo-isomerization reactions varies for the different types of azobenzene chromophores. Thus, the substitution properties of azobenzene are intimately tied to the kinetics of the photochemical processes as well as the *cis* lifetime and fraction. Other factors include the substituted position, electron-donating and electron-withdrawing groups, and steric hindrance.

Different azobenzene-based photo-responsive polymers have been explored by covalently attaching low molecular-weight azobenzene and its derivatives onto various sites of polymers, e.g., buried inside the polymer backbone,[135,136] end-capping the main chain,[115,137] or as pendent groups on the side chains.[138-140]

The photo-isomerization behaviour of azobenzene-based polymers depends on several factors, such as the chemical structure of the azobenzene moieties, the backbone, the glass transition temperature, and the crystallinity of the polymer.[108,134] The photo-isomerization rate of azobenzene-based polymers in solution is very sensitive to the local environment surrounding the azobenzene groups, which includes the solvent polarity, the polymer concentration, and the solution temperature.[141-145]

The reversible switching of the azobenzene chromophore as well as the resulting change in molecular physical properties and geometry could be used to regulate the macroscopic behaviour of polymers using an external light stimulus. The physical or functional properties of azobenzene-based polymers and materials that are controllable by photo-irradiation include their solubility, viscosity, phase separation, surface wettability, permeability, magnetic properties, mechanical effects, and reversible sol-gel transition. For example, Li *et al.* reported light-driven artificial muscles from side-on nematic elastomer actuators using two azobenzene chromophore monomers as side chains in the bulk polymerization of various acrylate monmers.[146] The elastomer with 25 % monomer 1 and 75 % monomer 2 can contracted up to 12-18 % after 130 s UV irradiation (100 mW/cm^2). A novel reversible photo-controlled pseudo-polyrotaxane hydrogel using the competition of host/guest interactions between PEG/α-CD pseudo-polyrotaxane hydrogel also was investigated.[147]

The azobenzene-based polymers have been studied both in the solid state and in solution. This section focuses not only on the azobenzene-based polymers, but also on polymers that can self-assemble in solution. Several research groups have carried out extensive studies in this research field. Prof. Zhao Yue, from the Universite de Sherbrooke Canada, summarized various types of light-responsive block copolymer micelles in 2012 (**Figure 2-9**).[148] It is a classic and widely adopted method to prepare photo-responsive self-assemblies of azobenzene-based polymers in aqueous solution.

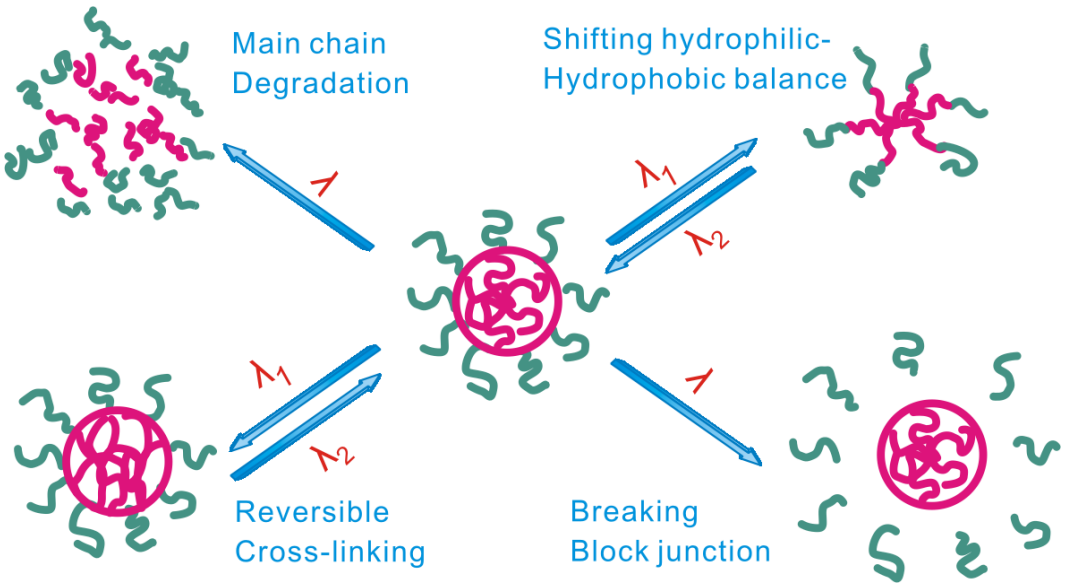

Figure 2-9 Schematic illustration of photo-responsive block copolymer core-shell micelles re-grouping into four different types of structures by light illumination.[148]

For over 10 years, our laboratory has been working on the synthesis, design and development of the azobenzene-based systems.[102,138,139,149-159] We have reported the self-arrangements of photo-switchable polymers in liquid crystalline organizations,[139] sol-gel transition complexes with cyclodextrins,[102] and their micellization.[152,154] This work will be reviewed in detail in following section.

The azobenzene-based liquid crystalline polymers have attracted considerable research interest.[160] The *trans* isomer of azobenzene exhibits a LC phase because it has rod-like shape when undergoing *trans*-*cis* isomerization upon photo-irradiation. The *cis* isomer of azobenzene does not exhibit a LC phase. It has been a great challenge to synthesize water soluble di-block copolymers and to construct the polymeric self-assembled structures in water. The polymer selected for the study is responsive to two different triggers, i.e., temperature and pH.

The schematic illustration (**Figure 2-10**) shows the concept of self-assembly of an amphiphilic double responsive di-block copolymer into well-defined micelles in aqueous solution, induced by both a thermal treatment and UV-irradiation. The LCST of the copolymer can be changed upon thermal treatment and light illumination. The polymer structure possesses one block that contains photo-sensitive azobenzene moieties in the pendant groups. Under visible light, the blocks containing *trans*-isomers render them hydrophobic and contribute to the micelle core formation. The amphiphilic di-block copolymers self-assemble into a compact core-shell micelle with the stabilization of other hydrophilic blocks. The polarity and solubility of the blocks can be photo-regulated by UV-Visible irradiation through the azobenzene photo-isomerization changing from *trans* to *cis* isomers. Upon UV absorption, the significant polarity increase of *cis*-isomers makes the hydrophobic block become more hydrophilic. The reversible isomerization can be achieved upon absorption of visible light with a wavelength of 410 nm, converting the *cis* isomers back into the initial *trans* isomers.

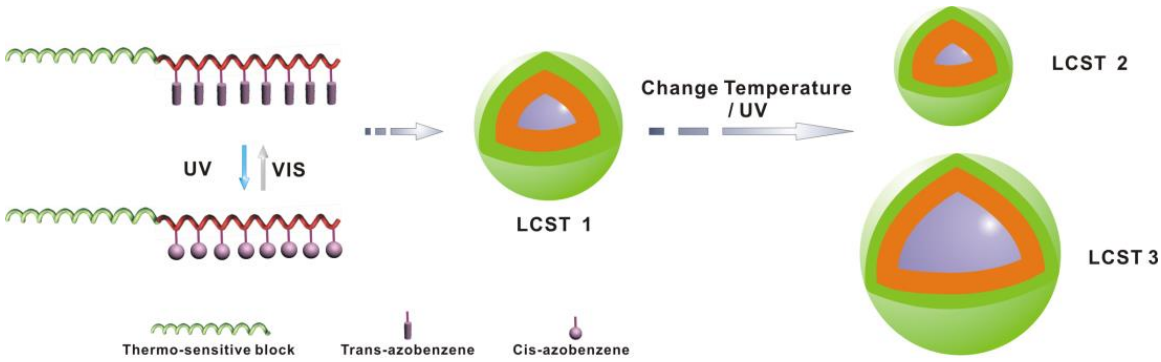

Figure 2-10 Schematic illustration of a thermo- and UV-responsive block copolymer self-assembled in the water with responsive LCST changes.

The concept and methodology were demonstrated by a series of block copolymers of 2-(dimethylamino) ethyl methacrylate (DMAEMA) and azobenzene methacrylate synthesized via atom transfer radical polymerization (ATRP).[102] These well-designed di-block copolymers possessed the azobenzene units as a photo-responsive trigger. They also possessed temperature-response and pH-response induced by the poly (DMAEMA) segments. Poly (DMAEMA-b-azo methacrylates) are a series of di-block copolymers with different chain lengths of the hydrophilic block [poly(DMAEMA)] and different substituted azobenzenes (H-, cyano- and butoxy- substituted). With azobenzene in the *trans*-form, the copolymer can readily form core-shell micelles in aqueous solution due to their amphiphilic behaviour. Those micellar aggregates displayed a photo-controllable effect on the LCST. Taking poly(DMAEMA172-b-PPHM9) as an example, the LCST could changed from 41.8 °C to 44.8 °C after UV-irradiation (λ=366 nm). The LCST increased because the *cis*-azobenzene is more hydrophilic than the *trans*-azobenzene. The micellization behaviour was also controlled by photo-irradiation, as confirmed by the surface tension versus concentration plots of the di-block copolymers before and after UV-irradiation.

Macromolecular self-assembly has been demonstrated to be a useful tool for fabrication of nano-scale functional architectures that can be reversibly controlled by external stimuli. An inclusion complex based on cyclodextrins (CDs) is attractive in bridging supramolecular chemistry and macromolecular self-assembly. CDs belong to a family of cyclic oligosaccharides, composing of 6, 7, or 8 glucopyranose units that are linked by α-1,4 glycosidic bonds. There are three different CDs that are called α-, β- and γ-CDs, respectively. CDs have been extensively used as host molecules since their truncated cone structure possesses a unique property. Their exterior surface is hydrophilic and the interior is hydrophobic. Inclusion complexes could be formed via CDs by accommodating a variety of guest molecules, e.g., azobenzene, adamantine, phenyl adamantine, and ferrocene. The *trans* isomer could form a stable host-guest inclusion complex with α-CD. The *cis* isomer of azobenzene is not able to form an inclusion complex. The host-guest inclusion of azobenzene and cyclodextrin has been employed to realize the reversible stimuli-responsive supramolecular complexes, such as sol-gel or hydrogel systems.

Figure 2-11 schematically illustrates the supramolecular complexes formed via α-CD and an azobenzene-modified random polymer.[102] The sol-gel transition of the supramolecular complexes is switchable by photo-irradiation with a photon of appropriate wavelength that controls the inclusion complex formed via α-CD and azobenzene groups.

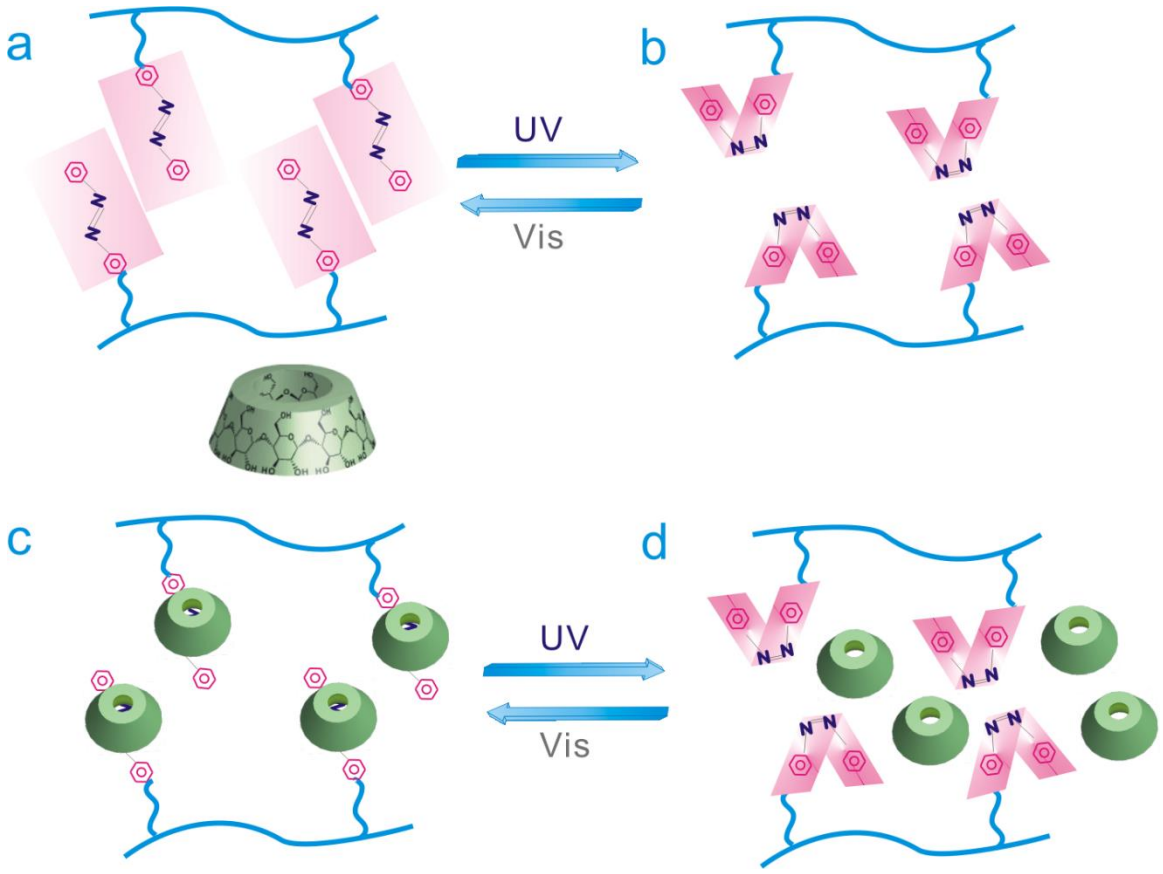

Figure 2-11 Schematic illustration of the supramolecular complexes formed via an α-CD and azobenzene-modified random polymer.[102]

The approach depicted in **Figure 2-11** was realized by our group through using novel azobenzene modified hydroxypropyl methylcellulose (azo-HPMC) to construct supramolecular complexes with α-CD.[102] It was determined by isothermal titration calorimetry that caused α-CD to form stable exothermic inclusion complexes with azo-HPMC with the stoichiometric ratio of 1:1. Our reported study is widely cited in the relevant research community. In the research design, HPMC was selected as a thermo-reversible polymer with a sol-gel transition in aqueous solutions. The other objective was to study the influence of the photo-switchable inclusion complexes on the sol-gel transition of HPMC. The *cis* isomers of azobenzene cannot form inclusion complexes with α-CD. The complexes of α-CD and azo-HPMC with a high degree of azobenzene moieties (DS_{azo}) were expected to undergo a phase separation or precipitation upon UV

irradiation. Surprisingly, they remained water-soluble after UV irradiation in our experiments. It could be explained by the fact that the *cis* isomers were less hydrophobic and only partially transformed from the *trans* isomers. The balance of the hydrophilic-hydrophobic interactions was intact under UV irradiation. The effect of temperature towards the sol-gel transition behaviour of azo-HPMC and their complexes with α-CD was also investigated. The sol-gel transition behaviour was confirmed to be reversibly regulated via photo-irradiation. The temperature of gelation increased after UV irradiation (e.g., azo-HPMC3, from 26.5 °C to.36.5 °C) without α-CD. The temperature decreased after UV irradiation (e.g., azo-HPMC3, from 57 °C to 49 °C) with α-CD. DS_{azo} in azo-HPMC polymers and the α-CD concentration in the solution are important parameters that affect the reversible photo-regulation of the sol-gel transition.

The above-mentioned systems have pointed out the great opportunity in studying azobenzene-based polymers. Other more simplistic model polymers, apart from random copolymers and di-block copolymers, are interesting candidates for studying the photo-switchable behaviour of azobenzene-based materials. In this study, end-capped lipid-like azobenzene-based polymers were chosen as the model system to further investigate the mechanism of the photo-driven behaviour of azobenzene-based polymers and materials.

2.5 Summary

In this chapter, the literature review underlines the importance and potential application of the research on biomimetic smart materials, biomimetic self-assembled materials, and self-assemblies from photo-sensitive polymers. There are many interesting physical and chemical phenomena left to be investigated and utilized for construction of novel reversible photo-responsive polymer systems. These systems have great potential for

various biological applications that require biocompatibility such as bio-sensors, bio-electronics, and drug delivery.

3 RESEARCH METHODOLOGY AND EXPERIMENT PROCEDURES

3.1 Materials

Chemicals used in the experiments were obtained from Sigma-Aldrich unless otherwise specified. Three different azobenzene derivatives (4'-substituted-4-hydroxyl azobenzene, i.e., R-Azo-OH, where the R group can be H-, CN- or C_4H_9O-) were obtained from Dr. Yu Hui (graduated co-worker). Poly(ethylene glycol) methyl ether with an average molecular weight of 5000 (**MeO-PEG 5000**) and poly(ethylene glycol) with an average molecular weight of 4600 (**PEG 4600**) were purchased from Sigma-Aldrich. Other PEGs were purchased from Polymer Source, Inc. They are **PEG 2100** (P4793-EG2OH, Mn 2100, PDI 1.04), **PEG 9800** (P4789-EG2OH, Mn 9800, PDI 1.04), and four-arm PEGs (for details: four-arm poly(ethylene oxide) hydroxy terminated, pentaerythritol core) including **PEG_{4ARM} 6700** (P1638-4EOOH, Mn 6700, PDI 1.14), **PEG_{4ARM} 10000** (P5474-4EOOH, Mn 10000, PDI 1.08), **PEG_{4ARM} 20000** (P8522-4EOOH, Mn 19000, PDI 1.09). The PEGs was dried by azeotropic distillation with toluene. 2-bromo-2-methylpropionyl bromide (Aldrich, 98%) and 4-(Dimethylamino)-pyridine (DMAP) (Aldrich, 99%) were used without further purification. Triethylamine (Aldrich, A.R. grade) was first refluxed using KOH and then distilled. Methylene dichloride (CH_2Cl_2) (Aldrich, A.R. grade) was first mixed with portions of concentrated sulfuric acid and shaken until the acid layer was colourless. CH_2Cl_2 was further washed by (i) water, (ii) 5% $NaHCO_3$ aqueous solution, and (iii) water again. The final step for the CH_2Cl_2 was distillation from CaH_2. There was no further purification for all the other chemicals (including solvents and reagents).

3.2 Synthesis of azobenzene based PEG (azo-PEGs)

3.2.1 Synthesis of bromine terminated polyethylene glycol (Br-PEG-Br)

Bromine terminated polyethylene glycol (**Br-PEG-OMe, Br-PEG-Br or Br_4-PEG_{4ARM}**) was prepared using the method reported by Jankova *et al.*[161] The experimental procedures described below take **Br-(PEG 4600)-Br** prepared from **PEG 4600** (PDI 1.06) as an example. The solution of 10 mL of dry THF, 0.45 mL of triethylamine, 0.5395 mmol **PEG 4600** was prepared in a three-necked, round-bottom flask (50 mL). It was equipped with a condenser, a magnetic stirrer, a gas inlet/outlet and a dropping funnel. After cooling to 0 °C, 3.24 mmol 2-bromoisobutyryl bromide (99 %) in THF (10 mL) was added drop-wise under nitrogen flow and gently stirred at 0 °C for an hour. The solution temperature was subsequently raised to 25 °C. The reaction continued for 24 hours under stirring at 25 °C. Then the solution was reduced to about 2 mL. Then it was precipitated in 40 mL cold ether. The synthesized product was obtained after precipitating into cold ether. It was then filtered, washed by ether, and dried under vacuum overnight. The synthesis yield was 93.1 wt % (2.51 g). The ^{1}H NMR spectra in $CDCl_3$ were recorded by a Bruker DMX-400 spectrometer: 4.35 ppm (t) (-OCH_2CH_2-OC=O), 3.66 ppm (s) (-OCH_2CH_2-)$_n$, 1.97 ppm (s) (-CH_3).[162]

3.2.2 Synthesis of azobenzene-based PEGs

In this second step, the azobenzene derivatives substituted with different groups were covalently incorporated in the chain ends of the PEG by an etherification with hydroxy-terminated azobenzene containing selected substituents with bromine-terminated PEGs synthesized in first step. The synthetic route of azobenzene-based PEGs (azo-PEGs) is outlined in **Figure 3-1**. Taking the synthesis of **(C_4H_9O-Azo)$_2$-PEG 4600** for example, 2.5 g of **Br-(PEG 4600)-Br** in 20 mL DMSO was placed in a round-bottomed flask (50

mL) and reacted under stirring overnight at 50 °C with an excess amount of R-Azo-OH. The details for the excess amount of R-Azo-OH were as follows: for synthesis of one end-capped azobenzene-based polymer, the molar ratio was kept at 1.2:1 (R-Azo-OH to MeO-PEG-Br), for synthesis of two end-capped azobenzene-based polymers, the molar ratio was kept at 2.1:1 (R-Azo-OH to Br-PEG-Br), for synthesis of azobenzene-based four-arm star polymers, the molar ratio was kept at 4.2:1 (R-Azo-OH to Br_4-PEG). After the solvent was removed by rotary evaporation, methanol (5 mL) was added. The mixture was poured into 100 mL ether for precipitation. The precipitate was washed by hexane after filtration. The product was prepared after drying under vacuum at 25 °C. The yield was 75 % for C_4H_9O-Azo-PEG 5000-OMe, 79 % for $(C_4H_9O\text{-Azo})_2$-PEG 2150, 84 wt % for $(H\text{-Azo})_2$-PEG 4600, 81 wt % for $(CN\text{-Azo})_2$-PEG 4600, 68 wt % for $(C_4H_9O\text{-Azo})_2$-PEG 4600, 61 wt % for $(C_4H_9O\text{-Azo})_2$-PEG 9800, 69 wt % for $(C_4H_9O\text{-Azo})_4$-PEG 6700, 63 wt % for $(C_4H_9O\text{-Azo})_4$-PEG 10000, and 64 wt % for $(C_4H_9O\text{-Azo})_4$-PEG 20000. The chemical structure of the synthesized product was confirmed by ^1H NMR spectra in $CDCl_3$. Gel permeation chromatography (GPC) was used to measure the weight-average molar mass (M_W) and polydispersity index (PDI).

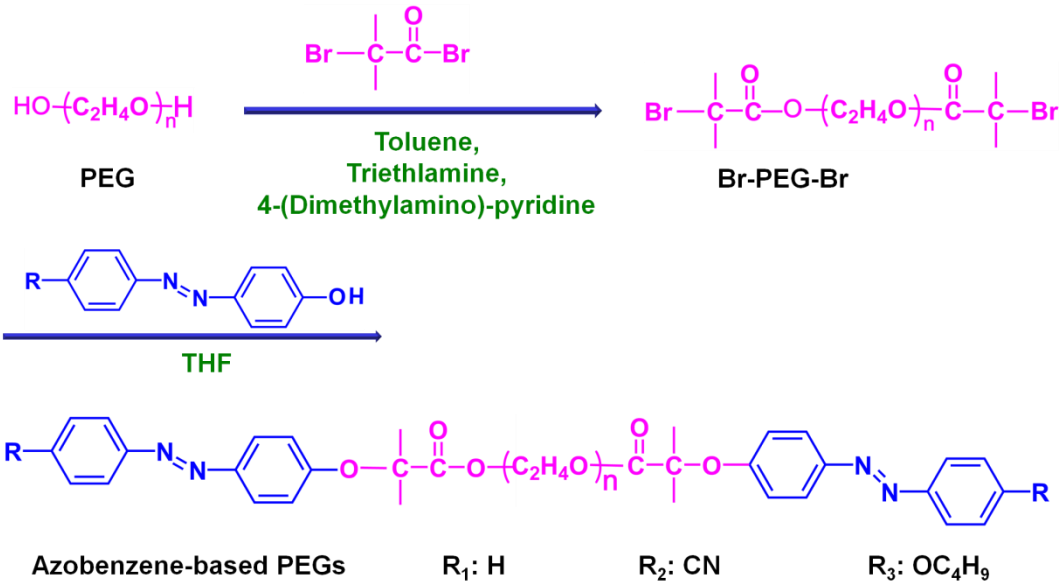

Figure 3-1 The representative synthesis routes of azo-PEGs. Taking the synthesis of the linear polymer (R-Azo)$_2$-PEG 4600 with three different R groups as example, the synthesis produces (H-Azo)$_2$-PEG 4600, (CN-Azo)$_2$-PEG 4600 and (C_4H_9O-Azo)$_2$-PEG 4600.

3.3 Preparation of self-assemblies from azo-PEGs

The self-assemblies in aqueous solutions were prepared by dissolution of the required amount of azo-PEGs in deionized water (DI water, Millipore Q, 18.2 MΩ cm) with vigorous stirring.

The self-assemblies in the mixed solvent were prepared as follows: (i) the required amount of polymer azo-PEGs were first dissolved in DI water. (ii) the aqueous solution of azo-PEGs were mixed under gentle stirring for 24 hours until complete dissolved. (iii) azo-PEGs self-assemblies were prepared by adding a predetermined amount of tetrahydrofuran (THF) into the azo-PEGs aqueous solutions (**Figure 3-2**).

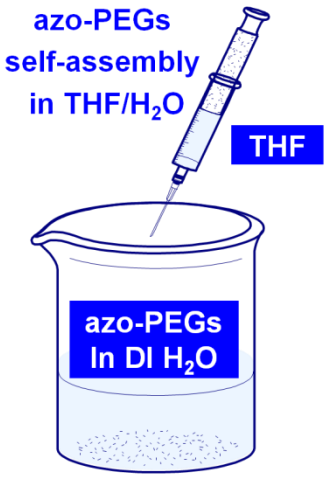

Figure 3-2 Illustration of the procedure to prepare the azo-PEGs vesicles in the mixed solvent via self-assembly. The amphiphilic azo-PEG polymers were first dissolved in DI water. After adding tetrahydrofuran (THF) drop by drop, the azo-PEGs self-assembled into vesicles.

3.4 *Trans-cis* Photo-isomerization

Photo-irradiation was carried out with a 500 W Hg ARC lamp (Oriel, model 68910) at room temperature in a dark room. UV and visible light were isolated by 370 nm and 410 nm interference filters, respectively. The irradiation power density was 0.8 mW/cm^2. Before characterization, all *trans* or dark-adapted samples ($\mathbf{S_{VIS}}$) were prepared after visible light (λ=410 nm) irradiation for 30 mins. Then the irradiated sample was kept in the dark as long as 72 hours. This made certain that all the azobenzene chromophores were in the *trans*-state. UV-irradiated samples were prepared under UV light (λ=370 nm) irradiation until the photo-stationary state, $\mathbf{S_{UV}}$, was reached. All measurements were repeated three times to ensure good reproducibility. Azobenzene moieties undergo *trans-cis* photo-isomerization under UV light irradiation. During the irradiation of UV light, the π-π* absorption of the *trans*-azobenzene gradually decreases. The n-π* absorption of the *cis*-azobenzene increases at the same time. The *cis* fraction ($\boldsymbol{f_z}$) at the photo-stationary state can be calculated using a method developed by Fischer.[163]

3.5 Characterizations

3.5.1 ^{1}H Nuclear Magnetic Resonance (^{1}H NMR)

The ^{1}H NMR spectra of the azo-PEGs were characterized using a Bruker DRX 300 instrument, with $CDCl_3$, D_2O, THF-*d8*, D_2O/THF-*d8*, H_2O/THF-*d8*, or D_2O/THF as solvents at 25 °C. The chemical compositions of the azo-PEGs were determined from ^{1}H NMR spectra in $CDCl_3$. The confirmation of the vesicle structure of the azo-PEGs self-assemblies was investigated by mixed deuterated solvents of water and THF.

3.5.2 Gel Permeation Chromatography (GPC)

GPC was done using an Agilent 1100 series GPC system with a LC pump, PLgel 5 MIXED-C column and RI detector. GPC determined the azo-PEGs molecular weights and molecular weight distributions. The GPC column was calibrated using Agilent EasiCal polystyrene standards having a narrow molecular weight distribution. THF (HPLC grade) was used as the mobile phase. It contained 1 % triethylamine, 2, 6-di-tert-butyl-4-methylphenol (BHT) was used as the stablizer. The flow rate was 1.0 mL/min.

3.5.3 UV-visible absorption spectroscopy

UV-visible absorption spectra were characterized by a Shimadzu UV-visible Spectrophotometer (UV-2501PC). The error of UV absorbance was within ± 0.001.

Calculation of *cis* fraction (f_z) at the photo-stationary state based on UV-visible absorption spectroscopy

When azobenzene is irradiated with any wavelength absorbed by both *trans* and *cis* isomers, a photo-stationary state will be established eventually.

$$Trans \underset{\phi_{Cis}}{\overset{\phi_{Trans}}{\rightleftharpoons}} Cis \qquad \textbf{(3.1)}$$

Where ϕ_{Trans} is the quantum yield of the *trans-to-cis* photo-isomerization. It is induced by irradiation of UV light. ϕ_{Cis} is the quantum yield of the *cis-to-trans* isomerization caused by irradiation of visible light.

Denote the extent of conversion of *trans-to-cis* at any particular wavelength λ of irradiation by α, the concentration ratio of *tran*-state/*cis*-state at a photo-stationary state, i.e., [*Trans*] and [*Cis*] can be expressed as **equation 3.2**:

$$\left(\frac{[Trans]}{[Cis]}\right)_{\lambda} = \left(\frac{1-\alpha}{\alpha}\right)_{\lambda} \qquad \textbf{(3.2)}$$

At a photo-stationary state attained with light at a certain wavelength λ, the concentration ratio of the *trans* isomer and *cis* isomer can be described by **equation 3.3**[163]

$$\left(\frac{[Trans]}{[Cis]}\right)_{\lambda} = \left(\frac{\phi_{Cis}}{\phi_{Trans}}\right)_{\lambda}\left(\frac{\varepsilon_{Cis}}{\varepsilon_{Trans}}\right)_{\lambda} = \left(\frac{\phi_{Cis}}{\phi_{Trans}}\right)_{\lambda}\left(\frac{A_{Cis}}{A_{Trans}}\right)_{\lambda} \qquad \textbf{(3.3)}$$

where A_{Trans} and A_{Cis} are the absorbance of a similar solution containing only the *trans* and *cis* isomers, respectively, i.e., the equilibrium of the *trans-to-cis* is shifted completely toward either the *trans* isomer or the *cis* isomer. ε_{Trans} and ε_{Cis} are the extinction coefficients of the *trans*-azobenzene and *cis*-azobenzene. $\varepsilon_{Trans}/\varepsilon_{Cis}$ can be calculated via the method reported by Fischer.[163]

In our study, under UV irradiation, the *cis* fraction increases quickly with increasing irradiation time within the first several minutes and reaches a plateau at a longer times, indicating that the photo-stationary state is reached. Upon irradiation at 370 nm, the

duration needed to reach the photo-stationary state is different for azo-PEGs with different end functional groups. The fraction of *cis* isomers (***f*****z**) can be determined from the **equation 3.4**:

$$f_z(t)=\left(\frac{[Trans]_t}{[Cis]_0}\right)_\lambda=\left(\frac{1\text{-}A_t/A_0}{1\text{-}\varepsilon_{Cis}/\varepsilon_{Trans}}\right)_\lambda \quad (\mathbf{3.4})$$

Where A_0 is the initial absorbance with all *trans*-isomers present at wavelength λ, and A_t is the absorbance of the *trans*-isomers at time *t*. The $\varepsilon_{Cis}/\varepsilon_{Trans}$ ratio for the azobenzene moieties in the present study is determined to be 0.05. This value is in agreement with reported values of 0.05 for azobenzene itself[164] and 0.055 for amphiphilic polyelectrolytes containing azobenzene moieties.[165]

3.5.4 Laser light scattering (LLS)

Dynamic light scattering (DLS) is used for the measurements of the scattering intensity. The normalized second-order autocorrelation function $G^{(2)}(t, \theta)$ can be calsulated by **equation 3.5**:[166,167]

$$G^{(2)}(t,\theta)=A[1+\beta\left|G^{(1)}(t,\theta)\right|^2] \quad (\mathbf{3.5})$$

Where *A* is the baseline, β is a parameter of the optical system (constant between 0-1), and *t* is the delay time. $G^{(1)}(t)$ is analyzed afterwards in terms of a continuous sum of exponential decays as **indicated by equation 3.6**:

$$G^{(1)}(t,\theta)=\int_0^\infty G(\Gamma)e^{-\Gamma t}d\Gamma \quad (\mathbf{3.6})$$

Where $G(\Gamma)$ is the distribution of decay rates Γ.

For block copolymers in mixed solvents, it is found that **equation 3.6** can be appropriately replaced by a discrete sum of single-exponential functions, each of them being characterized by a decay rate Γ.[168]

The decay rate (Γ) is proportional to the square of the scattering vector (q^2) (see **equation 3.7**). The distribution function affects the translation diffusion coefficient D of the scattering objects.

$$\Gamma = Dq^2 \qquad (\mathbf{3.7})$$

Where q is the magnitude of the scattering vector; it is the wave vector difference between the incident and the scattered light at a particular scattering angle θ. q is given by **equation 3.8**:

$$q = \frac{4\pi n}{\lambda} sin\frac{\theta}{2} \qquad (\mathbf{3.8})$$

Where n, θ and λ are the refractive index of the scattering, the refractive index of the solution, and the wavelength of the incident light, respectively.

For the DLS, the apparent hydrodynamic radius (R_h) can be calculated using the **Stokes-Einstein equation 3.9**:

$$R_h = K_b T / 6\pi\eta D_0 \qquad (\mathbf{3.9})$$

Where K_b is the Boltzmann constant, T is the absolute temperature, and D is the translational diffusion coefficient. For very dilute solutions, D is approximated to be D_0.[169] η is the solvent viscosity. For the selected samples in this study, the viscosity of the water/THF mixtures at 25 °C was extrapolated from the viscosities of the pure systems, η_{water} is 0.89 mPa·s and η_{THF} is 0.46 mPa·s.[170]

Static light scattering (SLS) is a technique to measure the intensity of the scattered light to obtain the average molecular weight M_W of a macromolecule like a polymer or a protein. In the SLS measurement, the angular dependence of the excess absolute time-averaged scattered intensity of a very dilute dispersion can lead to the root-mean square radius of gyration, which is also called the radius of gyration R_g. The values of R_g/R_h ratio can give us information about the morphology of the aggregates. Theoretically, the ratios of R_g/R_h are 0.774, 1.0, and 1.5-1.8 for a uniform solid sphere, a thin shell vesicle and a random coil respectively.[80]

A Zimm plot is a diagrammatic representation of data on scattering from large particles, corresponding to the Zimm equation (**equation 3.10**)

$$\frac{KC}{R(\theta)}=\left(\frac{1}{M_W}+2A_2C\right)\left(1+\frac{16\pi^2}{3\lambda^2}\langle R_g^2\rangle sin^2\frac{\theta}{2}\right) \quad \textbf{(3.10)}$$

Where K is an optical constant ($K=4\pi^2n^2(dn/dC)^2/N_A\lambda^4$, in which n is the refractive index of the solvent; dn/dC is the refractive index increment of polymer solution; N_A is Avogadro's constant, and λ is the wavelength of laser light.); $R(\theta)$ is the Rayleigh ratio at scattering angle θ; C is the concentration of the polymer solution; R_g is the radius of gyration; A_2 is the second virial coefficient, and M_W is the weight-average molecular weight.

For SLS, a set of light scattering experiments consists of measure $KC/R(\theta)$ for various concentrations and at various scattering angles. To get M_W, we can do a double extrapolation to zero angle and zero concentration. In the simplest form, the Zimm equation is reduced to **equation 3.11**:

$$\frac{KC}{R(\theta)}(\theta\to 0, C\to 0)=\frac{1}{M_W} \quad \textbf{(3.11)}$$

In detail, we first plot KC/R(θ) as a function of $\sin^2(\theta/2)$ at constant C gives a straight line with the following slope and intercept:

$$\text{slope}=(\frac{1}{M_W}+2A_2C)\frac{16\pi^2}{3\lambda^2}<R_g^2> \quad \textbf{(3.12)}$$

$$\text{intercept}=\frac{1}{M_W}+2A_2C \quad \textbf{(3.13)}$$

Next we plot the intercepts of the first plots (**equation 3.13**) as a function of concentration. The resulting plot should be a straight line with

$$\text{intercept}=\frac{1}{M_W} \quad \textbf{(3.14)}$$

The scattered intensity can be plotted as a function of the angle to give information on the R_g which can simply be calculated using the Guinier approximation as follows:

$$\ln(R(\theta))=1-(\frac{R_g^2}{3})q^2 \quad \textbf{(3.15)}$$

where $q=4\pi n_0\sin(\theta/2)/\lambda$. Hence a plot of the corrected Rayleigh ratio (R(θ)) vs $\sin^2(\theta/2)$ or q^2 will yield a slope $R_g^2/3$. However, this approximation is only true for $qR_g < 1$.

DLS and SLS experiments were done using a Brookhaven BI-200SM goniometer system equipped with a 522-channel BI9000AT digital multiple **τ** correlator. The light source was a power-adjustable argon ion laser with a wavelength of 488 nm or 632.8 nm. A PolyScience water bath was used for temperature control. The inverse Laplace transform of REPES (Regularized Positive Exponential Sum Program) in the Gendist software package was used to analyze the time correlation functions with the probability of reject setting at 0.5. Deionized water (DI water) was purified using 0.22 μm filters in a Millipore Alpha-Q purification system. The DLS was operated in the dilute regime in

order to minimize the effects of interactions on the diffusion coefficients. All measurements were repeated three times to ensure good reproducibility.

For DLS, the measurement angle was 90° and 3 min of correlation measurement was used. The cumulant analysis and CONTIN routes (a general-purpose constrained regularization method for continuous distributions, such as inverse Laplace transforms in relaxation studies and in dynamic light scattering) were used to fit the distribution averages and particle size distribution. All data were averaged over three repeated measurements.

For SLS, the instrument was calibrated with toluene first. This was to ensure that the scattering intensity from toluene had no angular dependence in the testing angular range. The sample solutions for light scattering were prepared using the same procedures described earlier for the UV-visible absorption analysis, except that they were filtered through a 0.8 μm filter. The Zimm plot of $(C_4H_9O\text{-}Azo)_2$-PEG 4600 is shown in **Figure A-4**. The Zimm plot of $(C_4H_9O\text{-}Azo)_2$-PEG 2100 is shown in **Figure A-7**. The values of R_g, M_W and the aggregation numbers of $(C_4H_9O\text{-}Azo)_2$-PEG 4600 are summarized (**Table 4-2**). The values of R_g, M_W and the aggregation numbers of $(C_4H_9O\text{-}Azo)_2$-PEG 2100 are summarized in **Table A-1**.

3.5.5 Real-time video observation under optical microscope

For real-time video observation, the suspended vesicle sample was dropped onto a special glass slide (purchased from Electron Microscopy Sciences Inc.). Each slide contained a built-in mini-Petri dish of 7 mm in diameter and 0.1 mm in depth. An inverted optical microscope (Nikon TE2000U) with a ×60 objective (NA=0.7) and a cooled CCD camera was used for the in vitro digital imaging. Both still and video images could be recorded.

Video recording was conducted, while the samples were subject to UV or visible irradiation in situ. The video is provided in an attached file (**Movie S1**).

3.5.6 Atomic force microscopy

Atomic force microscopy (AFM) characterization used a Digital Instrument Dimension 3100 AFM under ambient conditions. It could measure the thickness of the vesicles. The samples were freeze-dried on a silicon substrate. Tests were carried out using the tapping mode with an optical readout and Si cantilevers.

3.5.7 Transmission Electron Microscopy

TEM images were recorded on a JOEL 2010 at 200 kV. The samples for observation were freeze-dried samples. A single drop (~10 μL) of the vesicle solution was placed on a formvar coated copper grid first. The sample was rapidly frozen to the solid phase by projection into a cylindrical vial of liquid nitrogen. The substrates with the frozen samples were put into a freeze-drying flask then. The following freeze-dried process was done using a freeze-drying machine (model: TELSTAR cryodos freeze-drier), with an initial shelf temperature of -70 °C and an ultimate temperature at 25 °C at a pressure of 5 μ bar.

3.5.8 Scanning Electron Microscopy

SEM micrographs of freeze-drying sample on a silicon substrate were recorded at an accelerating voltage of 10KV using a JEOL 6360 scanning electron microscope.

3.5.9 Water Contact Angle

The water contact angle measurement was done to investigate the wettability of the surface. The samples were placed on the platform. A 5 mL syringe was used to push a

liquid droplet onto the tip of the syringe. The water contact angles were measured by dispensing a 2 µL DI water drop on the sample (under $\mathbf{S_{UV}}$ and $\mathbf{S_{VIS}}$) surface using a contact angle measurement system (FTA32, Analytical Technologies). The CCD camera was used to take the photographs of water droplets on the sample surface, showing the contact angle. The contact angle software was used to characterize the average contact angle. It calculated the contact angle of the droplet from both the left and right-hand side.

3.5.10 Surface Tension Measurement

The surface tension test was done to determine the values of the critical micelle concentration (CMC) of azo-PEGs self-assemblies under $\mathbf{S_{VIS}}$ and $\mathbf{S_{UV}}$. The measurement of the surface tension was carried out using a Dataphysics DCAT 21 tensiometer with a Wilhelmy plate. The measured surface tension was plotted against the concentration of the azo-PEGs.

3.5.11 Measurement of Electrolytic Conductivity

The electrolytic conductivity was measured using Metrohm Titrando 905 titration system connected with a conductivity module 856 coupled with a five-ring conductivity measuring cell (c=0.7 cm^{-1} with integrated Pt 1000). The calibration of the conductivity measuring cell used a standard potassium chloride solution with 100 ± 2 µS/cm.

3.5.12 Statistical Analysis of Experimental Replicates

All the measurements for DLS and conductivity test were repeated for at least three times to ensure good reproducibility. Results from replicated experiments were used to

calculate the average values. Standard deviation was also calculated to show the variation from the average values.

4 AZO-PEGS: SYNTHESIS AND THEIR SELF-ASSEMBLY IN THF/WATER MIXED SOLVENT

4.1 Introduction

4.1.1 Photo-driven biomimetic smart materials and their self-assembly

Artificial smart materials responsive to external stimuli are currently drawing considerable attention due to their potential to mimic the highly sophisticated hierarchical structures and novel functions of natural biological systems. In nature, photo-chromic molecules represent the basic molecular triggers in many essential biological photo-receptors. For example, bacteriorhodopsin, as a photo-chromic *trans*-membrane protein, has been demonstrated for photo-pumping of hydrated protons out of cells due to a photo-isomerization from the all-*trans* to 13-*cis* (**Figure 4-1**).[9] The structure resembles that of retinene found in cone-cell for transduction of light into visual signals (**Figure 4-1 b**).

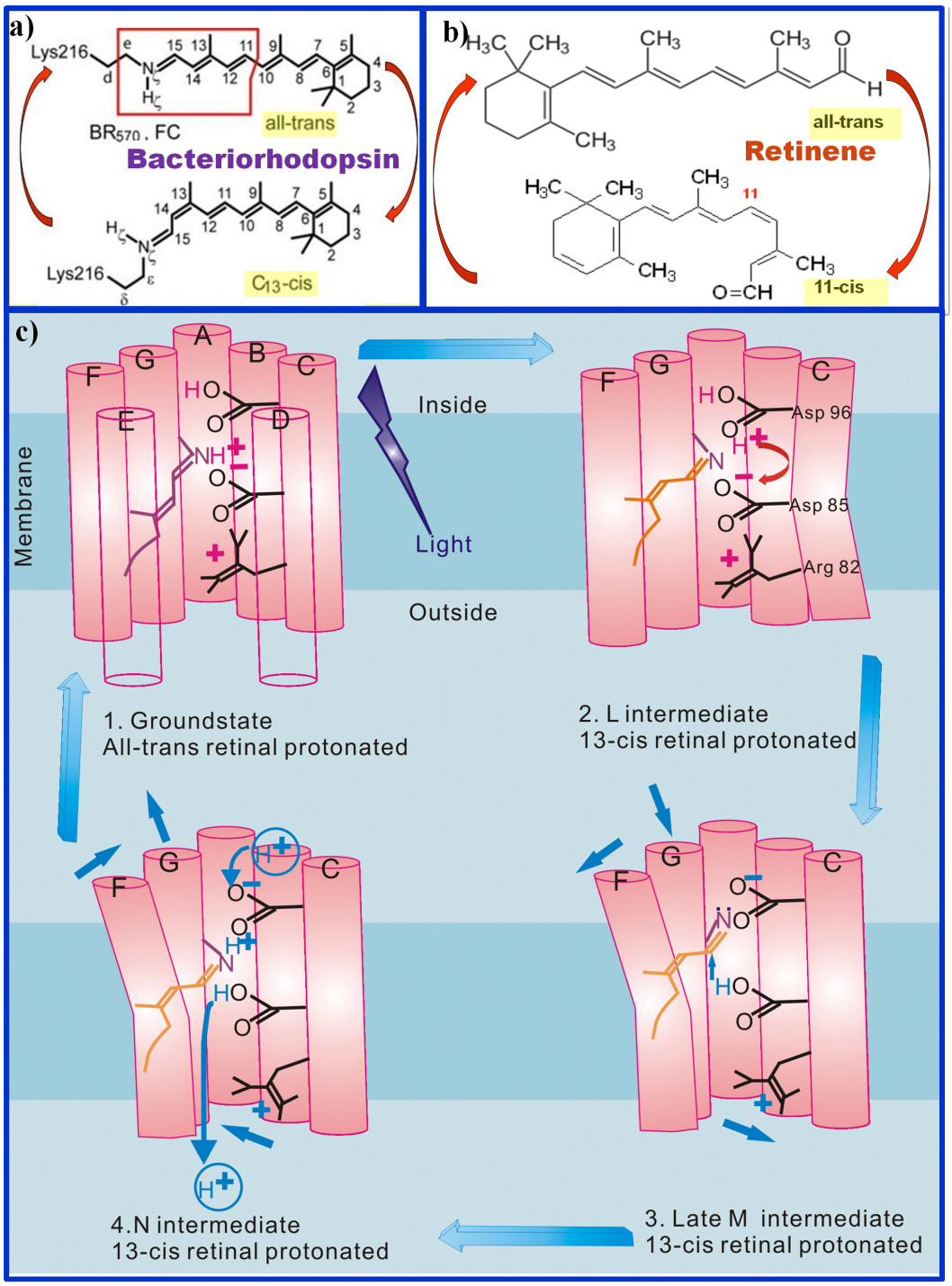

Figure 4-1 The chemical structures of (a) bacteriorhodopsin, and (b) retinene (for comparison), and (c) is the proton (H^+) pumping mechanism at the molecular level in bacteriorhodopsin.[9]

Photo-induced actuation, as an energy-saving, highly responsive and controllable approach, has been used for development of optical materials for medical applications,

functional micro/nano-devices, and even submersible tethered fiber optic cables.[171] Among the various photo-sensitive chromophores, azobenzene derivatives are utilized extensively because of the efficient and reversible *trans-cis* photo-isomerization. Azobenzene derivatives belong to a class of well-studied photo-responsive molecules.[102,130,140,151,152,154,156,172-175] They are able to trigger cascading changes in materials properties at the molecular, micro- to eventually macro-scopic scales depending on the molecular design and supramolecular organization.[159]

Self-assembly of block copolymers with behaviour akin to surfactant assembly has been explosively developed in past two decades. Functional groups are introduced into copolymers to design a self-assembly process triggered by external signals, in other words, to realize 'smart' self-assemblies that respond to light, pH, temperature, and even oxidation. When azobenzene is incorporated into the copolymer building-blocks, a model biomimetic photo-responsive system can be prepared that mimics naturally existing photoreceptors such as bacteriorhodopsin. It would be very interesting and important to combine block copolymer and photo-sensitive materials, i.e., photo-isomerization and self-assembly of azobenzene-based polymers. These smart polymers are very useful for applications in biomedicine, cosmetics, drug delivery, electronics, pollution control, and energy-related fields.

4.1.2 Self-assembly of azo-polymers into vesicles or hollow spheres

In Chapter 2, we have reviewed and discussed the utilization of novel amphiphilic polymers self-assembly to fabricate diverse morphologies. Among various morphologies, vesicles, especially the bilayer vesicles formed via the self-assembled synthetic amphiphiles, have attracted a lot of attention as they resemble the structure of biological

cell membranes. Self-assembled photo-sensitive vesicles utilizing azobenzene-based polymers have also been reported in recent years.

A novel advance involving the use of azobenzene with photo-switchable polarity to design photo-sensitive self-assemblies has been carried out by Liu and Jiang via the classic non-covalent connected micelles (NCCMs) strategy (see the details in Chapter 2 page 18).[174] They first prepared core-shell micelles in toluene by making use of the hydrogen bonding between the carboxyl group (the proton-donor group) end-capped polybutadiene and the pyridyl group (the proton-acceptor group) in poly(4-phenylazo-maleinanil-co-4-vinylpyridine) (AzoMI-VPy). After that, the pyridyl groups with 1,4-diiodobutene were chemically cross-linked. The core of the micelles was formed by AzoMI-VPy. Under visible light, the self-assemblies could swell into vesicles. The vesicles can further turn into micelles under UV-irradiation due to the polarity increase of *cis*-azobenzene. After the realization of photo-switchable self-assemblies from micelles to hollow spheres in toluene, they reported another NCCMs system utilizing the host-guest recognition between cyclodextrin and azobenzene in aqueous solution.[176] The vesicles could undergo photo-switchable self-assembly and disassembly under UV or visible irradiation.

Recently, Zhao *et al.* reported reversible aggregates and disaggregation of self-assembled micelles/vesicles using amphiphilic di-block copolymers i.e., azobenzene-containing polymethacrylate and poly(tert-butyl acrylate) (PAzoMA-b-PtBA) (**Figure 4-2 a**).[140] Zhang *et al.* also reported photo-responsive formation and deformation of giant micro-vesicles from poly(acrylic acid) and poly{6-[4-(4-methylphenylazo)-phenoxy]hexyl acrylate} based di-block copolymers (PAA-block-PAzoM) in H_2O/THF mixture (**Figure 4-2 b**).[177] Matthieu Bedar *et al.* fabricated micron-sized hollow capsules via layer-by-layer deposition of an azobenzene-containing polyelectrolyte.[178] The photo-responsive

capsule can experience photo-induced shrinkage under UV-irradiation (**Figure 4-2 c**). Han *et al.* also succeeded in achieving self-assembled micron-size vesicles of an azopyridine-containing copolymer in H_2O/THF mixture. The vesicles can increase 17 % in volume under UV-irradiation (**Figure 4-2 d**).[179]

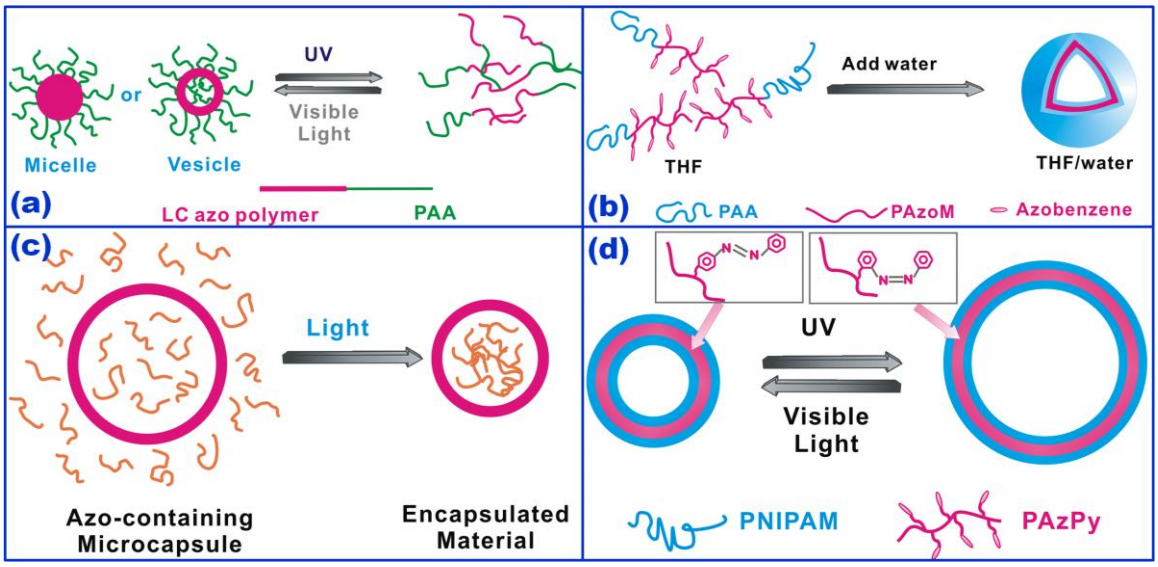

Figure 4-2 Representative examples of photo-sensitive vesicles via self-assembly of azobenzene-containing polymers: (1) Reversible changes of self-assembled aggregates (micelles or vesicles) from PAzoMA-b-PtBA.[140] (2) Photo-responsive formation and deformation of giant micro-vesicles of PAA-block-PAzoM in a H_2O/THF mixture.[177] (3) Photo-sensitive micron-sized hollow capsules.[178] (4) Micron-size vesicles increased 17 % in volume under UV-irradiation.[179]

4.1.3 Scope and objectives

It is of importance to study photo-sensitive azobenzene-based polymers, especially bilayer vesicles that are promising in bio-engineering and biomedical applications. The previously reported material systems provide convincing evidence on the versatility and functions of vesicle structure obtained via self-assembly of azobenzene-containing polymers. However, the limitations of these material systems for practical applications arise from the usually required use of an organic solvent (e.g., toluene[174]), the

disintegration of self-assemblies under repetitive UV-irradiation, the extremely large size (e.g., ~5μm[178]), and the relatively small volume change (e.g., 17%[179]). A more robust vesicle with a larger size/volume change under UV-irradiation is worthwhile and necessary for advanced applications such as nano-biophotonics, reversible encapsulation, and stochastic sensing.

In this part of the project, three kinds of azo-Poly (ethylene glycol) (azo-PEGs) with different end-capping terminal substituents were first synthesized. The end-capped azo-PEGs were selected due to their better-defined structures than those of block copolymers or complex dendrimers. The self-assembly behaviour of azobenzene-based polymers in mixed solvents was then studied. The representative and simplistic molecular design allows not only a more regular self-assembly, but also an easier understanding of the mechanisms involved in the observed changes. Lastly, the photo-switching properties of the self-assemblies under UV-visible light irradiation were investigated.

4.2 Results and Discussion

4.2.1 Synthesis of azo-PEGs

Poly (ethylene glycol) (PEG), as a polyelectrolyte, was selected as the main chain segment in this study. It possesses good thermal stability, favourable self-assembly properties, good aqueous solubility, and ability to improve the dispersion stability of small particles. In additional, PEG is a biocompatible polymer that exhibits no cell-toxicity. In this work, azobenzene derivatives substituted with different types of photo-sensitive groups were chosen as functional segments to be covalently incorporated in both chain ends of PEG (denoted as azo-PEGs in this thesis). The azo-PEGs were synthesized via esterification between PEG and 2-bromo-2-methylpropionyl bromide, followed by

etherification of first-step product with hydroxyl-terminated azobenzene containing substituents. The chemical structures of azo-PEGs were analyzed by GPC and ^{1}H NMR. From GPC analysis, the end functionalized PEG polymer possessed a narrow uni-modal peak. The weight-average molar mass (M_W) and polydispersity index (PDI) of each azo-PEG are as follows: (H-Azo)$_2$-PEG, M_W 7689 g/mol, PDI 1.039. (CN-Azo)$_2$-PEG, M_W 7748 g/mol, PDI 1.045. (C_4H_9O-Azo)$_2$-PEG, M_W 7932 g/mol, PDI 1.040. The structure of the synthesized polymers was confirmed by ^{1}H NMR spectroscopy. Figures (**Figure A-1** to **Figure A-3)** show the ^{1}H NMR spectra of three different azo-PEGs in $CDCl_3$. The chemical shift peaks at 7.6 and 8.0 ppm, which are assigned to the hydrogen on the azobenzene ring, clearly show the existence of azobenzene groups in the azo-PEGs. So far, highly mono-dispersed azo-PEGs with three different azobenzene derivatives have been prepared.

4.2.2 Self-assembly of azo-PEGs vesicles in THF/water mixture

(C_4H_9O-Azo)$_2$-PEG (M_W 7932 g/mol, PDI 1.040) was chosen in the study of the self-assembly behaviour of azo-PEGs. All of the following procedures were carried out inside the dark room. The self-assembly process was triggered by adding THF into an aqueous solution of (C_4H_9O-Azo)$_2$-PEG. This method is one of the major strategies used for achieving block copolymer self-assemblies, by changing the ratio of the selective solvents for the constituent blocks. The volume ratio of THF/water was varied within 1:10 to 1:1 (see **Table 4-1**). The size of the vesicle was measured by Dynamic Light Scattering (DLS). Furthermore, the stability of the vesicles was checked by using DLS to re-test the samples after 1 month. The results of the DLS measurement are included in **Table 4-1**. The mono-dispersed vesicles formed when the water content was fixed at 80 vol%. For further studies, 1:4 of THF/water volume ratio was selected since it gave stable vesicles

with a narrow size distribution. This property is suitable for applications related to cargo encapsulation and release.

Table 4-1 DLS results showing the self-assembly behaviour for (C_4H_9O-Azo)$_2$-PEG in THF/water mixed solvent under conditions of different THF/water volume ratios (values are mean ± standard deviation).

THF / water	1:10	1:9	1:8	1:7	1:6	1:5	1:4	1:3	1:2	1:1
DLS test done on the 1st day when the vesicles were prepared										
D_h(nm)	239 ±15	273 ±16	262 ±50	405 ±22	432 ±32	545 ±29	501 ±9	538 ±154	618 ±112	1003 ±68
PDI	0.13 ±0.1	0.15 ±0.02	0.16 ±0.1	0.13 ±0.05	0.11 ±0.05	0.07 ±0.05	0.05 ±0.01	0.1 ±0.1	0.14 ±0.1	0.3 ±0.1
DLS test done 30 days after the vesicles were prepared										
D_h(nm)	201 ±28	248 ±26	217 ±25	608 ±32	502 ±27	580 ±25	524 ±8	675 ±52	754 ±42	1415 ±210
PDI	0.22 ±0.1	0.21 ±0.1	0.24 ±0.05	0.25 ±0.1	0.26 ±0.1	0.19 ±0.05	0.14 ±0.05	0.15 ±0.1	0.27 ±0.1	0.33 ±0.2

*****The volume ratio of 1:4 was selected for further investigations.

4.2.3 *Trans-cis* photo-isomerization of azobenzene derivatives and azo-PEGs by UV-visible absorption spectroscopy

Azobenzene moieties undergo reversible *trans-cis* photo-isomerization upon UV or visible light irradiation. After irradiation with UV light, azobenzene moieties undergo *trans-cis* photo-isomerization, resulting in the gradual decrease of π-π* absorption of the *trans* isomers at 360 nm, as well as a gradual decrease of the n-π* absorption of the *cis* isomers at 430 nm. UV-visible absorption spectroscopy characterized the light irradiation effect based on the absorbance change of the solutions. **Figure 4-3** to **Figure 4-5** show the UV-visible absorbance of the azobenzene derivative, which is only soluble in THF (i.e., 4-hydroxy-4'-butoxyazobenzene), together with the azo-PEGs (i.e., C_4H_9O-Azo)$_2$-PEG) in aqueous and THF solution, respectively.

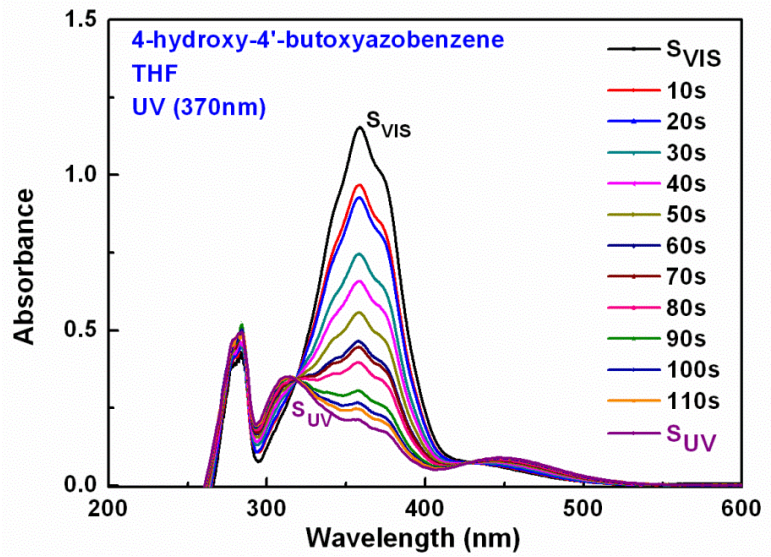

Figure 4-3 Time-dependent absorbance change showing the photo-isomerization of 4-hydroxy-4'-butoxyazobenzene (0.06 mg/mL) under UV irradiation.

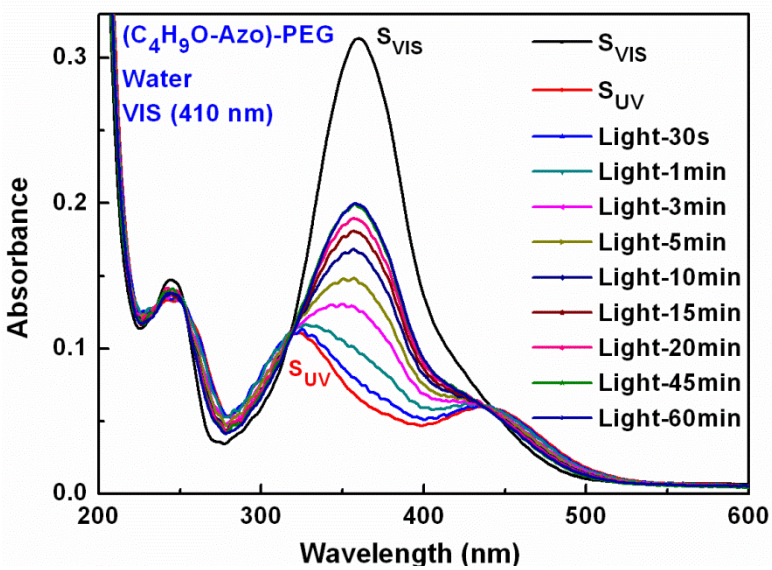

Figure 4-4 The UV-visible absorption spectra showing photo-isomerization from *cis*-to-*trans* states of $(C_4H_9O\text{-}Azo)_2$-PEG in aqueous solution under S_{UV} or light irradiation (410 nm filter) with a concentration of 0.3 mg/mL. The measurement started from the S_{UV} condition (bottom-most red curve); the absorption peak at around 360 nm increased in intensity with the duration of visible light irradiation.

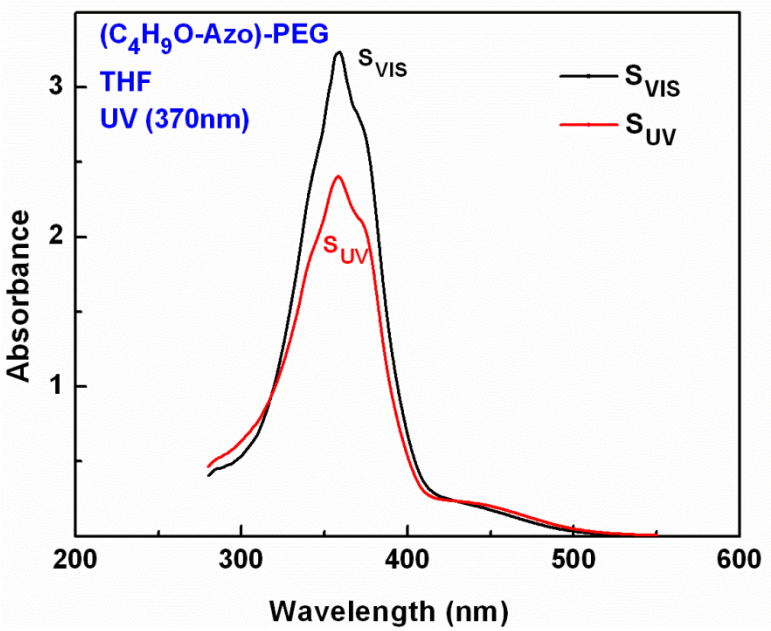

Figure 4-5 The UV-visible absorption spectra showing photo-isomerization from the *cis*-to-*trans* states of $(C_4H_9O\text{-}Azo)_2$-PEG THF solution under UV irradiation. Polymer concentration is 0.75 mg/mL.

The 4-hydroxy-4'-butoxyazobenzene in THF possesses a strong absorption peak at 359 nm and a weaker peak at 451 nm. The peaks are assigned to the π-π^* transition of the *trans* isomers of the azobenzene chromophore and the n-π^* transition of the *cis* isomers, respectively (**Figure 4-3**). Upon UV light irradiation, the azobenzene derivative showed *trans*-*cis* photo-isomerization. With an increase in the of UV-irradiation time, the intensity of the absorption peak at 359 nm progressively decreased until an equilibrium state was reached. The weaker peak at 451 nm was more pronounced at the same time. Moreover, it was also noted that the absorbance peak at 359 nm due to the π-π^* transition (*trans*-state) shifted to 315 nm with increased irradiation time. This blue shift is believed to be caused by two factors: (i) the decrease in the solvent polarity, also called the solvatochromic effect[180,181], and (ii) H-aggregation of the azobenzene groups through non-covalent aromatic-aromatic interactions. When azobenzene chromophores with a dipole moment are brought in close contact inside an ordered structure, excitation energy

levels splitting occurs. Consequently the absorption peak shifts consequently. This observation depends on the mutual orientation of the interacting dipole moments. When the dipole moments of azobenzene in the aggregates are parallel, a hypsochromic (blue) shift happens. H-aggregates have been reported by many researchers to have formed in azobenzene amphiphiles and polymers both in aqueous solution[182] and in aggregation form, e.g., micelles,[154] vesicles,[183] bilayers[184] or membranes.[185] By contrast, if the transition dipoles are in line (rather than parallel), the spectra exhibited a bathochromic (red) shift and the aggregates are, in this case, termed as J-aggregates.[186] In our case, when 4-hydroxy-4'-butoxyazobenzene was incorporated into the PEG, a blue shift was also noted in aqueous $(C_4H_9O\text{-}Azo)_2$-PEG solution under 370 nm UV-irradiation (**Figure 4-4**). The absorption peak intensity at 360 nm in *trans*-state decreased and shifted to 318 nm with increased UV-irradiation time. However, this shift was not observed in the absorption study done on $(C_4H_9O\text{-}Azo)_2$-PEG in THF (**Figure 4-5**), possibly due to the fast recovery.

Upon visible light irradiation, $(C_4H_9O\text{-}Azo)_2$-PEG experiences *cis* to *trans* photo-isomerization. In **Figure 4-4**, the intensity of the π-π* absorption peak of the *trans*-azobenzene moieties gradually increased. Meanwhile, the n-π* absorption of the *cis*-azobenzene moieties decreases. These observations showed a partial back-conversion of the absorption spectra.

4.2.4 Photo-driven pulsating behaviour of self-assembled azo-PEGs vesicles

4.2.4.1 Photo-driven size change of self-assembled vesicles

The size change of the self-assemblies under UV irradiation was studied by DLS. DLS results indicate a mean hydrodynamic diameter (D_h) of 510 nm (PDI<0.1) for the $(C_4H_9O\text{-}Azo)_2$-PEG self-assemblies in water/THF (4:1 volume ratio) for the photo-

stationary state upon visible light irradiation ($\mathbf{S_{VIS}}$). 15 min of UV irradiation was employed for the sample to ensure the completion of the *trans-cis* photo-isomerization. For the DLS on the self-assembly sizes in $\mathbf{S_{UV}}$, the dark-adapted samples would be first irradiated by 370 nm UV light, and DLS characterization would be done with the UV lamp turned off.

The measured size change was initially assumed to be related to the reversible cycle of disaggregation and reaggregation of self-assemblies. However, this assumption was ruled out by further measurement of the critical micellar concentration (CMC) values for $(C_4H_9O\text{-Azo})_2$-PEG self-assemblies (**Figure 4-6)**. The self-assemblies displayed the same CMC values under either visible light or UV light irradiation. This result clearly demonstrated that the remarkable decrease of the diameter was not caused by the disaggregation of the self-assemblies.

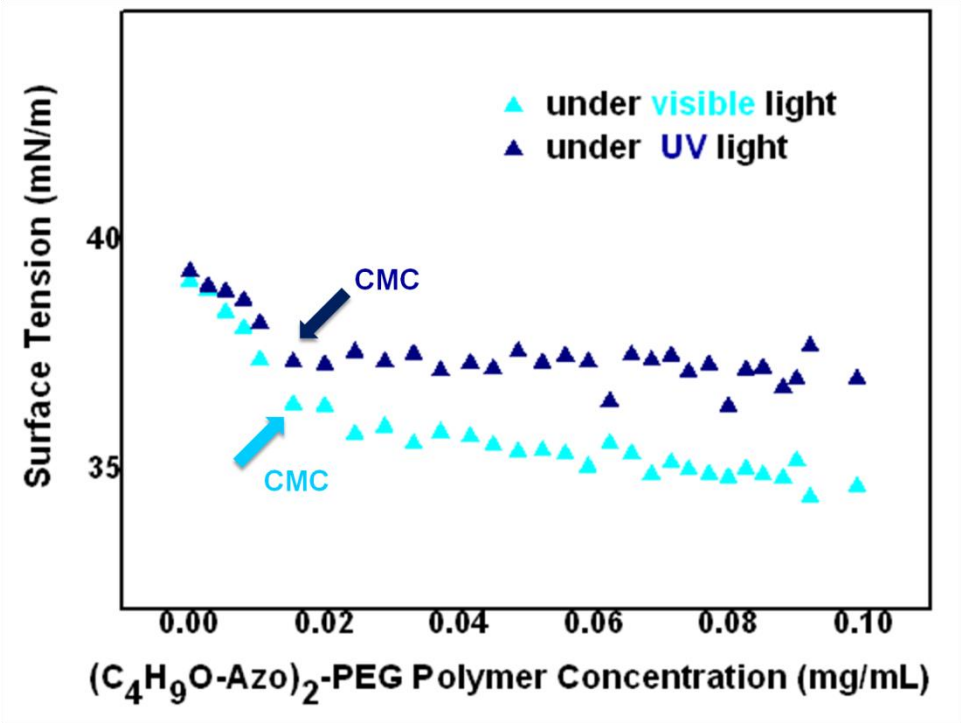

Figure 4-6 CMC of $(C_4H_9O\text{-}Azo)_2$-PEG as determined by surface tension measurement as a function of vesicle concentrations under the irradiation of both UV and visible light.

It is highlighted here that a continual size recovery was observed through time-resolved DLS on the UV irradiated samples (**Figure A-5**). This is due to the fact that the probing laser wavelength of the DLS is in the visible region (488 nm or 633 nm), which causes *cis* to *trans* photo-isomerization during the DLS measurement, inducing the growth of a particle size up to the original diameter. Such reversible size change could be observed by repeatedly turning on and off the UV light source. In all cycles, the size distribution of the vesicles maintained their good mono-dispersity (PDI < 0.1, see DLS plots in **Figure 4-7**).

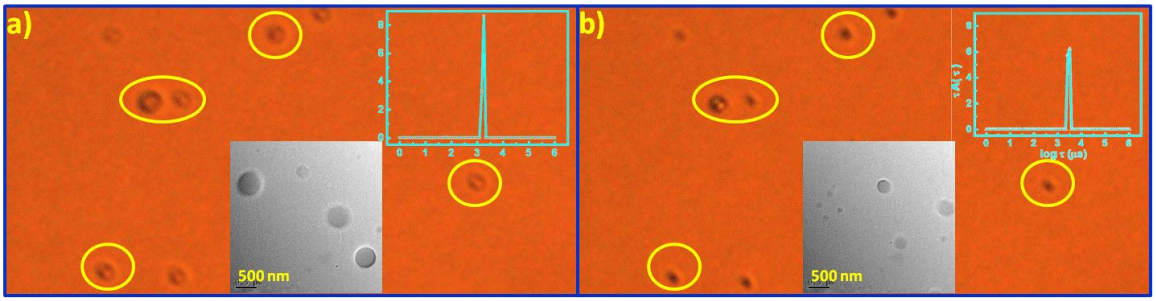

Figure 4-7 The optical microscopy images of (CN-Azo)$_2$-PEG vesicles on a glass slide (images taken from a continuous video recording, see Movie S1) of photo-stationary states (a) after dark-adapted treatment (S_{VIS}) and (b) after UV irradiation (S_{UV}). Corresponding TEM images of the vesicles are given as insets. Overlapped on the optical images are the DLS plots showing the size change while retaining a narrow size distribution.

In further experiments, real-time recording using optical microscopy was done to provide direct visualization of the pulsation of the vesicles, i.e., size change of the vesicles. D_h decreases substantially to 170 nm under UV irradiation for 10 min upon reaching the photo-stationary state ($\mathbf{S_{UV}}$). D_h recovered to the original size upon visible light irradiation ($\mathbf{S_{VIS}}$). This real-time observation of the vesicle pulsation behaviour ruled out the possibilities of cell or vesicle destruction-reformation[187] or division-fusion during the repeated UV-visible irradiation cycles. **Figure 4-7** shows the optical images (DLS results shown in insets) of the (CN-Azo)$_2$-PEG vesicles in solution at the beginning and the end of a video recording (**Movie S1**), i.e., during the photo-stationary states of $\mathbf{S_{VIS}}$ and $\mathbf{S_{UV}}$ respectively. Well-focused recording could be done on the (CN-Azo)$_2$-PEG vesicles because they could be immobilized on the petri dish surface. The other two types of vesicles tend to move randomly in the solutions. The video showed that the integrity of the vesicles was well-preserved while their diameter changed by 2.6 times during the repeating cycles. This indicated that a large amount of solvent was transported into and out of the vesicle through the membrane during visible and UV light irradiation cycles. This interesting phenomenon is important because it resembles the natural photo-

responsive protein bacteriorhodopsin, which shows a similar photo-driven mass transport through the purple membranes.[188] The real-time observation also gave a strong proof that the vesicle structures were not destroyed due to the large volume of solvent transported into and out of the vesicle membrane.

4.2.4.2 Reversibility and repeatability of photo-driven size change

The reversibility of the size change between $\mathbf{S_{VIS}}$ and $\mathbf{S_{UV}}$ was also investigated. The results are summarized in **Figure 4-8**. Excellent reversibility of continuous cyclic pulsation during UV and visible light irradiation cycles was observed, while vesicle integrity was maintained.

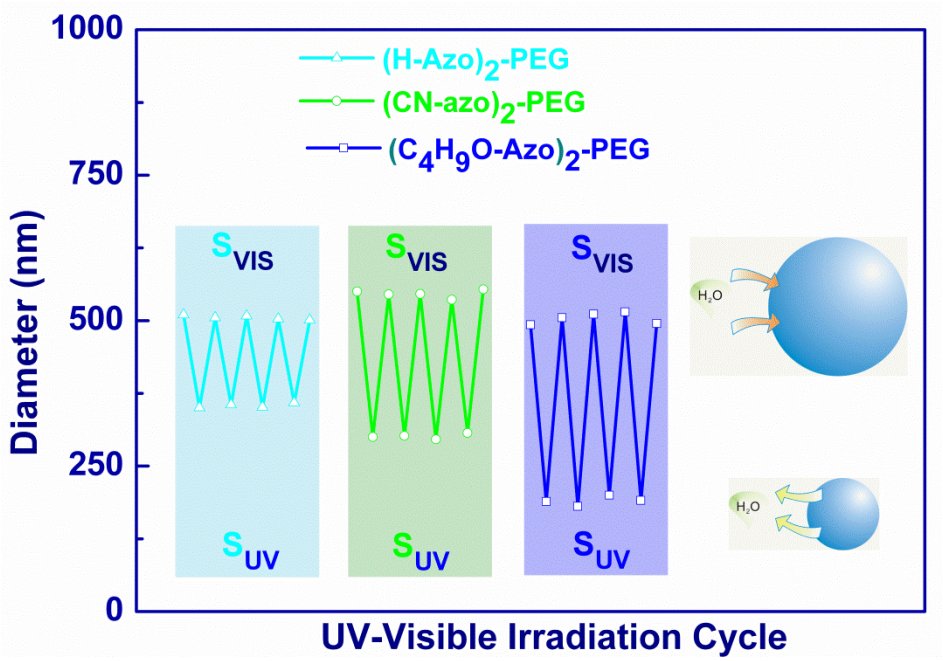

Figure 4-8 Consistent change of D_h during multiple UV-visible irradiation cycles showing good reversibility of the photo-driven pulsation behaviour of the three different azo-PEGs.

4.2.5 Vesicle structure of self-assembled azo-PEGs vesicles

4.2.5.1 Study on the conformational structure of self-assembled azo-PEGs vesicles by DLS

The morphology of the aggregates could be determined from the values of the R_g/R_h ratio. The theoretical ratios of the R_g/R_h ratio are 0.774, 1.0, and 1.5-1.8 for uniform solid spheres, vesicles, and random coils, respectively.[189] By combining DLS with static light scattering (SLS) analysis, the R_g/R_h ratios of different azo-PEGs vesicles were determined to be between 1.2-1.3. The actual values are included in **Table 4-2**. The R_g/R_h values obtained in this study, which are between 1.17 and 1.26, substantially deviate from 0.774 (the 'ideal' R_g/R_h value of a uniform sphere), but are close to 1.0, which is the R_g/R_h value for thin-layer hollow spheres. For example, a ratio of 1.15 was given as evidence for a hollow spherical structure in the literature.[80] Therefore, it is considered that a value of 1.2-1.3 concurs with a vesicle structure.[80] The aggregation number of $(C_4H_9O\text{-Azo})_2$-PEG vesicle was further determined to be ~10,000. Based on the theoretical size, the Flory radius for PEG 5000 is estimated to be 6 nm; thus, a fully stretched PEG 5000 chain should be ~20 nm when folded-back in half. In our case of the azo-PEGs self-assemblies, the PEG chains were believed to have partially stretched as depicted in **Figure 4-9**. It includes the proposed unilamellar bilayer vesicle formation from the self-assembled amphiphilic azo-PEGs in water/THF. This unique bilayer vesicle structure persuits a photo-driven pulsation. The observed reversible size change is similar to the function of some biological cells, e.g., hydration and dehydration of the erythrocyte,[190] where trans-membrane water exchange occurs.

Table 4-2 Summary of DLS and SLS Results[a]

Sample	R_h (nm)	R_g (nm)	R_g/R_h	M_W g/mol (aggregates)	M_w g/mol (polymer)	$N_{aggregation}$[b]
$(H\text{-}Azo)_2$-PEG	252	299	1.19	7.43×10^7	7.69×10^3	1.03×10^4
$(CN\text{-}Azo)_2$-PEG	273	334	1.22	7.95×10^7	7.75×10^3	1.03×10^4
$(C_4H_9O\text{-}Azo)_2$-PEG	250	318	1.27	8.20×10^7	7.93×10^3	1.05×10^4

[a] Test on dark-adapted samples, [b]$N_{aggregation}=M_W(aggregates)/M_W(polymer)$, the values of $M_W(polymer)$ are from GPC analysis.

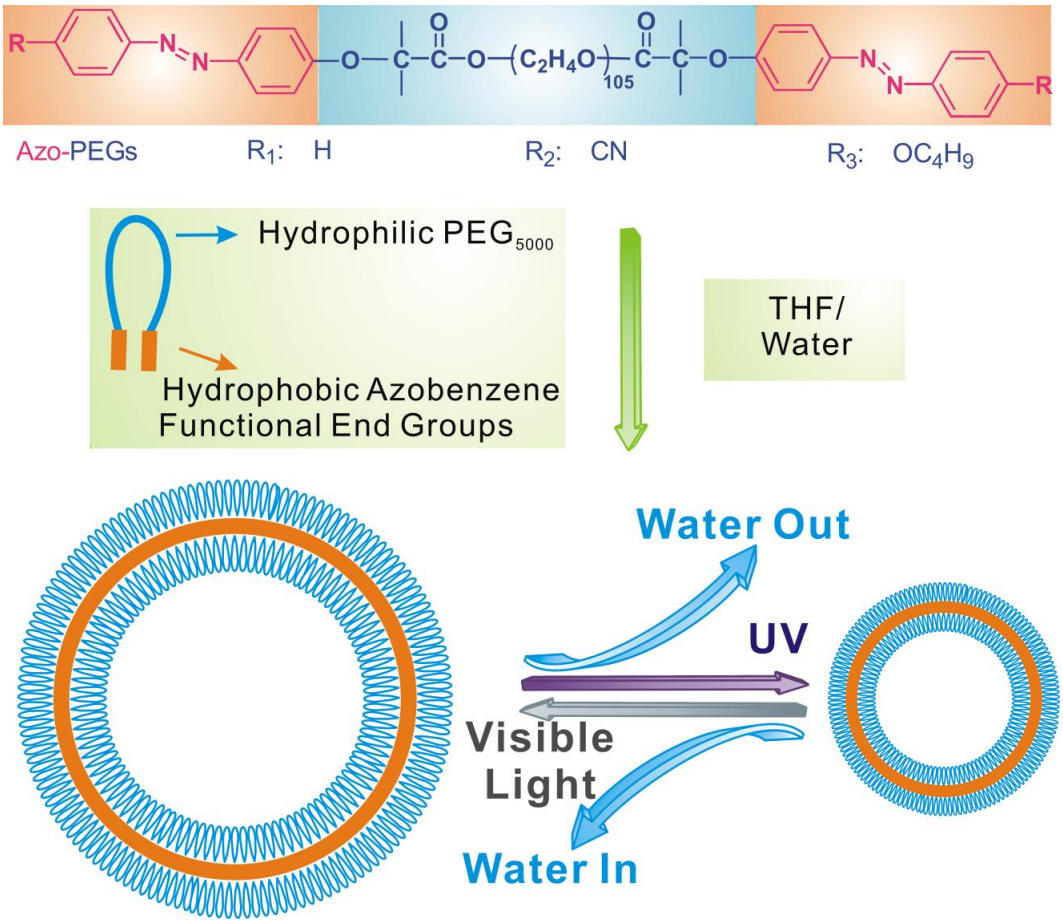

Figure 4-9 Illustration of the structure of azo-PEGs, their folded conformation, the proposed unilamellar bilayer vesicles self-assembly in water/THF mixed solvent, and their photo-driven pulsation behaviour under UV and visible light irradiation.

4.2.5.2 Azo-PEGs vesicle structure studied by AFM, TEM and SEM

The morphology of azo-PEGs self-assemblies was further investigated by AFM, TEM, and SEM to confirm the proposed unilamellar bilayer vesicle structure. All the samples for the AFM, TEM and SEM characterizations were rapidly freeze-dried after dropping 20μL of the vesicle solution onto a silica substrate or a TEM copper grid.

The AFM image (**Figure 4-10**) shows that the $(C_4H_9O\text{-Azo})_2$-PEG vesicles were flattened out on the substrate, with diameters between 1 to 2 μm and a height less than 100 nm. These dimensions are consistent with the proposed vesicle structure, since hollow vesicles would tend to collapse on the substrate. Similar observations were reported for other types of vesicles or hollow structures.[191] The thickness of a collapsed vesicle estimated from AFM images is in the range of 55-100 nm. This observation further supports the proposed unilamellar bilayer vesicle model.

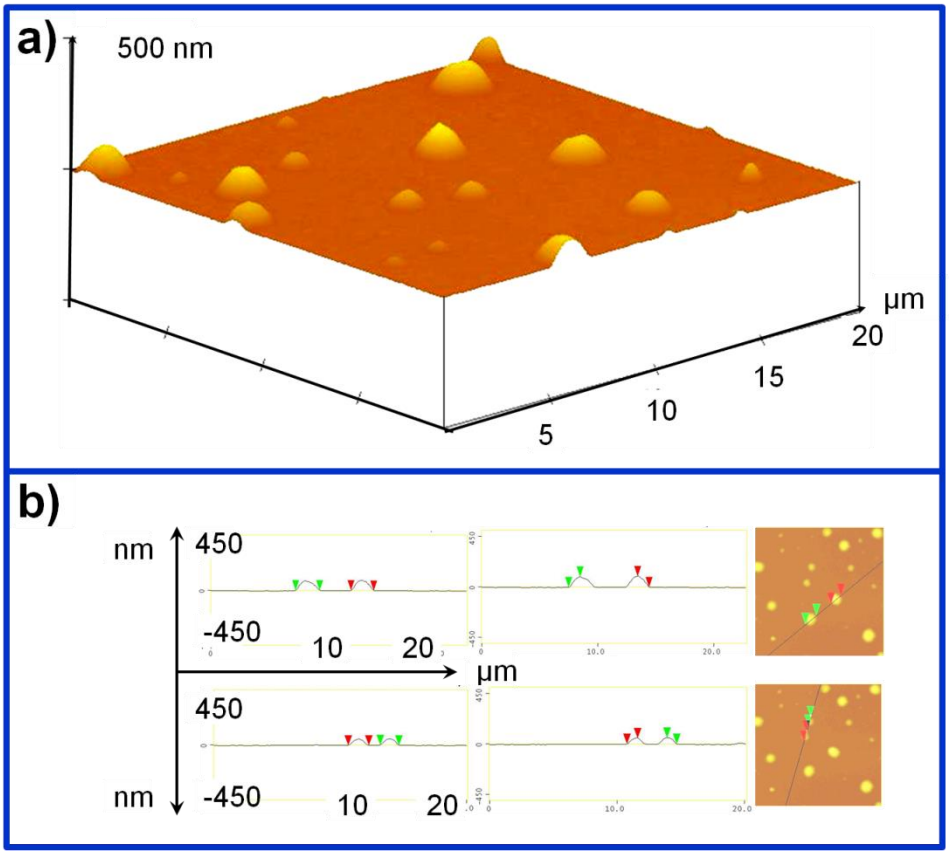

Figure 4-10 a) The AFM image of $(C_4H_9O\text{-}Azo)_2$-PEG vesicles in the dark-adapted state (S_{VIS}). Samples for AFM images were rapidly freeze-dried $(C_4H_9O\text{-}Azo)_2$-PEG vesicles under S_{VIS} with a concentration of 0.1 wt%. b) Cross-sections of the above AFM image. The diameter and height of the freeze-dried vesicles on the substrate can be observed through the analysis of the AFM-cross-section images.

TEM images of $(C_4H_9O\text{-}Azo)_2$-PEG vesicles in a dark-adapted state (**Figure 4-11 a**) and after UV irradiation (**Figure 4-11 b**) also confirmed size reduction after UV-irradiation. The original size of the vesicle was ~400 nm. After the UV irradiation, the size decreased to ~50 nm. SEM images of $(C_4H_9O\text{-}Azo)_2$-PEG vesicles in a dark-adapted state (**Figure 4-11 c**) and after UV irradiation (**Figure 4-11 d**) again confirmed the formation of self-assemblies with a diameter ranging from 400-1000 nm under $\mathbf{S_{VIS}}$ and 200-400 nm under $\mathbf{S_{UV}}$. The SEM showed large size compared to the TEM due to the spreading of the vesicle that might cause limit resolution limitations.

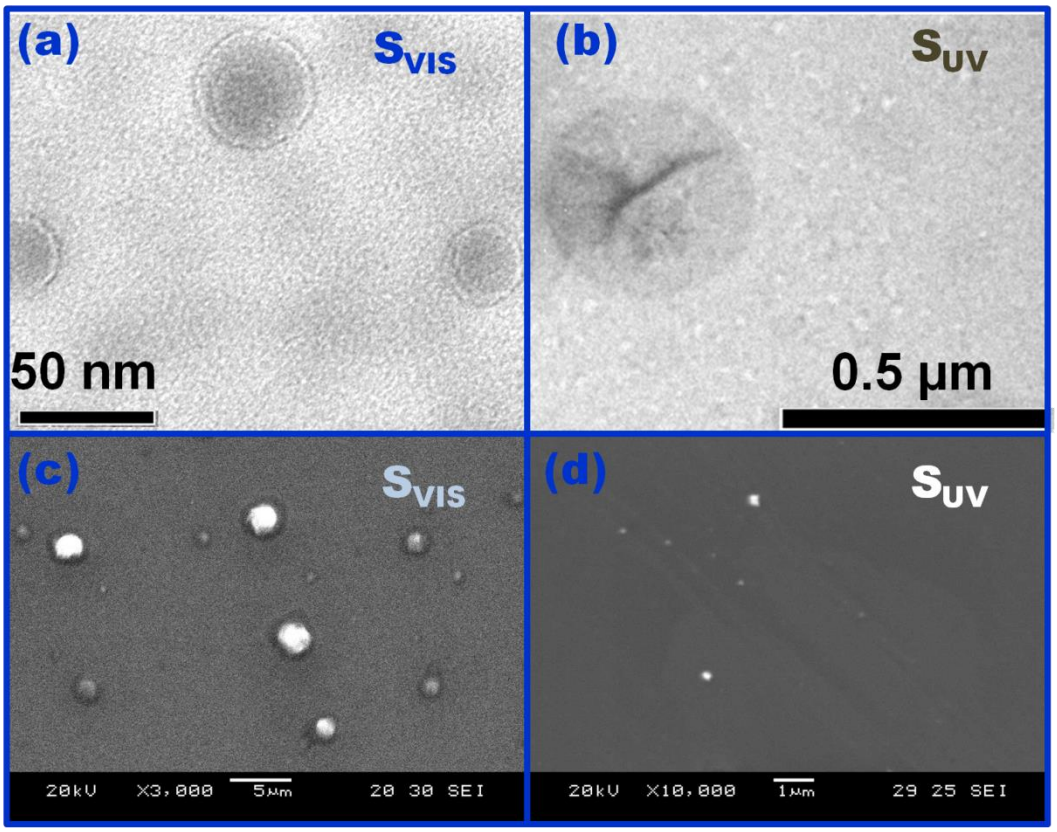

Figure 4-11 TEM images of $(C_4H_9O\text{-}Azo)_2$-PEG vesicles under S_{VIS} (a) and S_{UV} (b). SEM images of $(C_4H_9O\text{-}Azo)_2$-PEG vesicles under S_{VIS} (c) and S_{UV} (d). Samples for TEM and SEM images were prepared by rapidly freeze-drying $(C_4H_9O\text{-}Azo)_2$-PEG vesicles under S_{VIS} and S_{UV} conditions at a concentration of 0.1 wt%.

4.2.6 Mechanisms of self-assembly of azo-PEGs into vesicle structures and their photo-driven pulsation behaviour

The simplistic and representative molecular architecture of the azo-PEGs vesicles synthesized in this work allows a clear mechanistic interpretation on the dramatic photo-driven pulsation phenomenon observed. It is believed that a liquid-liquid phase separation accused owing to a partition of the solvents as the vesicles formed in a water/THF mixture. According to this proposed mechanism, THF should be preferentially associated with the hydrophobic azobenzene groups (see also in **Figure 4-13**). In other word, THF is compartmentalized within the assembled azobenzene groups after the self-assembly of the azo-PEGs. To prove this point, ^{1}H NMR analysis of the vesicle assembly in THF/D_2O

(1:4) (**Figure 4-12**) was conducted. **Table 4-3** shows the signal intensity ratio. It was found that the THF signals in the ^{1}H NMR spectra progressively decreased with increased azo-PEGs concentrations.

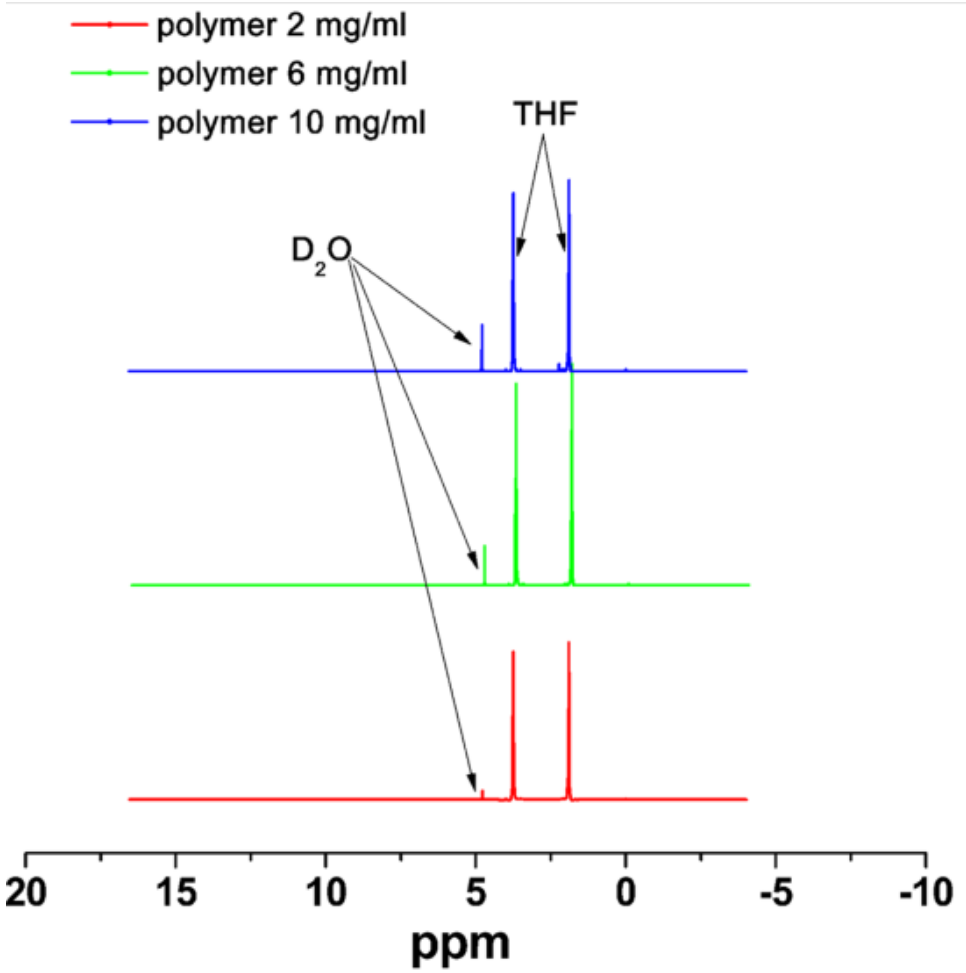

Figure 4-12 **^{1}H NMR spectra of $(C_4H_9O\text{-Azo})_2$-PEG polymer in THF/D_2O (vol/vol=1:4) with different polymer concentrations. The signal at δ 4.8 ppm is assigned to D_2O. The signals at δ 3.7 ppm and δ 1.8 ppm are assigned to THF.**

Table 4-3 **Summary of ^{1}H NMR results in Figure 4-12.**

Polymer Concentration	$I_1 : I_2 : I_3$*	I_2 / I_1 (or I_2 / I_3)
2 mg/ml	0.01 : 1 : 1	100
6 mg/ml	0.03 : 1 : 1	33
10 mg/ml	0.06 : 1 : 1	17

* The I_1 (at δ4.8 ppm, D_2O), I_2 (at δ3.7 ppm, THF), and I_3 (at δ1.8 ppm, THF) refer to the integral peak intensities of D_2O and THF.

The ^{1}H NMR results directly support the scenario of preferential association of THF with the assembled azobenzene groups, since THF signal is expected to decrease if the THF increasingly phase separates into the D_2O-free centre layer of the vesicle membrane. It is known that the ^{1}H NMR signal of an organic compound cannot be detected when it is isolated from any deuterated solvent. The unilamellar bilayer vesicle structure, which was already confirmed by morphological studies (AFM, TEM, and SEM), is assumed to be made up of individual lipid-like molecules that self-fold into a flower petal loop. This is similar to the behaviour of a fullerene-end-capped PEG.[162] The hydrophobic and rigid azobenzene groups at the chain ends aggregate in the THF-rich phase, driven by the hydrophobic π-π interactions. The hydrophilic PEG chains thus assemble in the water-rich phase forming the inner and outer layers of the membrane. An illustration of the water-rich phase and THF-rich phase within a self-assembled vesicle of azo-PEGs in a THF/H_2O mixed solvent is shown in **Figure 4-13**. From a thermodynamic viewpoint, these vesicles are potentially thermodynamically equilibrium structures.[192] In particular, the interfacial energy between the hydrophobic core and the more polar solvent is the key factor that governs the vesicle formation.

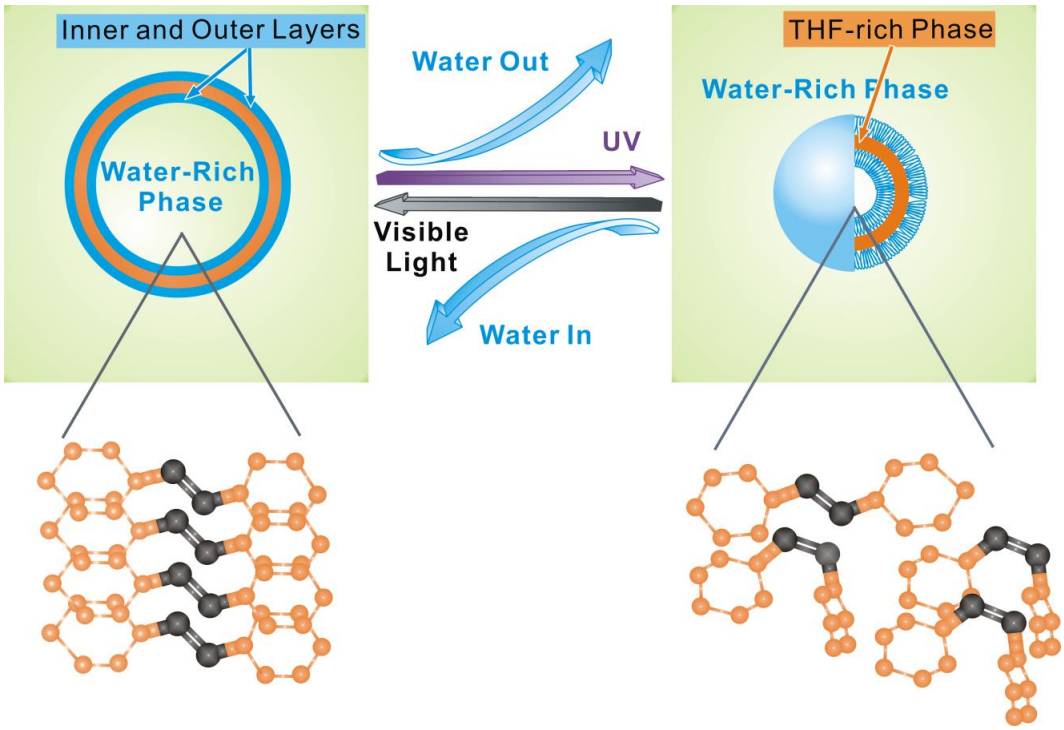

Figure 4-13 Illustration of the unilamellar bilayer vesicles self-assembly in a water/THF mixed solvent and their light-driven pulsation behaviour under UV and visible light irradiation accompanied with water transport in and out through the vesicle membrane.

In these azo-PEGs, the *cis*-isomers of azobenzene have a higher dipole moment and higher surface free energy. As a result, the interfacial energy between the bilayer and water increases under UV-irradiation, causing the vesicle to contract in order to minimize the total interfacial area. The mechanisms can also be explained from a molecular viewpoint. The photo-isomerization of *trans-cis* isomers is the ultimate cause of this unusually large size change of the vesicle, which can be viewed as the differences in polarity and geometry between the two isomers. It is believed that the *cis* isomers formed during UV-irradiation are expelled from the parallel *trans* isomer aggregation. Corralling of the remaining *trans* isomers results in the size reduction of the vesicle. However, the expelled *cis* isomers are likely to stay in the vicinity of the azobenzene aggregation, keeping the vesicle integrity. The reason is that the *cis* isomers are still hydrophobic (although with increased polarity), and prefer to be in the THF-rich phase. Therefore,

when the *cis* isomers are converted back into *trans* form, they are able to re-enter the aggregation, resulting in the recovery of the vesicle size. The quantum of the size change should be a function of the *trans*/*cis* isomer compositions. As mentioned earlier, the large size change of a vesicle indicates substantial photo-pumping of water across the membrane. Although the exact mechanism is believed to be complex, it is postulated here that the photo-driven expulsion and re-entry of the azobenzene isomers are responsible for creating water channels in the lipid-like membrane on the vesicle surface.

Additional evidence for our proposed vesicle structure, in which the azobenzene groups of the azo-PEGs are in the THF rich phase, was obtained from the photo-isomerization study of azo-PEGs in different solvents. This can be clearly observed by re-visiting the UV-visible absorption results. **Figure 4-14** compares the UV-visible absorption spectra of $(C_4H_9O\text{-}Azo)_2$-PEG in the dark-adapted and UV-irradiated photo-stationary states in (a) THF/water mixed solvent, (b) pure THF, and (c) pure water. The *trans-cis* photo-isomerization behaviour of the $(C_4H_9O\text{-}Azo)_2$-PEG vesicles in the THF/water mixed solvent (**Figure 4-14 a**) resembles that in pure THF (**Figure 4-14 b**), and is quite different from that of the $(C_4H_9O\text{-}Azo)_2$-PEG in pure water (**Figure 4-14 c**). This is understandable because the isomerization of azobenzene is sensitive to its solvent environment polarity.

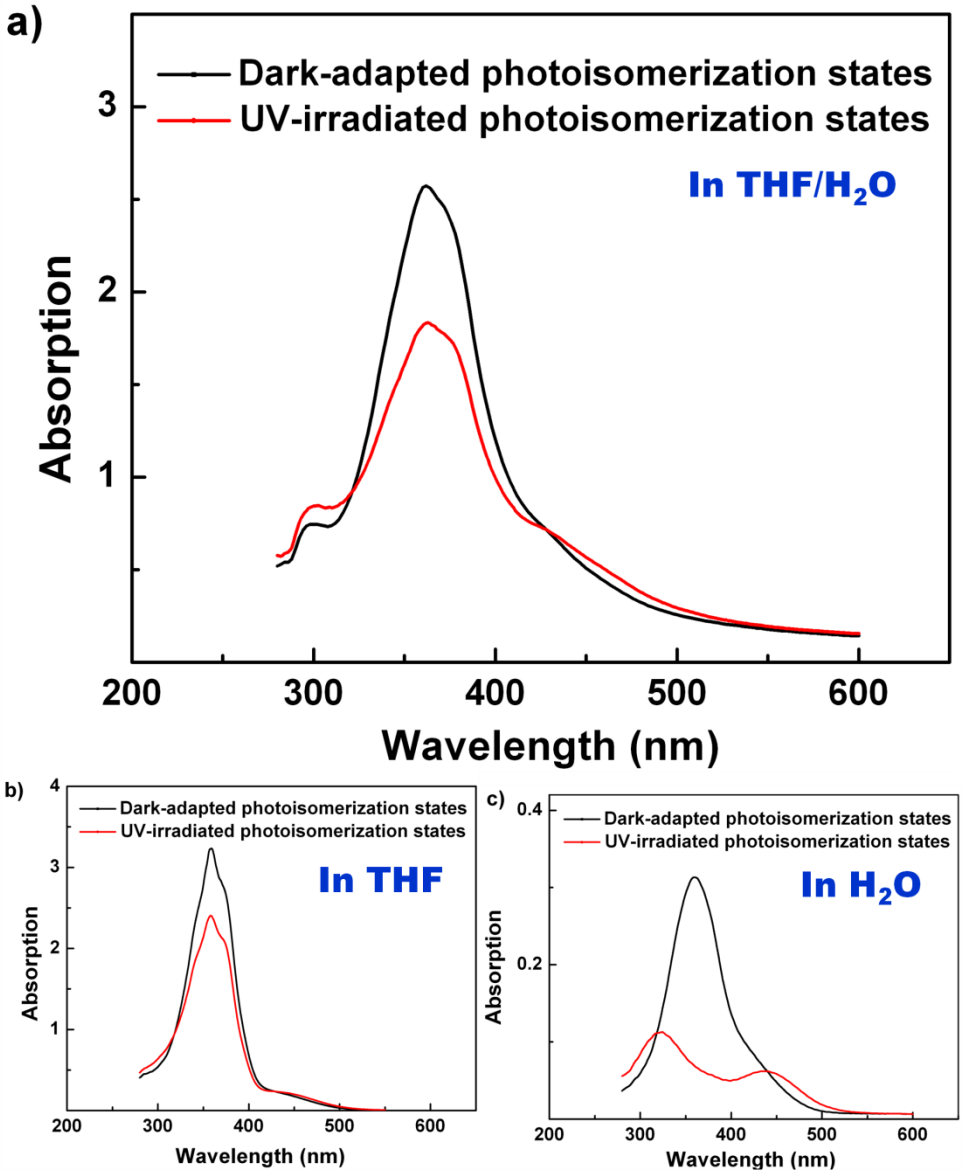

Figure 4-14 UV-visible absorption spectra of the dark adapted (S_{VIS}) and UV-irradiated photo-stationary (S_{UV}) $(C_4H_9O\text{-Azo})_2$-PEG (a) 0.24 mg/mL in THF/water (1:4) mixed solvent, (b) 0.75 mg/mL in pure THF and (c) 0.3 mg/mL in pure water.

4.2.7 Regulation of photo-driven pulsating behaviour of self-assembled azo-PEGs vesicles

Although $(C_4H_9O\text{-Azo})_2$-PEG is mainly discussed in order to clearly illustrate the concept and results of this project, nevertheless the controllable photo-driven pulsating behaviour of the vesicles has been successfully demonstrated for all azo-PEGs with three different terminal substituents of azobenzene, i.e., $(H\text{-Azo})_2$-PEG, $(CN\text{-Azo})_2$-PEG and $(C_4H_9O\text{-}$

Azo)$_2$-PEG. The terminal substituent groups are known to affect the photo-isomerization process of azobenzene. (H-Azo)$_2$-PEG contains an amino-type azobenzene. (CN-Azo)$_2$-PEG, similar to (C_4H_9O-Azo)$_2$-PEG, includes a push-pull-type azobenzene that has electron-donating and electron-withdrawing groups at the ends of the azobenzene. Since they are classified into different polymer categories, they should undergo different photo-isomerization processes, exert different influences towards the photo-driven deformation of vesicles, and offer the possibility to tailor the pulsating behaviour and water transport.

As expected, the vesicle from the azo-PEGs with different functional end groups showed different rates of diameter change and flexibility. Quantitative analysis of the photo-isomerization of the three types of azo-PEGs vesicles was carried out using UV-visible absorption spectroscopy to determine the *cis* isomer fractions ($\boldsymbol{f_z}$ [163], see Chapter 3 page 43 **equation 3.4**). The pulsating behaviour can be deduced from the $\boldsymbol{f_z}$ and D_h, as summarized in **Table 4-4**.

Table 4-4 ***Cis*** **isomer fractions ($\boldsymbol{f_z}$) and the corresponding mean hydrodynamic diameters ($\boldsymbol{D_h}$) at the two photo-stationary states ($\mathbf{S_{VIS}}$ and $\mathbf{S_{UV}}$) of the three different azo-PEGs vesicles.**

Vesicles	(H-Azo)$_2$-PEG		(CN-Azo)$_2$-PEG		(C_4H_9O-Azo)$_2$-PEG	
	S_{VIS}	S_{UV}	S_{VIS}	S_{UV}	S_{VIS}	S_{UV}
f_z (%)	0	18.4	0	52.2	0	54.0
D_h (nm)	505	354	547	301	501	190

The differences of D_h between the two photo-stationary states of the (C_4H_9O-Azo)$_2$-PEG, (CN-Azo)$_2$-PEG and (H-Azo)$_2$-PEG vesicles, i.e., ΔD_h, are 311, 246 and 151 nm respectively. The ΔD_h shows that end groups dramatically impacted the degree of size change of vesicles, the corresponding vesicle volumes shrank by 15, 6 and 2 times of (C_4H_9O-Azo)$_2$-PEG, (CN-Azo)$_2$-PEG and (H-Azo)$_2$-PEG vesicles. (H-Azo)$_2$-PEG

vesicles has the smallest fraction of *cis* isomers at the $\mathbf{S_{UV}}$ state and hence the least size change (ΔD_h = 151 nm). It is interesting to note that similar *cis* isomer fractions in (CN-Azo)$_2$-PEG and (C_4H_9O-Azo)$_2$-PEG does not result in the same degree of size reduction. Nevertheless, the results clearly indicate a close correlation between the size change and the *cis* isomers fraction at the photo-stationary state after UV-irradiation. This could be due to additional factors such as the different polarity of the end groups may influence the aggregation of the self-assemblies. Furthermore, the butoxy group in (C_4H_9O-Azo)$_2$-PEG is more hydrophilic than the CN or H group and was larger than the CN or H group in size. The bulky hydrophilic substituents may also change the inner-layer structure of the vesicle. Therefore, the functional group, i.e., H, CN or C_4H_9O, not only affects the isomerization, but also affects aggregation of azobenzene in $\mathbf{S_{VIS}}$. Furthermore, different azobenzene end groups also affect the change in surface energy between the two photo-stationary states in the vesicles, hence the resultant solvent transport across the vesicle membrane.

This part of the project shows clearly that the employment of different substitutions on the azobenzene group can tailor the reversible pulsating behaviour of the vesicles and the solvent transport across the vesicle membrane.

4.3 Conclusions

In this work, a unique photo-driven pulsating behaviour of robust artificial cells based on self-assembled vesicles of azobenzene end-capped polyethylene glycol (Azo-PEGs) has been investigated.

This was achieved by firstly preparing the lipid-like azobenzene-containing PEG by systematically incorporating three different types of azobenzene moieties into the chain

ends of PEG. The GPC and ^{1}H NMR confirmed the existence of azobenzene chromophores in azo-PEGs.

Secondly, the process of amphiphilic azo-polymer self-assembly has been studied. By adjusting the molar ratio of mixed solvents, i.e., water / THF, mono-dispersed vesicles can be prepared from photo-responsive lipid-like molecules based on the azobenzene end-capped PEGs. The UV-visible absorption study, surface tension measurement, DLS, SLS, AFM, TEM and SEM clearly demonstrated the vesicle structure of the self-assemblies.

Thirdly, the mechanism of the self-assembly and photo-isomerization of the azo-PEGs in different solvents has been discussed and experimentally verified. The vesicles undergo a photo-isomerization induced pulsation upon UV-visible light irradiation cycles, during which a large amount of solvent is transported across the vesicle membrane. To achieve controllability of the pulsation, different approaches can be adopted, e.g., changing the substitutes of azobenzene and tailoring the visible light power.

The simplicity of our molecular design enables a clear understanding of the mechanisms from the viewpoints of both thermodynamics and structural changes during the photo-isomerization of azobenzene. The azobenzene groups, acting as a photo-trigger that allows water transport across the vesicle membrane, have a similar function to the bacteriorhodopsin protein in the purple membranes.

In summary, a robust bilayer vesicle with large photo-induced size change was successfully prepared (**Figure 4-15**). It possibly resembles the bateriorhodopsin in the purple membrane that is able to pump protons out of the cell membrane. Understanding of such reversible photo-responsive materials may lead to the development of advanced responsive systems for applications in biomimetic sensing, controlled drug release, and various separation processes.

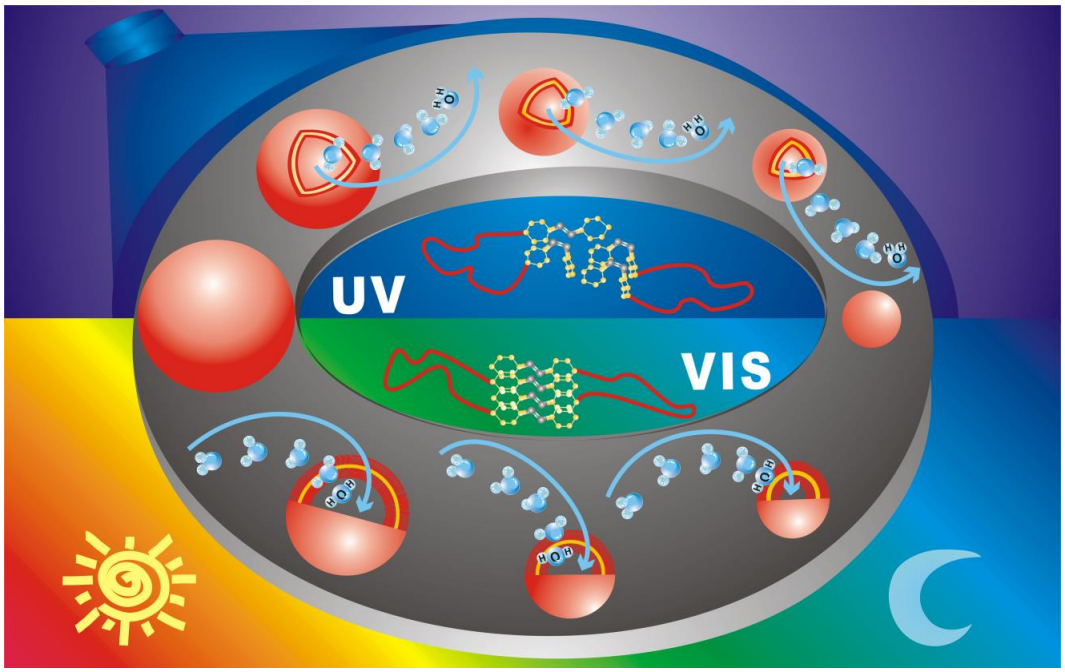

Figure 4-15 Illustration of photo-responsive pulsation of the unilamellar bilayer vesicles. The lipid-like photo-sensitive polymer (azo-PEGs) folded into a loop induced by the hydrophobic interaction of trans-azobenzene under visible light irradiation. Under UV irradiation, azobenzene terminal groups undergo *trans-to-cis* photo-isomerization. The rearrangement of azobenzene molecules expelled the *cis* isomers from the parallel *trans* isomers and corralling of the remaining *trans* isomers. Thus the vesicle exhibited a large size change associated with substantial transmembrane water transport. The size change is reversible and can be cyclically performed under UV-visible light irradiation.

5 AZO-PEGS SELF-ASSEMBLY IN AQUEOUS SOLUTIONS

5.1 Introduction

5.1.1 Biomembranes and gated channels

Biomimicry, meaning learning from nature, has become a widespread and rapidly expanding scientific branch.[193] Besides building materials with optimized mechanical properties, [31,32] 'Biomimetic Chemistry' aiming at investigating bio-membranes has been studied since the 1970s.[194] The well-known example, i.e., liposomes of a lipid bilayer, forms through a self-assembly process and establishes a continuous impermeable membrane resembling cell walls.[195-199] In an actual living cell, the membrane regulates the trans-membrane mass exchanges under various biological activities or external stimuli via specific membrane channel proteins. For example, aquaporin (AQP, see **Figure 5-1**), a water channels protein, can selectively transport water molecules from inside the cell to the outside of the cell, while preventing the passing of ions or other salts.[200] Recently, AQP has been studied intensively for its potential application in sea water desalination.[201,202] Gated biological channels[203-206] can interrupt the flow of ions (e.g., K^+, Na^+, Ca^{2+}) by switching between open and closed states (**Figure 5-2**).

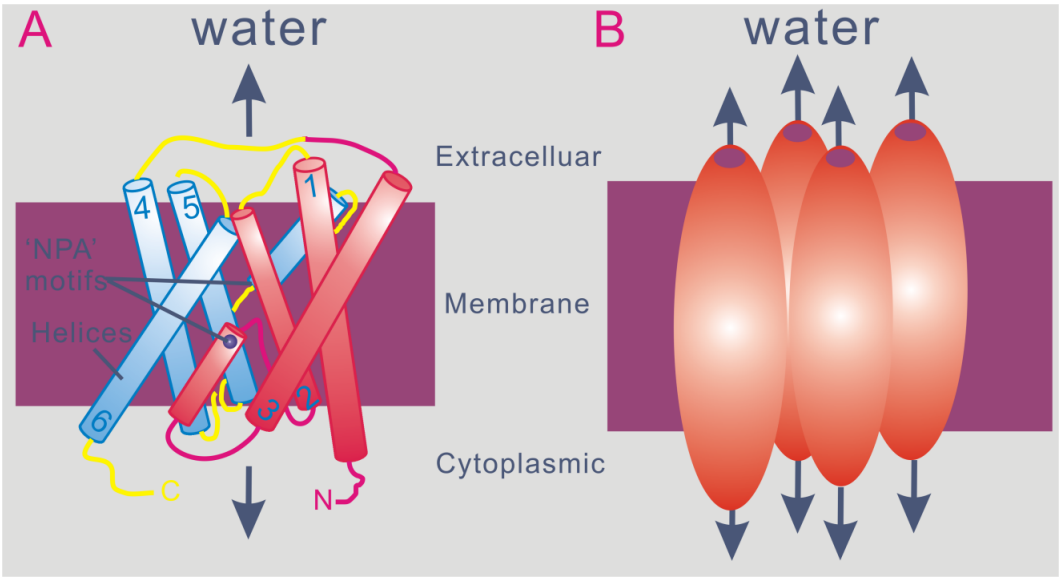

Figure 5-1 The structure and organization of the aquaporin (AQP) water channel molecule. A: Six trans-membrane domains in the AQP monomer. B: tetramers of aquaporin.[207]

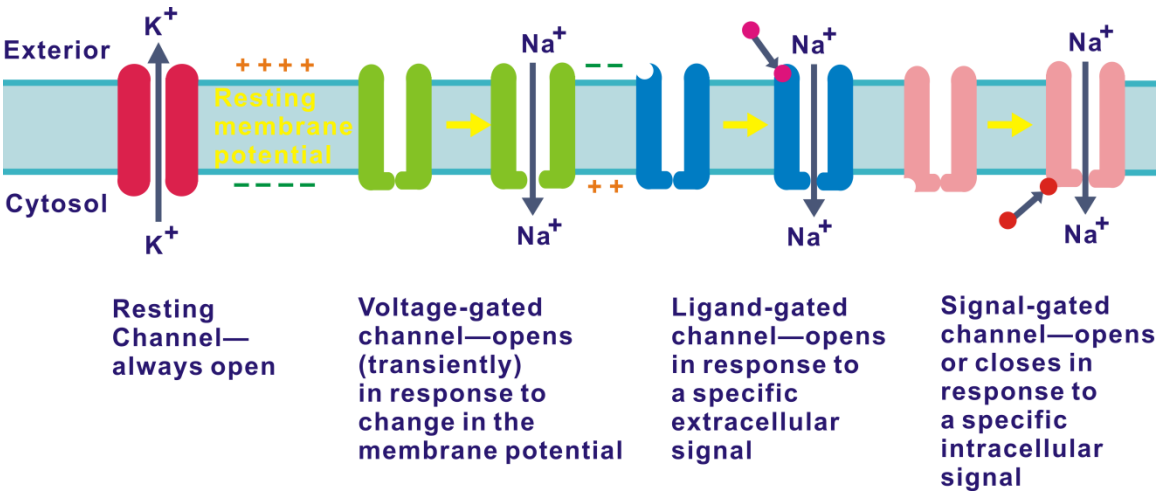

Figure 5-2 Illustration showing different types of gated channels.[208]

5.1.2 Light-driven smart biomimetic membranes

Stimuli responsive smart molecules are promising candidates as different signal-dependent switches for membranes. A light induced molecular switch[209] is especially appealing for building a controlled gating channel in membranes, since light is non-invasive. In fact, bacteriorhodopsin, a naturally occurring membrane protein, has a

demonstrated photo-pumping function of hydrated protons across the cell membranes. Recently, photo-responsive molecules, such as hemithioindigo, spiropyran/merocyanine, and azobenzene, have been used to modify the channel proteins in biological cells to render their light regulated permeation selectivity.[210-213]

Stimuli-driven pulsating self-assemblies are considered as promising approaches towards tackling one of the ultimate scientific challenges to develop artificial pulsating organs such as cardiac muscle cells.[2] Previous work on the responsive pulsating vesicles included the pH-triggered breathing vesicles[1] highlighted by ***Nature*** in 2009.[214] Yu *et al.* reported a pH-induced pulsation behaviour of vesicles that experience reversible size change in solution with different pH values.[1] The breathing vesicle can swell via protonation in acid solution and shrink via deprotonation in basic solution. This work was highlighted with potential applications in biomedicine, e.g., drug-delivery devices and chemical reaction nano-vessels. Thermally responsive nano-tubules, recently reported in ***Science***, can undergo shrinkage upon heating and expansion upon cooling.[2,215] Huang *et al.* reported a thermo-induced pulsation behaviour of nano-tubes that undergoes shrinkage and expansion induced by thermo-responsive dehydration and hydration upon heating and cooling, respectively. This work was highlighted with the expectation of capability to transport cargos using thermal energy. In the previous chapter, we have discussed a new pulsating system using photo energy as the driving force based on the lipid-like azo-PEGs. In this chapter, a further investigation on the photo-driven pulsating vesicles was carried-out. The photo-driven changes can be detected conveniently when azobenzene materials are embedded in a biological cell membrane,[216] artificial vesicle membrane,[217] polyelectrolyte multilayer membrane,[218] or when densely packed inside a micro-porous ceramic[219] or zeolite[220] membrane. These membranes made from or modified with

azobenzene-based polymers have been studied for their selective permeability in water treatment[216,221-225] and gas separation.[220]

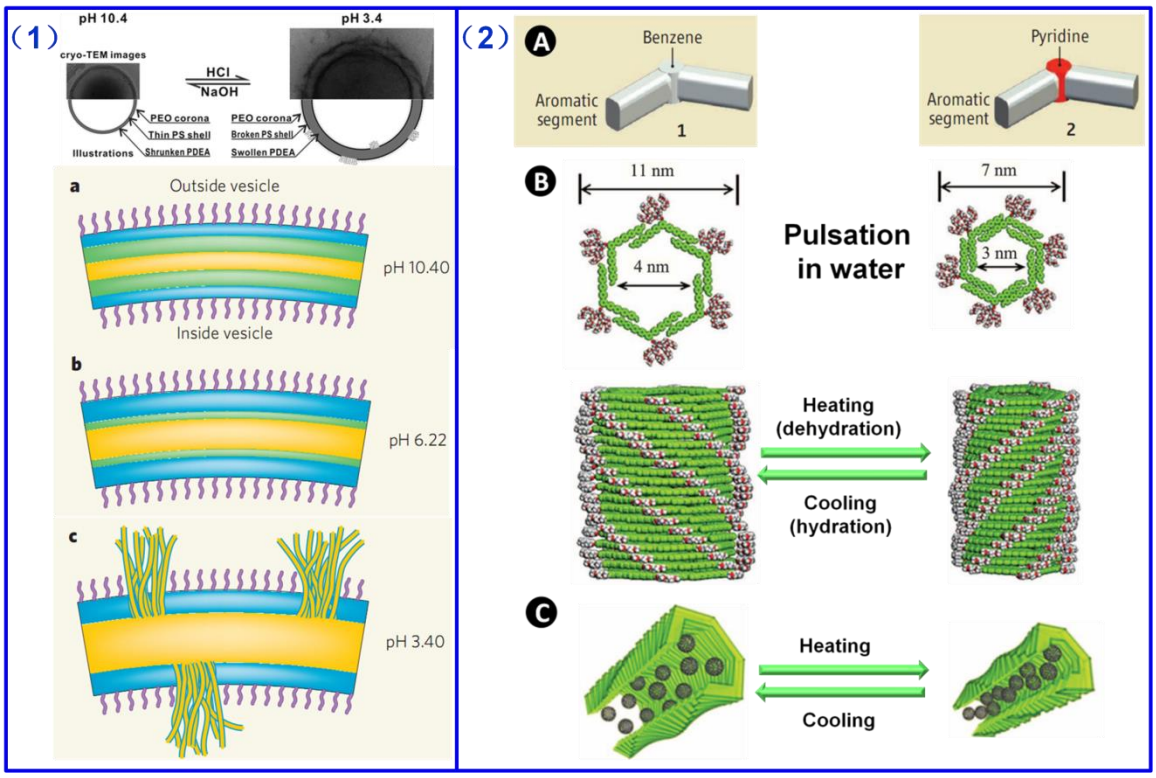

Figure 5-3 Illustration of (1) pH-induced pulsating vesicle[1,214] and (2) thermal-induced pulsating nano-tubules.[2,215]

5.1.3 Scope and objectives

A series of lipid-like azobenzene-based polymers (azo-PEGs) have been studied in Chapter 4. The azo-PEGs form bilayer vesicles in organic/aqueous mixed solvents that possess unique 'photo-respiring' or 'photo-pulsating' characteristics, whereby considerable change in the vesicle diameters were seen before and after UV irradiation. These vesicles effectively 'respire' as a large amount of solvent transport across the bilayered membrane occurs during UV or visible light irradiation.[159] It would be highly interesting to study the ionic permeation behaviour of such photo-responsive bilayer

membranes. However, the above azo-PEGs were found to be unsuitable because the presence of an organic solvent makes the analysis difficult and data interpretation ambiguous. In this chapter, we optimized the chain length of azo-PEG so that it could form similar bilayer vesicles in aqueous media, i.e., DI water, or dilute aqueous salt solutions of lithium chloride (LiCl), sodium chloride (NaCl), and potassium chloride (KCl). The permeation behaviour of the vesicle membrane was investigated based on a carefully designed electrolytic conductivity experiment.

5.2 Results and Discussion

5.2.1 Synthesis of Azo-PEG

Azo-PEG has been synthesized and named as $(C_4H_9O\text{-}Azo)_2$-PEG 2100 (M_W 2144 g/mol, PDI 1.2, from GPC). The product was a dark bronze thick soft solid after drying under vacuum (yield 69 wt %). ^{1}H NMR in $CDCl_3$ (**Figure A-6**): 7.0-7.8 ppm (-C_6H_6-) , 4.32 ppm (-OCH_2C-), 3.6 ppm (-OCH_2CH_2)$_n$, 1.67 ppm (s) (-CH_3).

5.2.2 Vesicle assembly in solutions and pulsating behaviour investigation

Vesicles of $(C_4H_9O\text{-}Azo)_2$-PEG 2100 were prepared in DI water, KCl solution (0.005-0.015 M), NaCl solution (0.005-0.015 M), and LiCl solution (0.005-0.015 M) separately. The concentration of $(C_4H_9O\text{-}Azo)_2$-PEG 2100 polymer was kept at 1 mg/mL. Light scattering data of $(C_4H_9O\text{-}Azo)_2$-PEG 2100 assemblies under $\mathbf{S_{VIS}}$ in DI water and different salt solutions are shown in **Table 5-1**.

Table 5-1 Light scattering data of (C_4H_9O-Azo)$_2$-PEG 2100 assembled in DI water and different salt solutions.

Salt Concentration	DLS Result	**KCl solution**	**NaCl solution**	**LiCl solution**
0 M	D_h (nm)	**667**		
	PDI	**0.01**		
0.005 M	D_h (nm)	**914**	**825**	**730**
	PDI	**0.23**	**0.16**	**0.01**
0.01 M	D_h (nm)	**929**	**849**	**770**
	PDI	**0.12**	**0.05**	**0.05**
0.015 M	D_h (nm)	**928**	**856**	**742**
	PDI	**0.29**	**0.11**	**0.01**

Table 5-1 shows that (C_4H_9O-Azo)$_2$-PEG 2100 is able to self-assemble in both DI water and aqueous media of different salts, such as KCl, NaCl and LiCl, within the rather dilute concentration range used in this investigation, although the salt solutions seem to have an effect on the diameter and PDI of the assembly. This is not unexpected. The assemblies are usually larger and with broader size distribution in salt containing aqueous media in comparison to those obtained in the pure DI water. The light-driven pulsating behaviour of vesicles was investigated first by the diameter change recorded using DLS measurement. The actual diameter and corresponding PDI data are summarized in **Table 5-2**, which shows a substantial size change of the vesicles in DI water and different salt solutions.

Table 5-2 Light scattering data of (C_4H_9O-Azo)$_2$-PEG 2100 vesicle in DI water and different salt solutions under the two different photo-stationary states (S_{VIS} and S_{UV}). The data after recovery from the S_{UV} state are also given for comparison.

		Vesicle in DI water	Vesicle in Salt solution (0.01 M)		
			LiCl	**NaCl**	**KCl**
S_{VIS}	D_h (nm)	**667**	**770**	**849**	**929**
	PDI	**0.01**	**0.05**	**0.05**	**0.12**
S_{UV}	D_h (nm)	**330**	**640**	**570**	**638**
	PDI	**0.01**	**0.10**	**0.13**	**0.30**
S_{VIS} (recovery)	D_h (nm)	**643**	**730**	**867**	**933**
	PDI	**0.01**	**0.19**	**0.23**	**0.18**

Table 5-2 shows that the pulsating behaviour was maintained as the diameter of the vesicles reversibly changed between the two different photo-stationary states, i.e., $\mathbf{S_{VIS}}$ and $\mathbf{S_{UV}}$, during a UV-visible irradiation cycle regardless of the media. But the percentage of the size change between the $\mathbf{S_{VIS}}$ and $\mathbf{S_{UV}}$ is lower in comparison to that in DI water. For example, the mean hydrodynamic diameters at $\mathbf{S_{VIS}}$ and $\mathbf{S_{UV}}$ are 667 and 330 nm, respectively, in DI water, whereas the corresponding values are 928 and 540 nm in 0.015 M KCl solution. The $\mathbf{S_{UV}}$ state is sufficiently established after UV irradiation at a wavelength of 370 nm for 60 min in this study. It seems that the salt solutions can affect the assembly as well as the pulsating behaviour. The recovery of the size change was captured by a time resolved DLS analysis of the UV irradiated samples with a continuous increase of the diameter to its original size (see video taken of the computer screen during the DLS experiment, **Movie S2**). Perhaps it should be mentioned that it is the visible light probing laser light source (632.8 nm) that caused the diameter increase during the DLS experiment. This can be ultimately traced back to azobenzene isomerization from the *cis* isomer to *trans* isomer in the vesicles. While DLS data for the samples at $\mathbf{S_{UV}}$ photo-stationary state show clearly a single modal distribution, a bimodal distribution profile appeared during the continuous DLS run. In fact, a single modal distribution is also seen for samples in the $\mathbf{S_{VIS}}$ photo-stationary state. An interim bimodal distribution is conceivable because the probing laser is a focused beam passing and scattering through the sample cuvette, which is unlikely to have a uniform intensity throughout the sample.

The photo-isomerization behaviour was observed for all samples (**Figure 5-4**). In **Figure 5-4**, the characteristic decrease of the π-π* absorption of the *trans* isomers and the increase of the n-π* absorption of the *cis* isomers were observed for all the self-assemblies upon UV-visible irradiation.

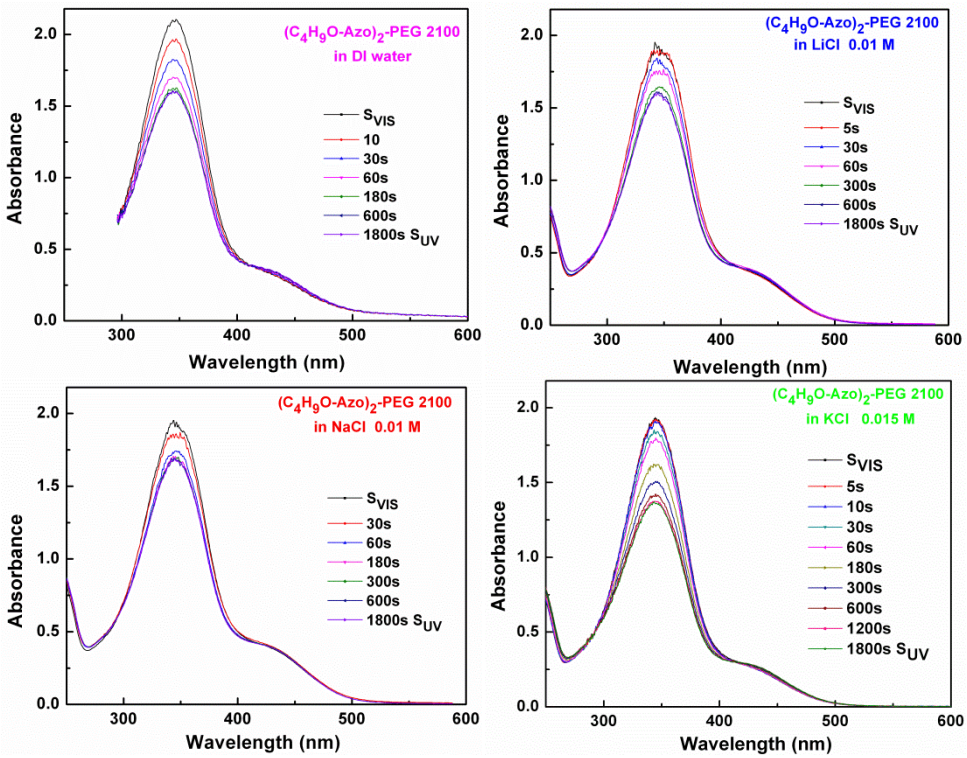

Figure 5-4 UV-sisible absorption spectra of the dark adapted (S_{VIS}) and UV-irradiated photostationary (S_{UV}) of (C_4H_9O-Azo)$_2$-PEG 2100 vesicle in DI water and in different salt solutions (0.01 M LiCl, 0.01 M NaCl, and 0.015 M KCl). Vesicles in different solutions were prepared with the polymer concentration kept at 1 mg/mL. The polymer concentration of all the samples used for the tests was diluted to 0.25 mg/mL.

The light regulated size change in the (C_4H_9O-Azo)$_2$-PEG 2100 vesicles was induced by the photo-isomerization of the azobenzene moieties in the lipid-like bilayer; the detailed schematic illustration is shown in **Figure 5-5**.

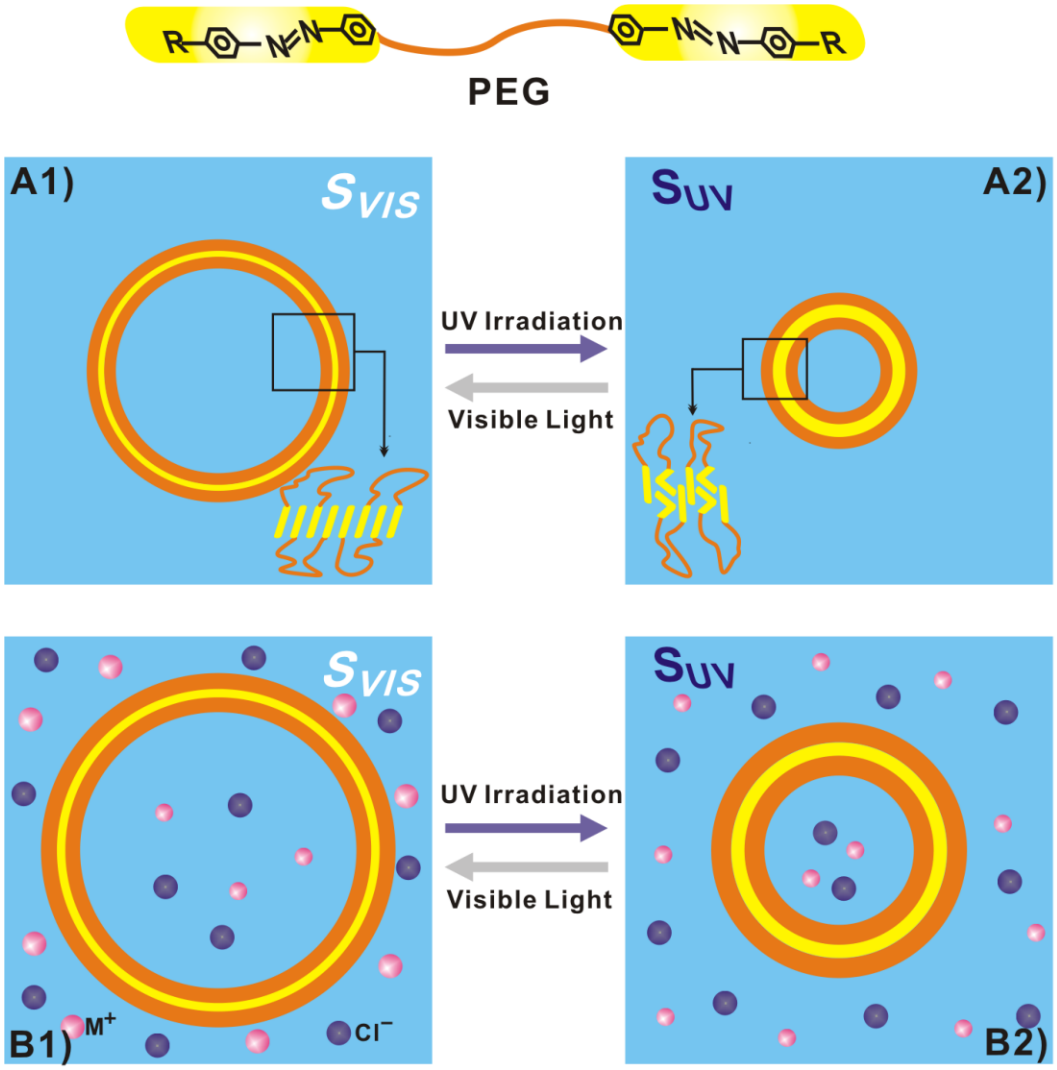

Figure 5-5 Structure of polymer (C_4H_9O-Azo)$_2$-PEG 2100 and schematic illustration of photo-regulated size change during UV-visible irradiation of its self-assembled state in aqueous (A1 S_{VIS} and A2 S_{UV}) and in a salt solution (B1 S_{VIS} and B2 S_{UV}). Violet sphere: anion (Cl^-). Pink sphere: cation (M^+: Li^+, Na^+, K^+).

5.2.3 Vesicle structure of assembly in DI water and salt solutions

The R_g/R_h ratio of the assembly is 0.94 (see **Table A-1**), supporting a hollow vesicle morphology.[226] It is concluded that (C_4H_9O-Azo)$_2$-PEG 2100 self-assembles into unilamellar bilayer vesicles in which each lipid-like molecule self-folds into a flower petal loop (**Figure 5-5 a**).[159,227] The assembly is similar to the self-assemblies in

THF/water mixed solvent aided via a solvent compartmentalization mechanism. However in this work the PEG chain length is tuned such that the $(C_4H_9O\text{-}Azo)_2$-PEG 2100 could self-assemble in DI water without the organic solvent.

The vesicle structure was further studied by AFM and TEM analyses. For the vesicle samples self-assembled in DI water and KCl solution, AFM images (**Figure 5-6**) show flattened particles on the substrate with diameters ~1.1 μm while their height is around 34-57 nm. Similar observations of collapsed hollow vesicles on silicon wafers were reported earlier for other types of vesicles or hollow structures.[159,228] According to the calculation, if a sphere with a diameter of 660 nm is stretched into a flattened out membrane, the diameter of the membrane should be 1050 nm, which is quite close to the 1.1 μm determined from the AFM imaging. If the amphiphilic $(C_4H_9O\text{-}Azo)_2$-PEG 2100 self-assembles into the proposed cell-like unilamellar bilayer vesicle, the thickness is calculated to be around 35 nm. It is also comparable with the thickness determined by AFM imaging (34-55 nm). The dimension of the particles measured from AFM images is consistent with that of the proposed vesicle structure. TEM images of $(C_4H_9O\text{-}Azo)_2$-PEG 2100 vesicles in DI water under a dark-adapted state ($\mathbf{S_{VIS}}$) and after UV irradiation ($\mathbf{S_{UV}}$) (**Figure 5-7**) also indicate size shrinkage after UV irradiation. Thus, the unilamellar bilayer structure of the vesicle via self-assembled $(C_4H_9O\text{-}Azo)_2$-PEG 2100 in DI water is fully confirmed. For the samples self-assembled in 0.015 M KCl salt solution, the flattened particles under $\mathbf{S_{VIS}}$ are as large as 1.1 μm~2 μm, while their heights are between 213 to 452 nm. The vesicles under $\mathbf{S_{UV}}$ shrink to 752-878 nm, and the thickness is around 40-60 nm. The dimensions of the self-assemblies in 0.015 M KCl salt solution also suggest the vesicle structure.

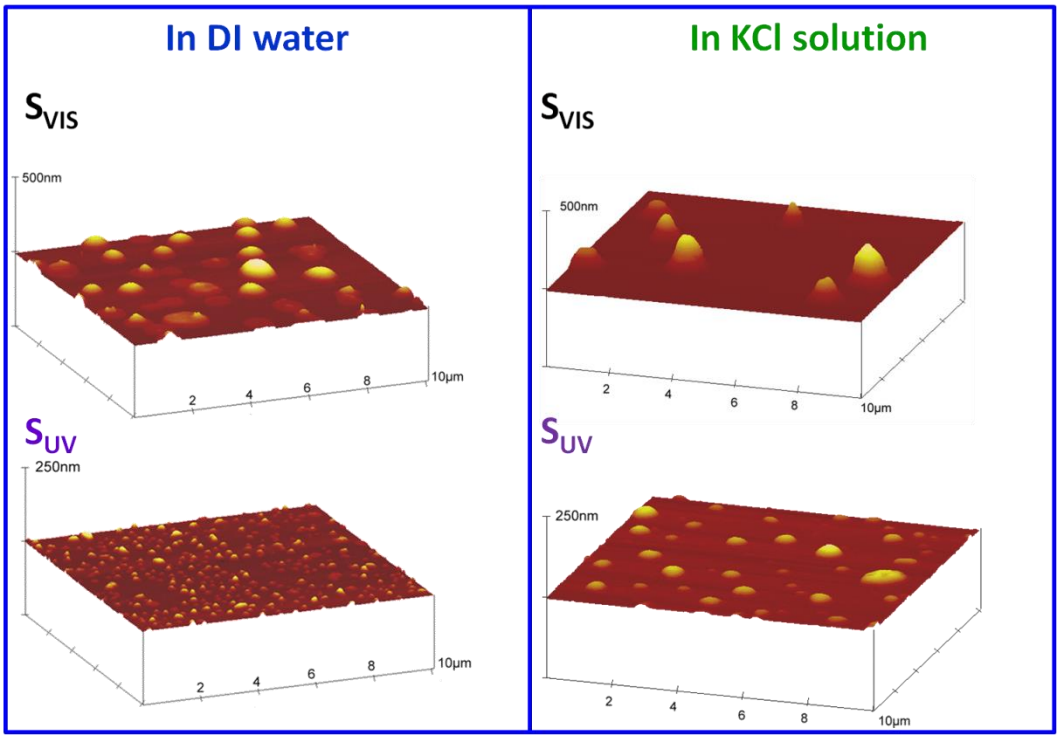

Figure 5-6 AFM images of $(C_4H_9O\text{-}Azo)_2$-PEG 2100 vesicles self-assembled in DI water (Left) and in 0.015 M KCl salt solution (Right). Their photo-stationary states after dark-adapted treatment (S_{VIS}) and after UV irradiation (S_{UV}) are characterized.

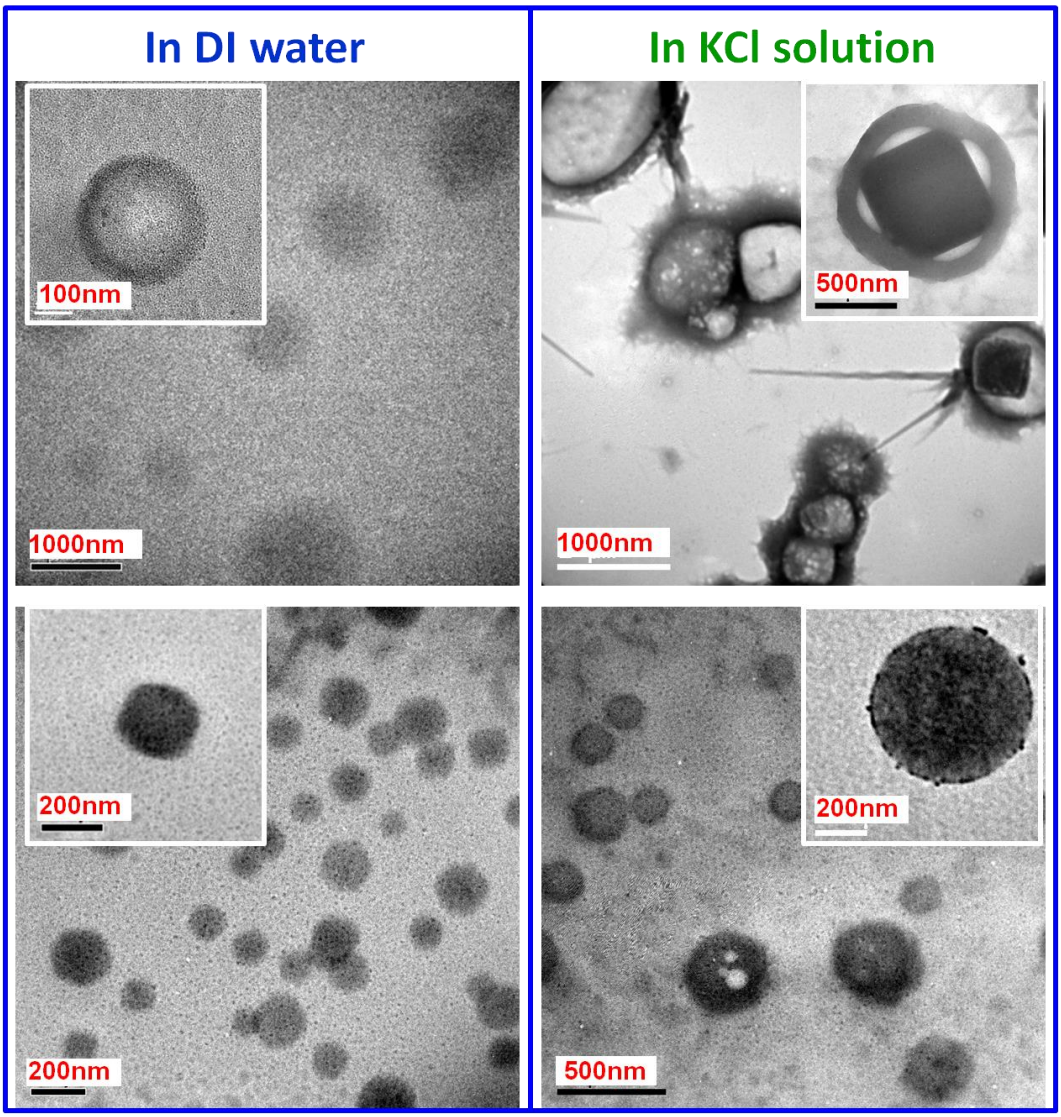

Figure 5-7 TEM images of $(C_4H_9O\text{-Azo})_2$-PEG 2100 vesicles self-assembled in DI water (Left) and in 0.015 M KCl salt solution (Right).

5.2.4 Investigation of vesicle membrane permeability and ion selectivity

According to **Table 5-2** and discussion thereafter, the integrity of the vesicles can be well preserved while their size changes. The volume change of the vesicles in DI water is up to 8 times with their diameter changing from 667 nm to 330 nm (volume=π/6 D^3). The volume change of the vesicles in 0.015 M KCl solution is about 5 times with their diameter changing from 929 nm to 638 nm during the repeating cycles between $\mathbf{S_{VIS}}$ and

S_{UV}. It was anticipated that the only possibility is the transport of a large amount of liquid through the vesicle membrane during alternating visible and UV light irradiation. A membrane separation function was proposed as a potential application in Chapter 4. However, for the system studied in Chapter 4, a limitation arises due to the usage of THF as the inner layer of the vesicle. By tuning the molecular structure, the $(C_4H_9O\text{-}Azo)_2$-PEG 2100 vesicle can self-assemble in DI water and salt solution with a similar robustness and a comparable size change. In the next step, the permeability of the vesicle membrane was studied. The first choice for characterization is using the stopped-flow technique. However, the light scattering signal of the stopped-flow tests was influenced by the fluorescence signal intrinsically emitted from the azo-PEGs self-assembly. Therefore, it was unable to produce accurate information about the membrane permeability. Hence an alternative method, i.e., electrolytic conductivity measurement, was used to study the transport-related properties of $(C_4H_9O\text{-}Azo)_2$-PEG 2100 vesicles in different salt solutions during the UV-visible irradiation cycle. The measured electrolytic conductivity can be correlated to the salt (e.g., KCl) concentration outside the vesicles. By monitoring the conductivity value during the UV-visible cycle, we could probe the water transport and salt rejection of the vesicle membrane. The change in salt solution concentration under pulsation cycles was directly visualizable by the corresponding change in the conductivity under UV-visible irradiation. The photo-driven behaviour of $(C_4H_9O\text{-}Azo)_2$-PEG 2100 vesicles in different salt solutions with different concentrations was studied. The quantitative analysis of the change in electrolytic conductivity in different salt solutions across the membrane is summarized in **Table 5-3** that shows different electrolytic conductivities outside the vesicle membrane before and after UV-irradiation. The conductivity difference suggested a solvent exchange across the vesicle membrane when it was in the **S_{UV}** photo-stationary state. Within the conditions used in

our experiments, the salt concentration does not play a key role in the electrolytic conductivity difference.

Table 5-3 The electrolytic conductivity and corresponding concentration data of the $(C_4H_9O\text{-}Azo)_2$-PEG 2100 vesicle in different salt solutions under both the S_{VIS} and S_{UV} photo-stationary states. The concentrations of the salt solutions were varied from 0.005 M to 0.015 M.

Salt	Concentration of salt solution (M)	Conductivity of salt solution without vesicles (mS/cm)	Conductivity of salt solution with vesicles (mS/cm)*	
			$\kappa_{Svis(OUT)}$	$\kappa_{Suv(OUT)}$
KCl	0.005	0.703	0.754±0.009	0.690±0.008
	0.01	1.413	1.426±0.006	1.298±0.020
	0.015	1.995	2.103±0.015	1.922±0.018
NaCl	0.005	0.589	0.627±0.009	0.587±0.010
	0.01	1.185	1.211±0.021	1.126±0.013
	0.015	1.668	1.714±0.092	1.605±0.092
LiCl	0.005	0.534	0.560±0.001	0.529±0.003
	0.01	1.073	1.084±0.017	1.020±0.015
	0.015	1.532	1.580±0.026	1.483±0.017

*$\kappa_{Svis(OUT)}$ and $\kappa_{Suv(OUT)}$ are the salt electrolytic conductivities of the salt concentration outside the vesicle membrane at the dark-adapted and UV-irradiated photo-stationary states, respectively.
**Conductivity of salt solution with vesicles is higher than that of salt solution without vesicles caused by the salt in the azo-PEGs, which is the impurity from synthesis. The conductivity of the vesicles with a comcentration of 1mg/ml in DI water is 0.02 ms/cm.

The electrolytic conductivity change is mainly caused by the water flux transported across the vesicle membrane upon UV exposure. This photo-induced electrolytic conductivity change is repeatable for at least 5 cycles for samples in different salt solutions (**Figure 5-8**).

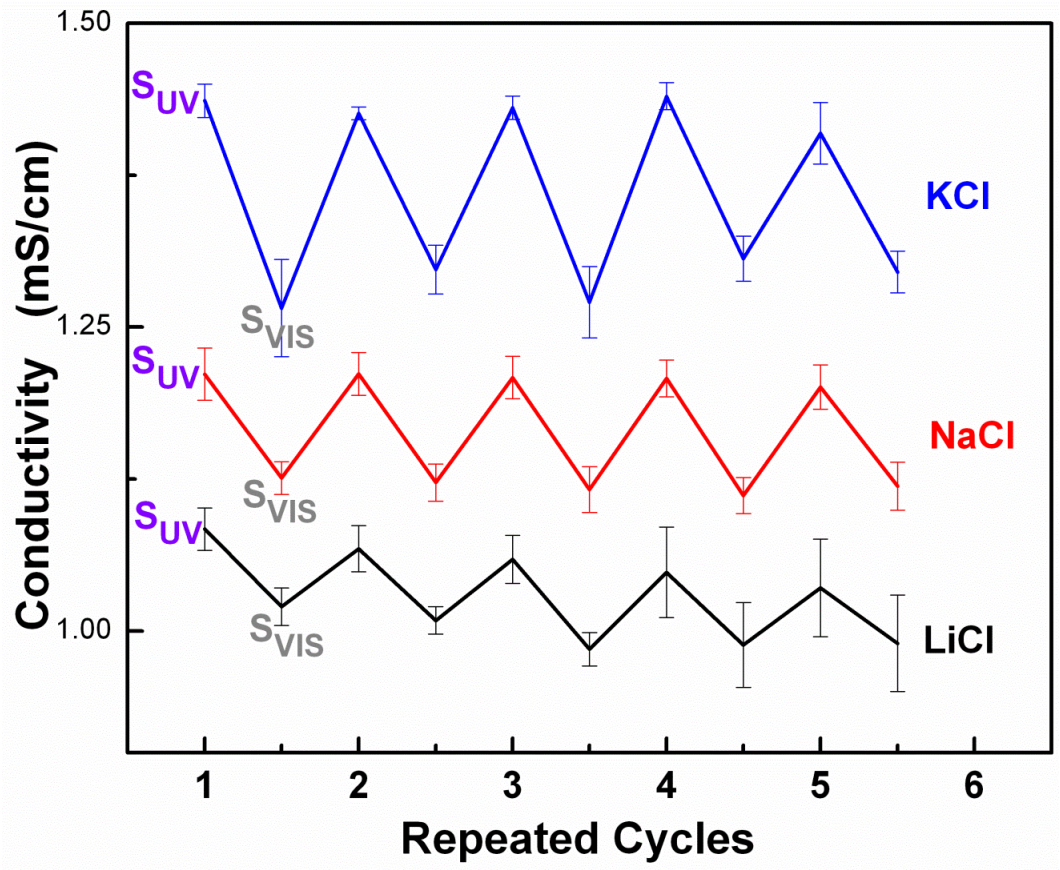

Figure 5-8 The repeated electrolytic conductivity changes outside the $(C_4H_9O\text{-}Azo)_2$-PEG 2100 in 0.01 M KCl, NaCl, and LiCl solutions (polymer concentration 1 mg/mL).

5.3 Conclusions

In this chapter, mono-dispersed self-assembled vesicles in aqueous solution were prepared from photo-responsive lipid-like molecules based on azobenzene end-capped PEG. The shortening of the PEG chain length contributed to the successful vesicle assemble in pure water, previously only achievable in THF/water mixed solvent. The azobenzene groups act as a photo-trigger to allow formation of water channels within membrane. In the presence of salts, such as potassium chloride (KCl), a selective permeation of the vesicles results in a unique electrolytic conductivity gradient across the membrane. During the UV irradiation, water is effectively transported from interior to the exterior of the vesicles. The membrane vesicles are sufficiently robust during the UV-

visible light irradiation cycles, going through generation of the electrolytic conductivity gradient during the UV cycle and size recovery during the visible light cycle. Similar observations were made when different salts were used. The reduction in the conductivity demonstrates the dilution of the salt concentration outside the vesicles. This demonstrates the possiblities of using the vesicles for separation processes by the selective transport of water from inside to outside of the vesicle membrane while screening the salt ions inside the vesicle membrane. The vesicles in the mimicked cells possess built-in artificial channels for trans-membrane solvent transport that can be regulated by photo-irradiation. Such vesicle membranes with photo-controllable pulsating water channels provide many promising applications in membrane separations.

6 INVESTIGATION OF SELF-ASSEMBLY BEHAVIOUR OF STAR-SHAPED AZO-PEGS IN SOLUTION

6.1 Introduction

6.1.1 Self-assembly of multi-arm polymers

The significant progress in polymer synthesis over past decades has enabled creation of new polymers with various novel architectures. Examples of such polymers with sophisticated structures include dendrimers,[229,230] cyclic copolymers,[231,232] and multi-arm polymers (**Figure 6-1**). The conceptual methodologies to obtain well-defined star polymers have been established, e.g., the arm-first methodology using living anionic polymerization.[229] The relationship between molecular architecture and self-assembly has received progressively more attention as various types of star polymers have been reported.

There are many studies on the multi-arm polymers, such as star-branched polymers, H-shaped polymers and 'palm-tree' polymers.[229,233] Theoretical studies on the micellization models of multi-arm polymers have been developed. **Figure 6-2** shows the theoretical model of polystyrene-polyisoprene star-shaped copolymers.[233]

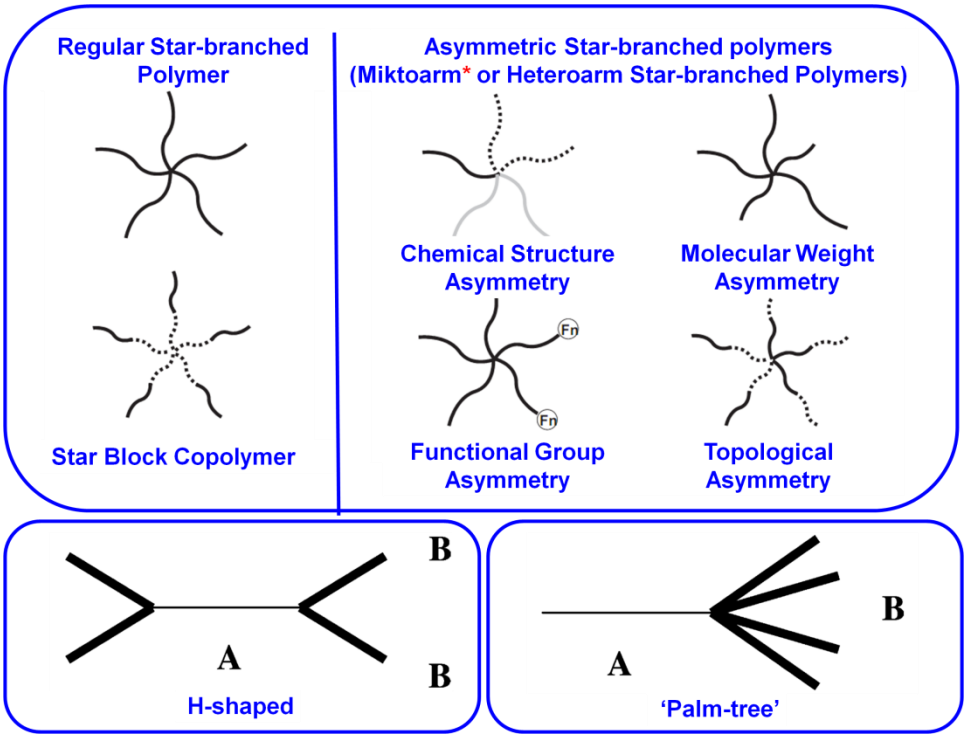

Figure 6-1 Schematic representations of major types of multi-arm polymers.[229,233] *Miktoarm star-branched polymer is a special class of asymmetric star-branched polymer with various molecular weighs or chemically different branch chains radiating from the same central core.

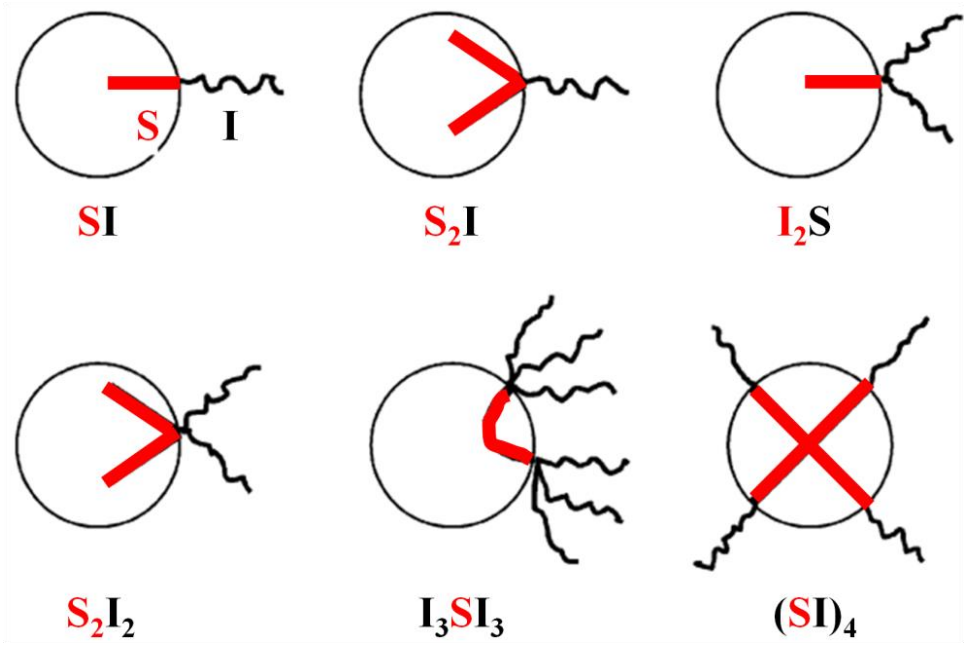

Figure 6-2 Illustration of micellar structures of polystyrene (S)-polyisoprene (I) multi-arm polymers.[233]

Block copolymer self-assemblies have been studied for their potential applications in drug delivery, encapsulation of catalysts and in sensing devices. However, the majority of the studies deal with the linear di-block copolymers or tri-block copolymers. Recently, the multi-arm amphiphilic polymers have received more attention for several reasons. First, their architectures are less entangled. Thus, compared to linear polymers, the multi-arm polymers have lower viscosity, lower glass transition temperature, and higher solubility.[229,234-236] It is also important that more functional end groups can be introduced into the multi-arm polymers. The study on the multi-arm polymers, such as self-assembly behaviour, therefore, is very interesting from a theoretical viewpoint. Another advantage is their increased stability when self-assembled into aggregations with different morphologies.[232] It is also essential to study the multi-arm polymer self-assemblies from a practical pointview. By tuning the architecture of the multi-arm polymers, such as the length of hydrophilic/hydrophobic blocks and the functional end-groups, their self-assemblies can be used for well-designed drug delivery systems.

For the four-arm polymers, polymeric self-assemblies with tunable architectures were reported. K.C. Tam *et al.* synthesized a four-arm poly(ethylene oxide)-b-poly(methacrylic acid) (PEO-b-PMAA) that exhibits pH-responsive association behaviour.[237] The star-shaped polymer self-assembled into core-shell micelles with variable sizes under different degrees of neutralization (α): 46 nm at α = 0.1, 63 nm at α = 0.2, and 84 nm at α = 0.3. When α was lower than 0.02, larger spherical aggregation appeared because of the hydrogen bonding between methacrylic acid groups.

Karel Prochazka *et al.* reported a similar investigation on star polymers. They studied two different four-arm copolymers of poly(ε-capro-lactone)-block-poly(ethylene oxide) [$(PCL–PEO)_4$] and polylactide-block-poly(ethylene oxide) [$(PLA–PEO)_4$]. It was found that the $(PLA–PEO)_4$ four-arm copolymers self-assembled into micelles with core/shell

flower-like structures, while the $(PCL–PEO)_4$ associated into large aggregates with interconnected individual micelles.[238]

6.1.2 Scope and objectives

In the Chapter 4 and 5, the studies on the linear PEG polymers end-capped with rigid and hydrophobic azobenzene groups revealed several interesting phenomena. It is postulated that the change in molecular shape from linear to star-shaped will provide more complicate self-assembly behaviour. However, the studies of the star-shaped polymers have been far less extensive compared to those of the linear polymers. Therefore, in this chapter, we shall discuss the unique self-assembly behaviour of azobenzene end-capped four-arm PEG.

6.2 Results and Discussion

6.2.1 Self-assembly of azobenzene end-capped four-arm PEG in aqueous solution

This section aims to discuss the diversified morphologies of four-arm Azo-PEG self-assembled in aqueous solution together with our proposed most plausible formation mechanisms. Because the polymer architecture directly influences the resultant aggregate morphology, this study started by screening the self-assembly behaviour of azo-PEGs with different molecular designs, i.e., (i) linear azo-PEGs with different PEG chain lengths, and (ii) four-arm azo-PEGs in an aqueous environment. The self-assembly behaviour of different azo-PEGs in aqueous solution was monitored by DLS analysis, and the results are summarized in **Table 6-1**.

Table 6-1 The DLS results showing self-assembly of different azo-PEGs in aqueous solution

	Sample	Concentration (mg/ml)	Intensity (Kcounts)	D_h (nm)	PDI	Self-assembly in DI water
One end-capped linear azo-PEGs	C_4H_9O-Azo-PEG 5000-OMe	5	42.8	1190.7	1.592	Random aggregated
Two end-capped linear azo-PEGs	$(C_4H_9O$-Azo$)_2$-PEG 2100	1	270	667	0.05	Good Single-modal
	$(C_4H_9O$-Azo$)_2$-PEG 4600	1	16.2	/	/	Dissolution
	$(C_4H_9O$-Azo$)_2$-PEG 9800	40	9.2	/	/	Dissolution
Four end-capped four-arm star azo-PEGs	$(C_4H_9O$-Azo$)_{4ARM}$-PEG 6700	1	82.7	570.6	0.293	Good Bimodal
	$(C_4H_9O$-Azo$)_{4ARM}$-PEG 10000	40	37.7	577.5	0.397	Poor
	$(C_4H_9O$-Azo$)_{4ARM}$-PEG 20000	40	15.2	1261	1.008	Poor

The PEG with only one chain-end capped with an azobenzene derivative, i.e., C_4H_9O-Azo-PEG 5000-OMe, cannot self-assemble into regular structures. Since the wide PDI is larger than 1.5, it experiences the problem of weak hydrophobic interaction.

For the PEG with both chain-ends capped with an azobenzene derivative, a well-known theory makes a good explanation for our experimental results. Theoretically the ratio of the hydrophilicity to hydrophobicity plays key factor for polymeric self-assembly. From the investigation in Chapter 4, it has been confirmed that $(C_4H_9O$-Azo$)_2$-PEG 4600 could readily self-assemble in a THF/water mixed solvent and the azobenzene groups were inside THF-rich phase. According to the studies in Chapter 5, it was found that (C_4H_9O-

Azo)$_2$-PEG 2100 could successfully self-assemble into vesicles. The shorter PEG chain length can induce self-assembly in aqueous solution due to higher hydrophobicity to hydrophilicity ratio. From the results in **Table 6-1**, when the PEG chain length increases (e,g., (C_4H_9O-Azo)$_2$-PEG 4600 and (C_4H_9O-Azo)$_2$-PEG 9800), there is no inefficient self-assembly formed since the increased hydrophilicity favors the azo-PEGs dissolution in aqueous solution. For the four-arm azo-PEGs, self-assembly can only be achieved for (C_4H_9O-Azo)$_{4ARM}$-PEG 6700 in aqueous solution.

The subsequent section discusses in detail the self-assembly behaviour of a four-arm (C_4H_9O-Azo)$_{4ARM}$-PEG 6700 in aqueous solution. The same method as described in Chapter 3 was used to prepare (C_4H_9O-Azo)$_{4ARM}$-PEG 6700 self-assembly in DI water. Interestingly, in our experiment, three distinct morphologies were observed when 1 mg/mL (C_4H_9O-Azo)$_{4ARM}$-PEG 6700 self-assembled in aqueous solution (see **Figure 6-3** to **Figure 6-5**).

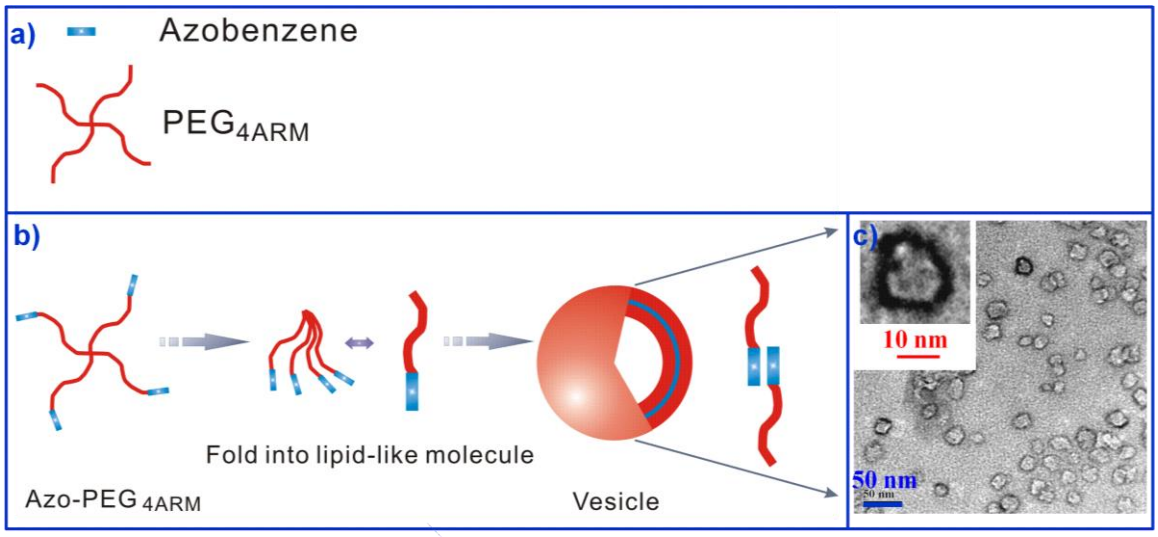

Figure 6-3 (a) The structure of four-arm azo-PEG. (b) The schematic illustrations of a self-assembled bilayer vesicle of four-arm azo-PEGs in aqueous solution. (c) TEM images of (C_4H_9O-Azo)$_{4ARM}$-PEG 6700 assemblies showing small vesicles (less than 20 nm).

As seen in **Figure 6-3 c**, the diameter for the small vesicles is ~20 nm and their thickness is less than 5 nm. Based on these dimensions, we propose a formation mechanism that is schematically illustrated in **Figure 6-3 a**. The four-arm azo-PEGs can fold into lipid-like molecules due to the aggregation of azobenzene end group. The lipid-like molecules subsequently self-assemble into bilayer vesicles in aqueous solution. The entangled PEG chain for PEG 5000 is ~ 4 nm. Thus, the thickness of the proposed bilayer structure is around 4 nm. This is consistent with the thickness observed from the TEM imaging which is less than 5 nm.

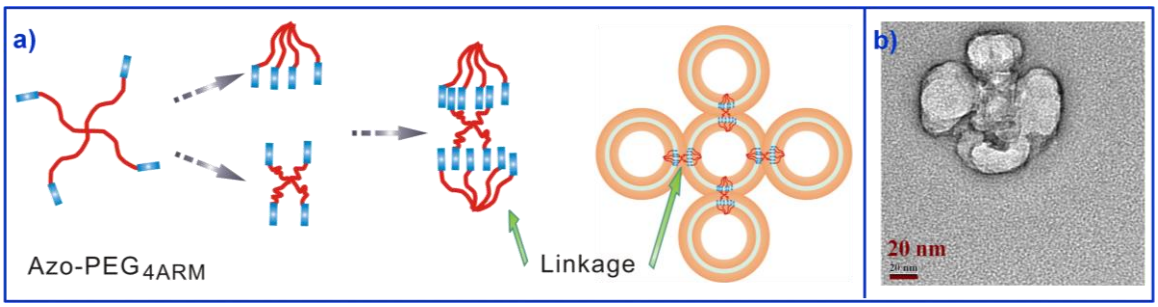

Figure 6-4 (a) Schematic illustration of flower-like aggregations via vesicles linked by the stretched four-arm azo-PEGs. (b) TEM image of (C_4H_9O-Azo)$_{4ARM}$-PEG 6700 assemblies showing flower-like aggregations via vesicles linked by the stretched four-arm azo-PEGs.

The proposed formation of the flower-like small aggregations with a diameter ~ 80 nm (see TEM image, **Figure 6-4 b**) is illustrated in **Figure 6-4 a**. In this case, the four-arm azo-PEGs chains are fully stretched with both ends containing functionalized azobenzene, acting as a linkage or bridge for both vesicles. The size of the flower-like small aggregations is ~ 80 nm, which is consistent with the dimension of the observed individual vesicle (~ 20 nm).

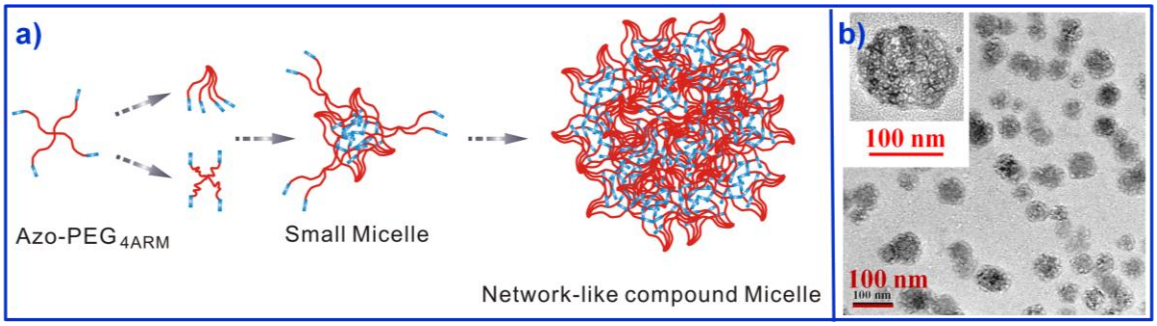

Figure 6-5 (a) Schematic illustration of network-like structure of 'sub-assembly' via small micelles linked by the stretched azo-PEGs as bridges. (b) TEM images of (C_4H_9O-Azo)$_{4ARM}$-PEG 6700 assemblies showing network-like aggregations.

The proposed formation mechanism of observed large aggregations with a diameter around 100 -150 nm (see TEM image, **Figure 6-5 b**) is illustrated in **Figure 6-5 a**. Firstly, the four-arm azo-PEGs self-assemble into small micelles. After that, the formation of large network-like aggregations is further induced by the stretched four-arm azo-PEGs (as described earlier) that provide inter-micellar linkages. The network-like structure is assumed to possess a microgel-like structure. The photo-responsive behaviour of the microgel-like structure is also very interesting and should be investigated in the future.

6.3 Conclusions

In this chapter, the self-assembly behaviour of four-arm azo-PEGs was investigated. The four-arm azo-PEGs can self-assemble into structures with different morphologies in aqueous solution, i.e., ~20 nm vesicles, ~80 nm flower-like aggregations, and ~150 nm network-like compound micelles. The four-arm azo-PEGs can act as a linkage to bridge small micelles into a network-like complex.

7 CONCLUSIONS, RECOMMENDED FUTURE WORK AND OUTLOOK

7.1 Conclusions

The summary of major findings and key proposed mechanisms is given in this chapter, accompanied by a brief discussion on the recommended future work. The project scope as defined clearly in Chapter 1 is to investigate the photo-responsive smart materials based on the azobenzene-based polymers. The end-capped lipid-like polymer, distinctly different from the widely studied di-block or tri-block copolymers, is believed to possess a simple structure that favours the mechanisms that has been discussed. It is interesting to combine interdisciplinary concepts related to biomimetic materials, smart materials, and self-assembly process into fabrication of controllable photo-driven polymeric self-assemblies.

7.1.1 Molecular design and synthesis of lipid-like azobenzene-based polymers

Azobenzene derivatives with different end groups were chosen as functional groups to modify the PEG polymer chains. The azo-PEGs with different molecular shapes, from linear to four-arm star-shaped, were successfully synthesized via an esterification between PEG and 2-bromo-2-methylpropionyl bromide, followed by further esterification with hydroxyl terminated azobenzene containing selected substituents. The synthesized azo-PEGs were found to be able to self-assemble in solution as they possess a hydrophilic PEG chain and two hydrophobic azobenzene end-groups. When they are dissolved in the solution, as the hydrophobic azobenzene moieties tend to gather together, the azo-PEGs can fold into a loop and act as a conventional lipid molecule. In this case, the azo-PEGs become lipid-like with non-polar heads (i.e., the azobenzene derivatives) and polar tails

(i.e., PEG chain). The simplicity of this molecular design enabled a clear understanding of the vesicle self-assembly mechanisms. The analysis is based on: (i) a thermodynamics viewpoint and (ii) the morphology change of molecules self-assembling via azobenzene photo-isomerization induced by UV-visible irradiation.

7.1.2 The photo-driven pulsating vesicles in mixed solvent and aqueous solutions

Specific focus is given to the photo-pulsating vesicles in both THF/water mixed solvent and aqueous solutions. On top of the self-assembly process driven by the hydrophobic groups, the azobenzene groups also act as photo-triggers that allows deformation of the assemblies. In this study, the azo-PEGs self-assembled vesicle is a photo-responsive system with a shape change originating from the morphology change of the molecular assembly based on the *trans-cis* photo-isomerization of azobenzene. The large size change is associated with significant trans-membrane solvent transport, which is sensitive not only to the degree of isomerization but also to the para-position substituents on the azobenzene. This process is believed to mimic the water pumping function of the bacteriorhodopsin protein in the purple membranes. The term 'photo-driven pulsation' is used to describe this process and has been cited as an example of a photo-triggered pulsating vesicle.[215] It is noted that this photo-driven vesicle is structurally strong enough to experience several cycles of UV-visible irradiation (at least 5 times) with solvent being repeatedly pumped in or out of the vesicles. The vesicles have the potential to be used as biomimetic membranes for various separation processes. The further investigation of azo-PEGs vesicles in different dilute salt solutions confirmed the possibility that these photo-driven vesicles possess water channels with ion-selectivity.

7.1.3 The micellization behaviour of star-shaped azo-PEGs with or without linear azo-PEGs vesicles in aqueous solution

The star-shaped azo-PEGs could self-assemble into different structures from small vesicles to network-like compounds in aqueous solution. With the addition of linear azo-PEGs, polymer-induced micellization was observed. If the photo-trigger is introduced, more interesting phenomena should be observed. The network-like compounds could be a photo-responsive gel-like system that could release encapsulated cargo under UV-visible irradiation. The mixture micellization system will also display special photo-responsive behaviour such as aggregation and disggregation upon UV-visible irradiation. This suggested for future work.

7.2 Recommended future work

7.2.1 Host-guest inclusion interaction between azobenzene and cyclodextrin (CD)

Cyclodextrin (CD) with a characteristic hydrophilic exterior surface and hydrophobic interior cavity (**Figure 7-1**) can accommodate a wide range of molecules as guests including azobenzene.[239] It have been confirmed that α-CD forms a stable inclusion complex with azobenzene in the stoichiometry of 1:1.[156]

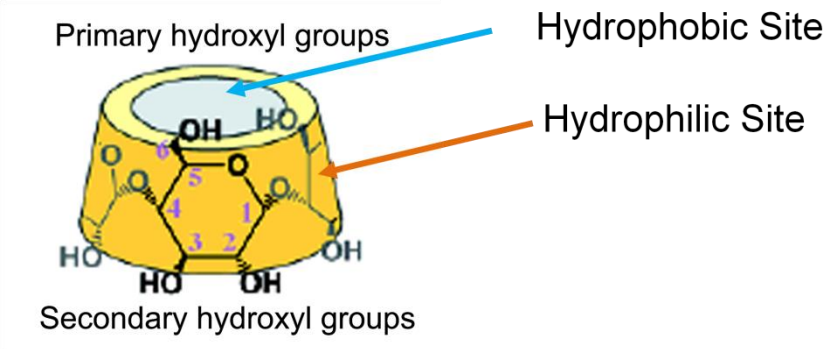

Figure 7-1 Structure of cyclodextrin with a hydrophilic exterior surface and a hydrophobic interior cavity.

Recently, host-guest inclusion interaction has been introduced as a driving force for a self-assembly process. A reversible sol-gel transition has been reported in various systems. For example, azobenzene-functionalized HPMC (AZO-HPMC) polymers can form complexes with α-CD in aqueous solutions that exhibited a photo-regulated sol-gel transition.[102] When the inclusion interaction was further introduced into 'organic/inorganic nanocomposites', an interesting responsive hybrid hydrogel was reported based on the complex of cyclodextrin modified graphene and an azobenzene end-functionalized copolymer, i.e., poly-(N,N-dimethylacrylamide)-b-poly(N-isopropylacrylamide) (AZO-PDMA-b-PNIPAM).[240] The host-guest inclusion interaction can also induce the reversible aggregation of gold nanoparticles as reported by Li and Jiang.[241]

7.2.2 Azobenzene modified surfaces with photo-driven wettability

Surfaces with specially designed wettability have attracted great interest due to their wide applications in industry and agriculture.[52] Smart surfaces with switchable wettability have been achieved based on various external triggers including pH,[242] temperature[243] and light-irradiation.[244] Azobenzene is a good candidate for photo-responsive smart surfaces due to the different dipole moments of *trans* and *cis* isomers triggered by UV-visible irradiation. Such photo-switchable wettability has been realized in monolayers,[245] Langmuir–Blodgett (LB) films,[246] and electrostatically layer-by-layer (LBL) self-assembled thin films based on azobenzene.[247] Kiwon Cho *et al.* fabricated a photo-responsive smart surface by electrostatically LBL self-assembled film of poly(allylamine hydrochloride) / SiO_2 modified with fluorinated azobenzene molecules. This smart surface can change from super-hydrophobicity to super-hydrophilicity under UV-visible irradiation.[248]

7.2.3 Preliminary study on azobenzene modified surface with photo-driven wettability

Recently, smart surfaces with photo-controllable wettability have drawn increasing attention in surface science. Azobenzene modified films are considered as good candidates for optical storage devices and photo-switchable bio-sensors. It is well-known that when azobenzene changes from the *trans* state to the *cis* state, the size of the molecule decreases from 9.0 Å to 5.5 Å. Its dipole moment also increases from 0.5 to 3.1 Debye, along with the loss of molecular planarity. These property differences between the *trans*- and *cis*-isomers lead to the different surface wettability. In the presence of α-CD, the *trans*-azobenzene moieties form inclusion complexes with equivalent α-CD by hydrophobic and van der Waals interactions.

This thesis work deals more with the self-assembly of azo-PEGs in the solution phase. The proposed future work will focus on photo-responsive surfaces via self-assembly assisted by the host-guest inclusion interaction between azobenzene and cyclodextrin.

The preliminary study on an azobenzene modified surface with photo-driven wettability has been done. The mono-6-thiol-α-cyclodextrin (SH-α-CD, supplied by Duan HW group, NTU) formed a tightly packed monolayer on a gold coated substrate (see **Figure 7-2 a**). The α-CD coated substrate was immersed in the 50 mg/ml $(C_4H_9O\text{-}Azo)_{4ARM}$-PEG 6700 supersaturated solution with vigorous stirring in the dark. After 3 days, the α-CD coated substrate was covered with azo-PEGs (denoted as the Azo-PEGs@α-CD surface) via the host-guest inclusion interaction of *trans*-azobenzene and α-CD (see **Figure 7-2 b**). As we know, the *cis*-azobenzene is unable to act as the guest of α-CD (due to change of dipole moment and morphology); moreover, it is more hydrophilic comparing to *trans*-azobenzene. Based on this mechanism, a concept of a photo-sensitive smart surface is proposed (See **Figure 7-3**). This photo-sensitive surface will be more hydrophilic upon

UV-irradiation. The wettability is reversed when visible light is employed. The smart surface can be simply prepared with facile chemical modification. In the reported systems, the electrostatic LBL self-assembly has been evaluated as a relatively simple and effective technique to construct a thin film, as compared to the chemisorption process and the Langmuir–Blodgett (LB) membrane. In our case, the methodology is a modified LBL self-assembly via an inclusion interaction.

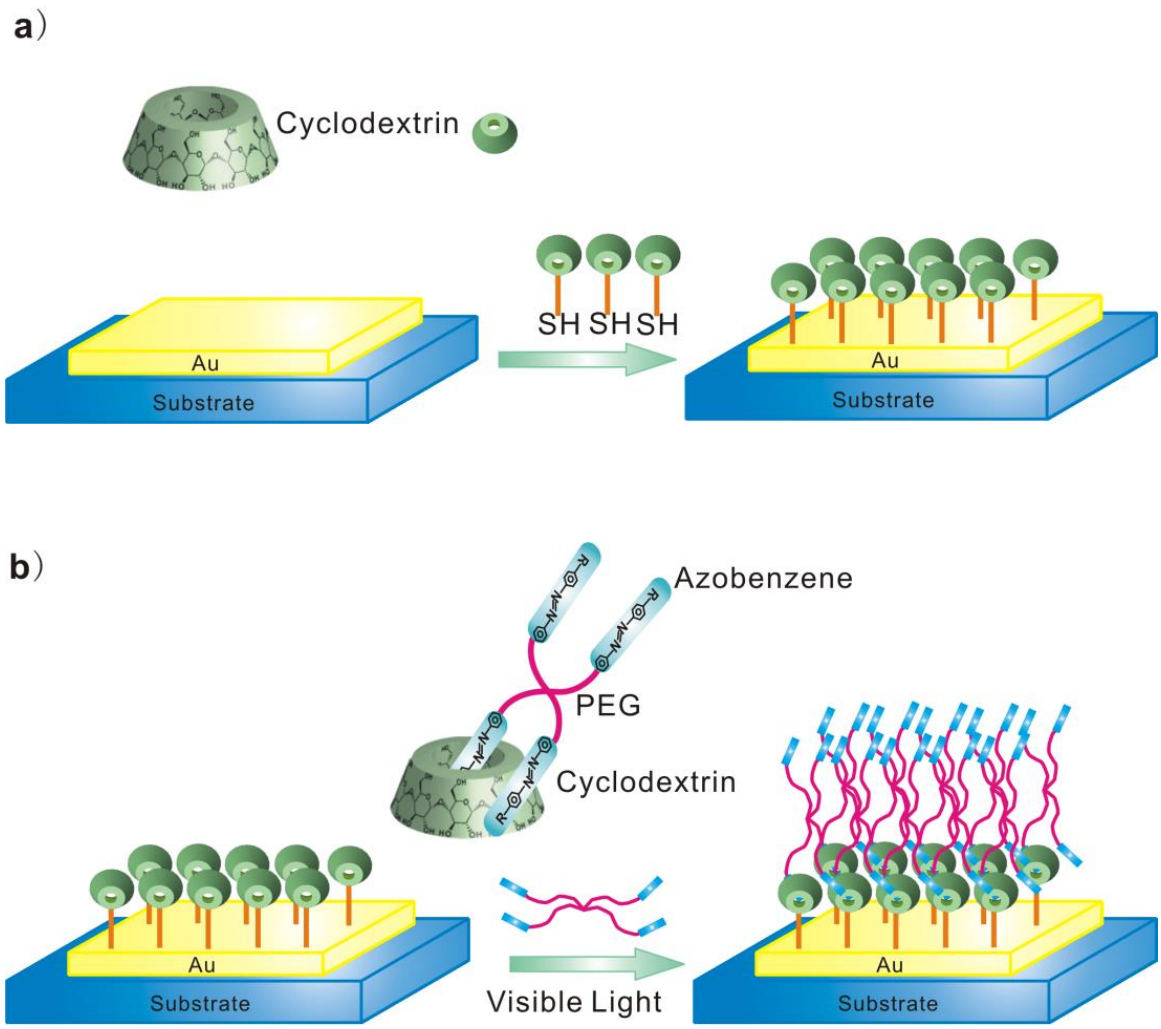

Figure 7-2 The schematic illustration of (a) α-CD immobilized onto a gold coated substrate via the interaction between the thiol group and gold, (b) the photo-responsive smart surface under S_{VIS} with *trans*-azobenzene inserted into the cavity of the α-CD via an inclusion interaction (denoted as the azo-PEGs@α-CD surface).

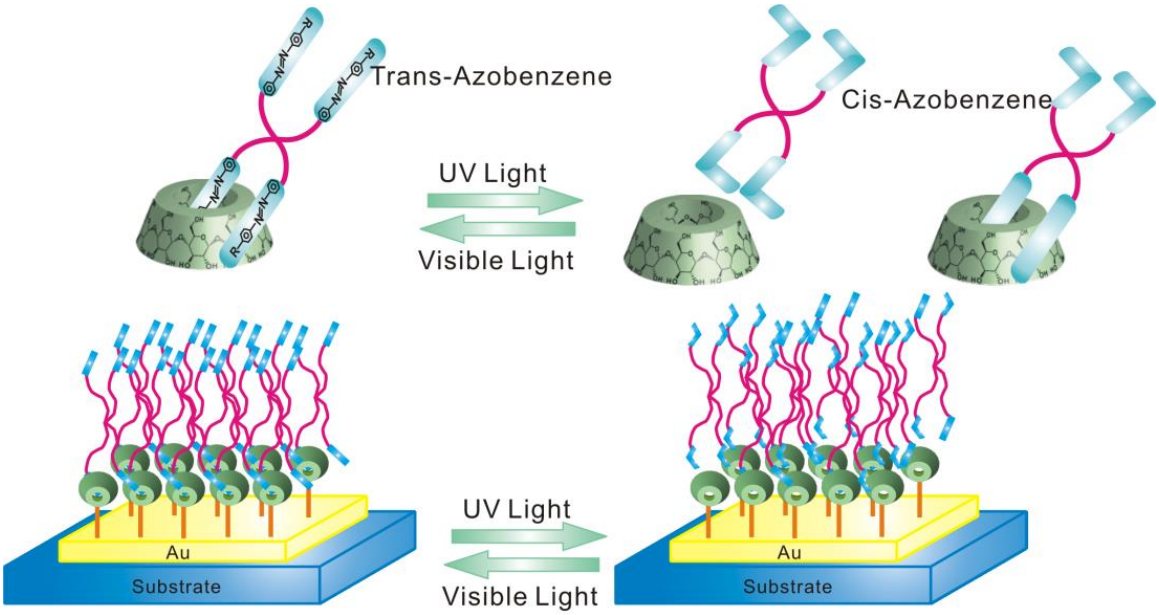

Figure 7-3 Schematic illustration of the photo-responsive smart surface.

The morphology of the substrate with immobilized α-CD and the self-assembled Azo-PEGs@α-CD surface was characterized by AFM (see **Figure 7-4**). The roughness of the surface under $\mathbf{S_{VIS}}$ (RMS=1.12, **Figure 7-4 a and b**) was higher compared with that after UV irradiation (RMS=0.96, **Figure 7-4 c and d**). The thickness of the surface changed from 2.5 - 4 nm under $\mathbf{S_{VIS}}$ to 1.5 - 3 nm under $\mathbf{S_{UV}}$. The reversible surface wettability was studied by measuring the water contact angle.

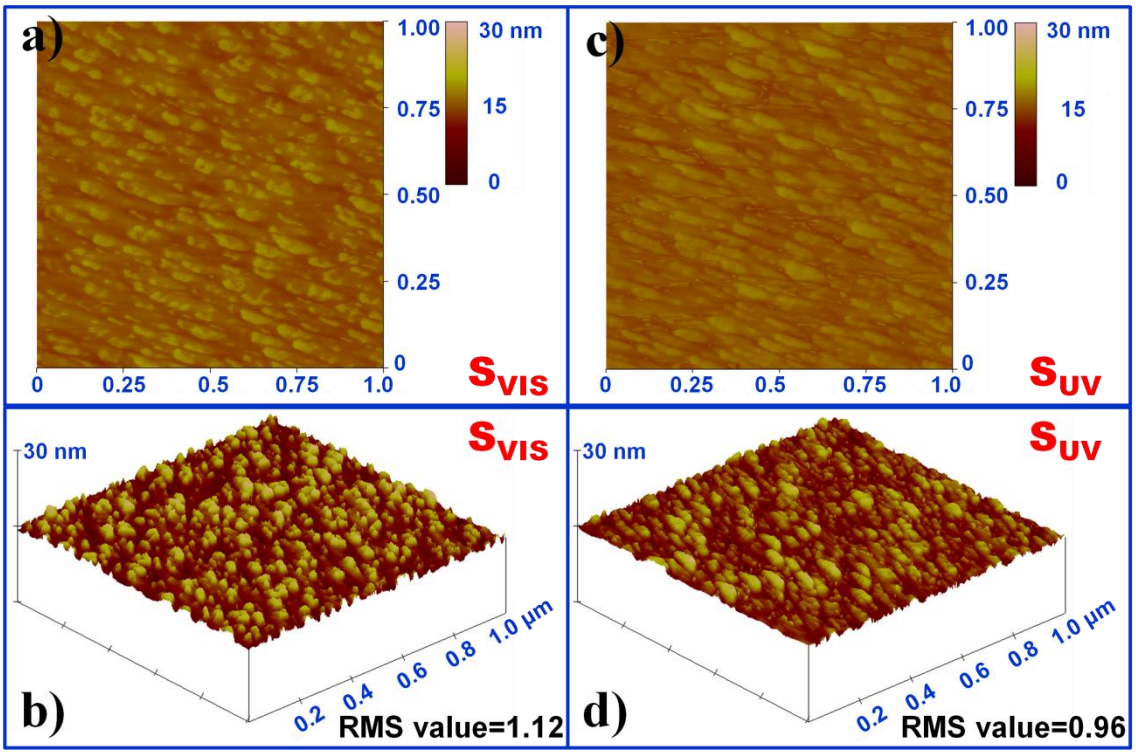

Figure 7-4 AFM image of a photo-responsive smart surface under (a) (b) S_{VIS}, and (c) (d) S_{UV}, respectively. The Root Meant Square (RMS) roughness for the surface under S_{VIS} and S_{UV} is 1.12 and 0.96, respectively.

The change of the water contact angles under $\mathbf{S_{VIS}}$ and $\mathbf{S_{UV}}$ is shown in **Figure 7-5**. A surface with a water contact angle > 65° is defined as hydrophobic.[249] The gold surface at 25 °C under room light was reported to be 57°.[250] The surface under $\mathbf{S_{VIS}}$ exhibited a hydrophobic property with a measured water contact angle of 91°. The surface under $\mathbf{S_{UV}}$ changed to more hydrophilic with a water contact angle of 45° upon UV-irradiation at 370 nm wavelength. The larger contact angle for the surface under $\mathbf{S_{VIS}}$ is consistent with the hydrophobic nature of *trans*-azobenzene. As for that of the surface under $\mathbf{S_{UV}}$, the larger hydrophilicity which leads to smaller water contact angle could be ascribed to the change of dipole moment from *trans*-azobenzene to *cis*-azobenzene.

Figure 7-5 Water contact angle of the photo-responsive smart surface in the cases under S_{VIS} and S_{UV}, respectively.

In comparison to the reported superhydrophobicity-to-superhydrophilicity system with an azobenzene derivative grafted onto the patterned substrate,[245] the result of this work does not appear to be fantastically striking at first. However, we would like to highlight that most studies on the water contact angle change based on simply a dipole moment change accompanied by azobenzene *trans-cis* isomerization only reported a change of ~10°.[246,251] The result of this work is quite interesting. In fact, in this work, when the *cis*-azobenzenes are expelled from the cavity of the α-CD, the diversification introduced by the host/guest inclusion complexes is more significant than the dipole moment change; this is associated with the change of the thin film morphology as observed in the AFM images (**Figure 7-4**). This morphology change may be brought about by the rearrangement of the azo-PEGs chains. As more PEG chains are exposed on the top of the surface, the surface hydrophilicity will increase. The scenario is schematically illustrated in **Figure 7-6**.

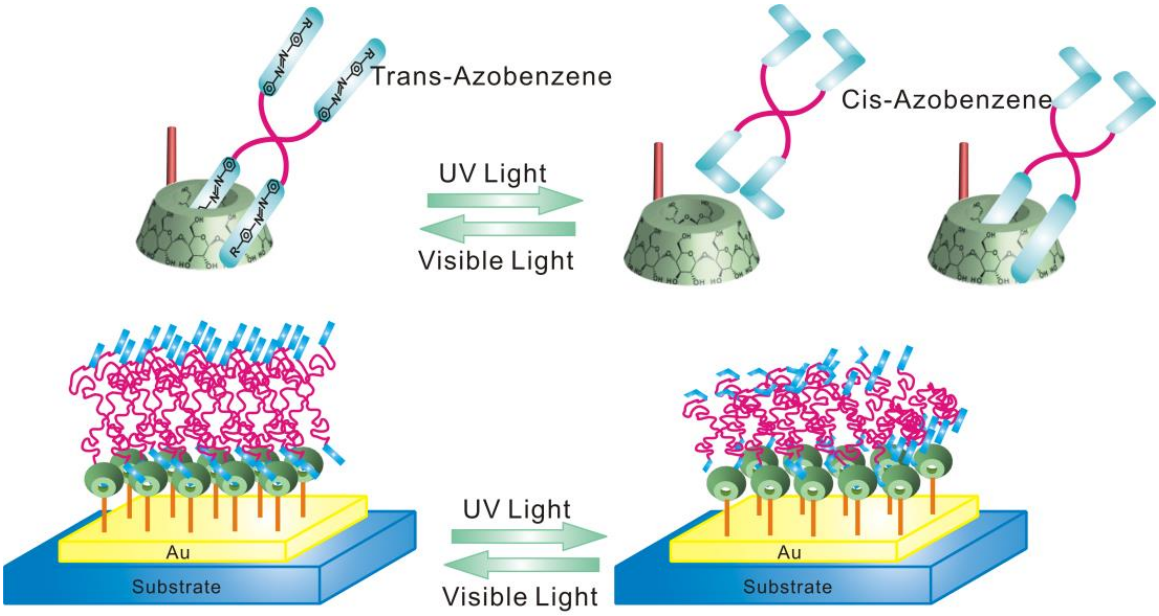

Figure 7-6 Schematic illustration of the photo-responsive smart surface based on the experimental investigation. After UV-irradiation, more PEG chains are exposed on the top of the surface, resulting in higher surface hydrophilicity.

We believe that this inclusion LBL strategy can be extended to a multi-layer structure if a polymer with both chain ends capped with CD is introduced into the system. It is also possible to design a patterned surface with selective-area grating of the α-CD with a thiol group to create patterned azo-PEGs@ α-CD smart surface. This prospective is recommended as future work, since much more work is needed to be done, such as studying the reversibility of the contact angle.

7.3 Outlook: biomimetic smart self-assembled materials

Smart materials, the Ithaca of most profound mystery in synthesis version, have attracted so much attention that progressively scientists have set sail to chase them. After decades of comprehensive investigation of molecular self-assemblies, it is now feasible to combine lessons from both nature and synthesis science to create higher-level smart material systems. Alice finds 12 ways to make herself grow and shrink to a particular size

in the Wonderland after she has fallen down into a rabbit hole. It is also amazing to scientifically make materials to change in size in response to different triggers.

Many artificial complex structures with novel functions have been achieved via self-assembly. However, synthetic science still pales in comparison to the marvels of nature. In an essay series published in celebrating the 125th anniversary of **Science** magazine in 2005, scientists brought up 125 big questions that will face scientific inquiry over the next quarter-century. Among the top 25 questions, 'How Far Can We Push Chemical Self-Assembly' was highlighted as the only urgent question to chemists. However, the concept and application of self-assembly is multi-disciplinary that requires the increased integration of knowledge in chemistry, biology and physics. The interdisciplinary efforts of scientists are needed to develop the hierarchical functional inorganic, organic, and biological materials. From the views of chemical and material engineering, there is growing interest in self-assembly at all levels, from the molecular level to the planetary level. One stimulating topic is to study nano-robots created through nanofabrication by a self-assembly process. The transfer of knowledge and techniques from self-assembly to netted systems (computers, sensors and controllers) remains a great challenge. Dynamic self-assembly is not well-understood and may provide great opportunities in the future. The ultimate goal is the ability to synthetically emulate the level of complexity and functionality of nature.

APPENDIX

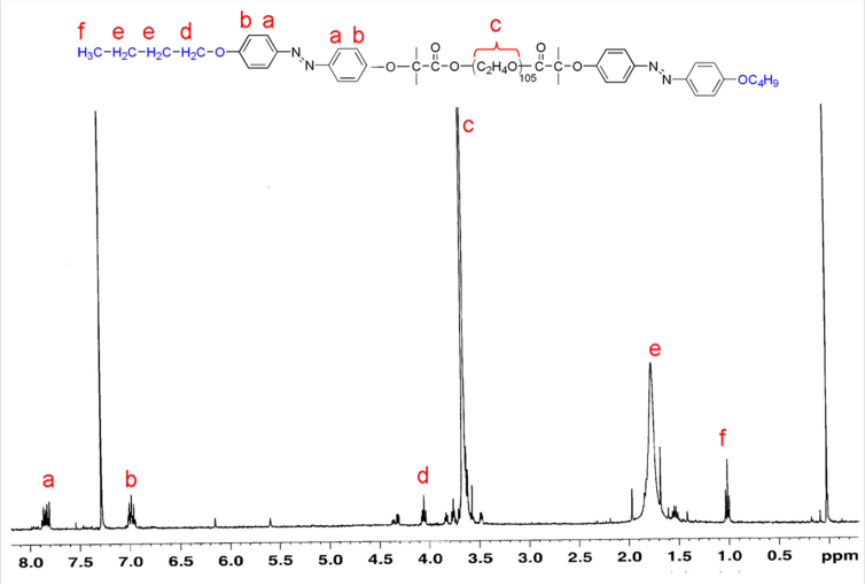

Figure A-1 **^{1}H-NMR spectrum of $(C_4H_9O\text{-Azo})_2$-PEG 4600 in $CDCl_3$ recorded by a Bruker DMX-400 spectrometer. The ^{1}H NMR spectra in $CDCl_3$ were: 4.35 ppm (t) (-OCH_2CH_2-OC=O), 3.66 ppm (s) (-OCH_2CH_2-)$_n$, 1.97 ppm (s) (-CH_3).[162] The chemical shift peaks at 7.6 and 8.0 ppm, which are assigned to the hydrogen on the azobenzene ring, clearly show the existence of azobenzene groups in the azo-PEGs.**

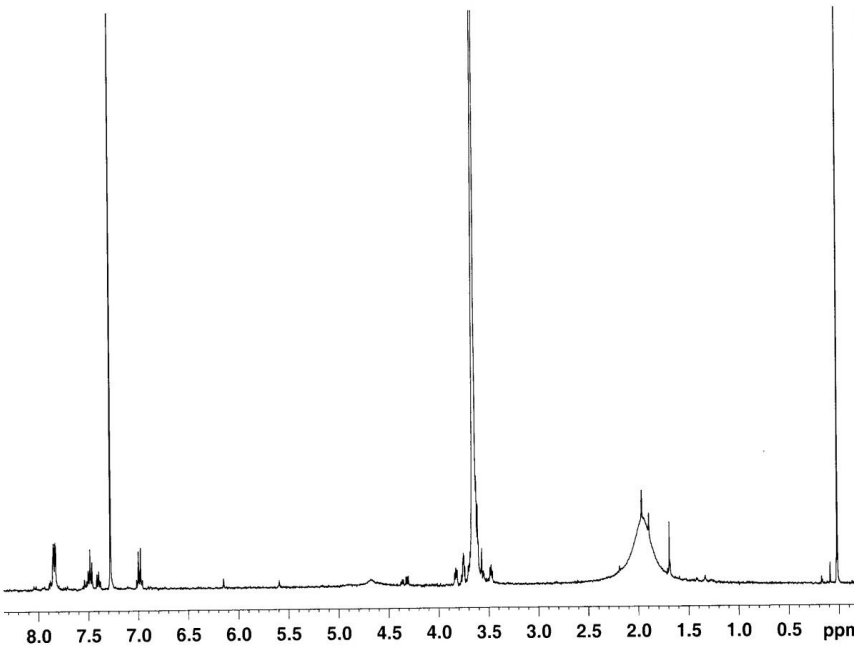

Figure A-2 **^{1}H-NMR spectrum of $(CN\text{-Azo})_2$-PEG 4600 in $CDCl_3$ recorded by a Bruker DMX-400 spectrometer which confirmed the successful synthesis of azobenzene-containing polymer.**

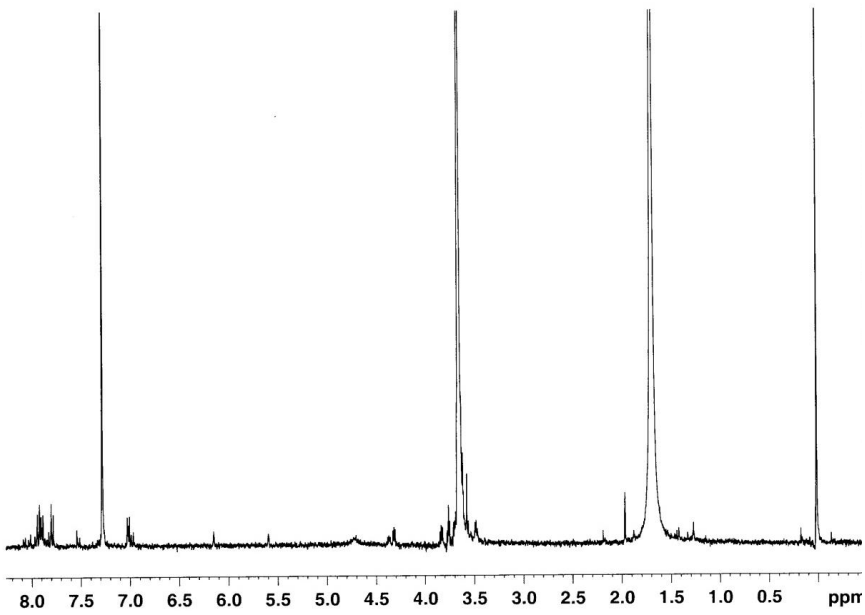

Figure A-3 **^{1}H-NMR spectrum of $(Azo)_2$-PEG 4600 in $CDCl_3$ recorded by a Bruker DMX-400 spectrometer which confirmed the successful synthesis of $(Azo)_2$-PEG 4600.**

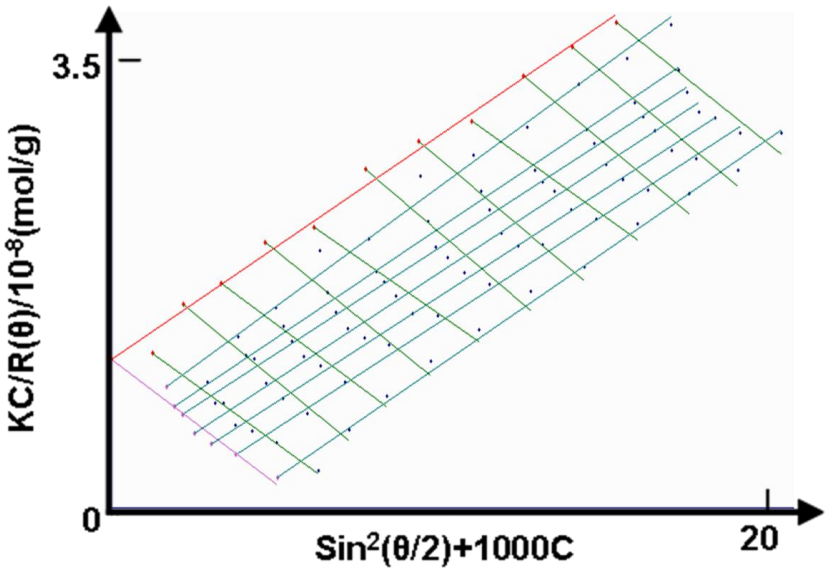

Figure A-4 **Zimm plot of aggregates formed from $(C_4H_9O\text{-}Azo)_2$-PEG in water/THF (volume ratio=4/1) with concentration range from 0.2-2.0 $\times 10^{-3}$ g/mL. According to the software calculation, the R_g of $(C_4H_9O\text{-}Azo)_2$-PEG vesicles in water/THF (volume ratio=4/1) was 318 nm. The M_W is 7.93×10^3.The data collected from the Zimm plot were summerized into Table 4-3.**

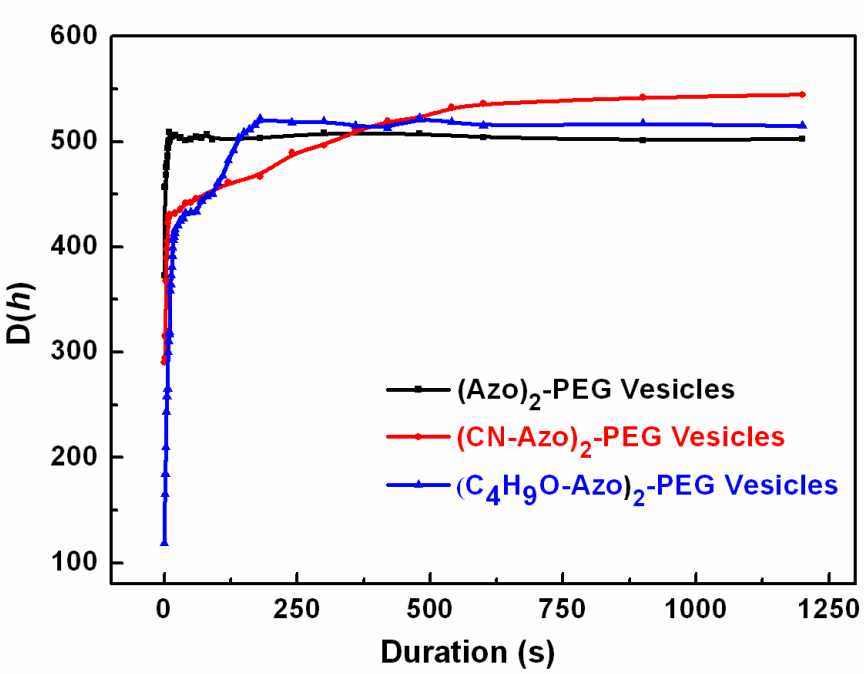

Figure A-5 **The continual size recovery through time-resolved DLS on the UV irradiated samples for three different kinds of azo-PEGs vesicles in THF/water (v/v 1/4).The continual size recovery is due to the fact that the probing laser wavelength of the DLS is in the visible region (488 nm or 633 nm), which causes *cis* to *trans* photo-isomerization during the DLS measurement, inducing the growth of a particle size up to the original diameter.**

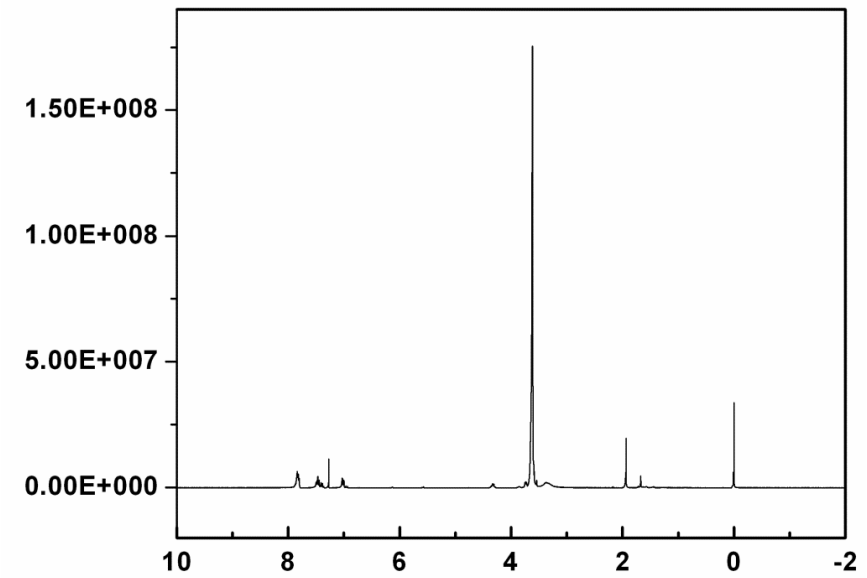

Figure A-6 **^{1}H-NMR spectrum of $(C_4H_9O\text{-}Azo)_2$-PEG 2100 in $CDCl_3$ recorded by a Bruker DMX-400 spectrometer which confirmed the successful synthesis of $(Azo)_2$-PEG 4600.**

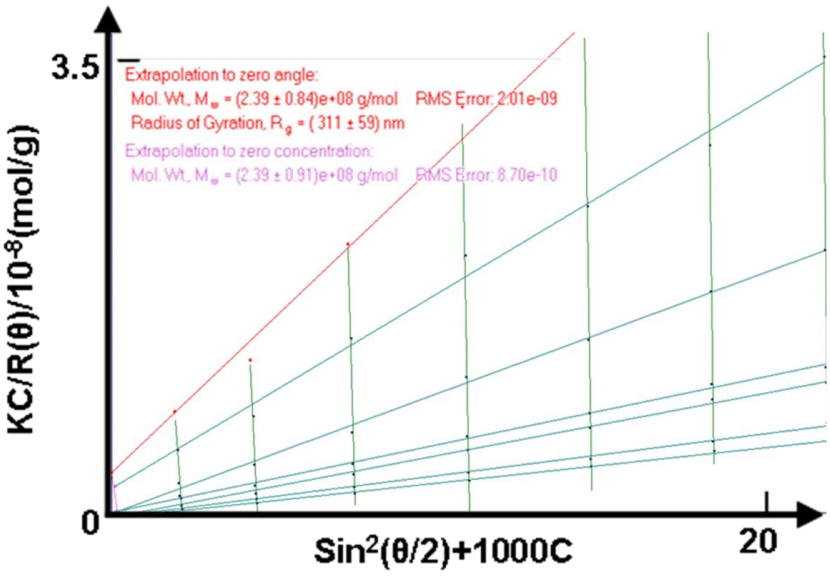

Figure A-7 Zimm plot of aggregates formed from $(C_4H_9O\text{-}Azo)_2$-PEG 2100 in water with concentration range from 0.1-1.0 $\times 10^{-3}$ g/mL. According to the software calculation, the R_g of $(C_4H_9O\text{-}Azo)_2$-PEG 2100 vesicles in water was 311 nm. The M_W is 2.39×10^8 g/mol.The data collected from the Zimm plot were summarized in Table A-1.

Table A-1 Summary of R_h, R_g, and aggregation number of PEG2100-$(C_4H_9O\text{-}Azo)_2$ vesicles in DI water from dynamic and static light scattering results and GPC results

$(C_4H_9O\text{-}Azo)_2$-PEG 2100	R_h		R_g/R_h (S_{VIS})	M_W g/mol (aggregates)	M_W g/mol (polymer)	$N_{aggregation}$ [b]
	S_{VIS}	S_{UV}				
In DI water	330 nm	165 nm	0.942	2.39×10^8	2.144×10^3	1.115×10^5

[a] Test on dark-adapted samples, [b] $N_{aggregation}=M_W(\text{aggregates})/M_W(\text{polymer})$

LIST OF PUBLICATIONS

1. **Jinhua Hu**, Hui Yu, Leong Huat Gan, and Xiao Hu, Photo-driven pulsating vesicles from self-assembled lipid-like azopolymers. *SOFT MATTER*, 7:11345-11350, 2011

2. Yen Nan Liang, **Jinhua Hu**, Kam Chiu Tam and Xiao Hu, *CuO_x Nanotubes via an Unusual Complexation Induced Block Copolymer-like Self-assembly of Poly(acrylic acid)*, *RSC Advances*, 2012,2, 9531-9537.

- **Manuscript:** "Photo-generated reverse osmosis in pulsating artificial membrane vesicles"
- Jinhua Hu, Yen Nan Liang, Wenming Shen, Ming Liu and Xiao Hu †,*
- In preparation (We have not yet decided the magazine to be submitted. There are some options including 'Nature Communications', 'Angewandte Chemie International Edition', 'Advanced Functional Materials' or 'Chemical Communications'.)

Conferences:

IUPAC 43rd World Polymer Congress, 2010, Glasgow, UK

Paper presented: "Unusual photo-driven size change in vesicles of azobenzene end-capped polyethylene glycol"

IUPAC 44rd World Polymer Congress, 2012, Virginia Tech Campus, Blacksburg, VA USA

Paper presented: 'Solvent Compartmentalization Study of Vesicles Self-assembled in Mixed Solvent'

REFERENCES

(1) Yu, S.; Azzam, T.; Rouiller, I.; Eisenberg, A. *Journal of the American Chemical Society* **2009**, *131*, 10557-10566.

(2) Huang, Z.; Kang, S.-K.; Banno, M.; Yamaguchi, T.; Lee, D.; Seok, C.; Yashima, E.; Lee, M. *Science* **2012**, *337*, 1521-1526.

(3) Berzelius, J. *Kungl. Svenska vetenskapsakademiens handlingar* **1830**, *49*, 49-80.

(4) "IUPAC Gold Book ". *PAC,* **1996**, 68, 2193 on page 2204

(5) "IUPAC Gold Book". *PAC,* **1996**, 68, 2193 on page 2203

(6) "IUPAC Gold Book". *PAC,* **1996**, 68, 2193 on page 1129

(7) Wasielewski, M. R. *Chemical Reviews* **2002**, *92*, 435-461.

(8) Doyle, D. A.; Cabral, J. M.; Pfuetzner, R. A.; Kuo, A. L.; Gulbis, J. M.; Cohen, S. L.; Chait, B. T.; MacKinnon, R. *Science* **1998**, *280*, 69-77.

(9) Kuhlbrandt, W. *Nature* **2000**, *406*, 569-570.

(10) Nagarajan, R.; Ganesh, K. *Journal of Chemical Physics* **1989**, *90*, 5843-5856.

(11) Whitesides, G. M.; Grzybowski, B. *Science* **2002**, *295*, 2418-2421.

(12) Bensaude-Vincent, B.; Arribart, H.; Bouligand, Y.; Sanchez, C. *New Journal of Chemistry* **2002**, *26*, 1-5.

(13) Steadman, P. *The Evolution of Designs Biological Analogy in Architecture and the Applied Arts*; the Syndics of Cambridge University Press: Cambridge, 1979.

(14) Merriam-Webster, I. *Merriam-Webster's Collegiate® Dictionary*; Eleventh Edition ed.; An Encyclopædia Britannica Company: Springfield, MA 01102, 2004.

(15) McCulloch, W. S. *Biological prototypes and synthetic systems proceedings*; Plenum Press: New York, 1962; Vol. 1.

(16) Benyus, J. M. *Biomimicry: Innovation Inspired by Nature*; HarperCollins: New York, 1997

(17) Lavine, M.; Vinson, V.; Coontz, R. *Science* **2005**, *310*, 1131-1131.

(18) Mossman, S. T. I. *The Development of Plastics*; Royal Society of Chemistry Cambridge, 1994.

(19) Shin, H.; Jo, S.; Mikos, A. G. *Biomaterials* **2003**, *24*, 4353-4364.

(20) Zhang, L. J.; Webster, T. J. *Nano Today* **2009**, *4*, 66-80.

(21) Jeong, K. H.; Kim, J.; Lee, L. P. *Science* **2006**, *312*, 557-561.

(22) Stupp, S. I.; Ciegler, G. W. *Journal of Biomedical Materials Research* **1992**, *26*, 169-183.

(23) Yu, J. H.; Shi, J. N.; Jin, Y. *Tissue Engineering Part B-Reviews* **2008**, *14*, 307-319.

(24) Risbud, M. V.; Sittinger, M. *Trends in Biotechnology* **2002**, *20*, 351-356.

(25) Klemm, D.; Schumann, D.; Udhardt, U.; Marsch, S. *Progress in Polymer Science* **2001**, *26*, 1561-1603.

(26) Baxt, W. G. *Lancet* **1995**, *346*, 1135-1138.

(27) Baughman, R. H. *Synthetic Metals* **1996**, *78*, 339-353.

(28) Ma, L.; Gao, C. Y.; Mao, Z. W.; Zhou, J.; Shen, J. C.; Hu, X. Q.; Han, C. M. *Biomaterials* **2003**, *24*, 4833-4841.

(29) Dickinson, M. H. *Proceedings of the National Academy of Sciences of the United States of America* **1999**, *96*, 14208-14209.

(30) Meyers, M. A.; Chen, P. Y.; Lin, A. Y. M.; Seki, Y. *Progress in Materials Science* **2008**, *53*, 1-206.

(31) Espinosa, H. D.; Rim, J. E.; Barthelat, F.; Buehler, M. J. *Progress in Materials Science* **2009**, *54*, 1059-1100.

(32) Lazaris, A.; Arcidiacono, S.; Huang, Y.; Zhou, J. F.; Duguay, F.; Chretien, N.; Welsh, E. A.; Soares, J. W.; Karatzas, C. N. *Science* **2002**, *295*, 472-476.

(33) Kasemo, B. *Surface Science* **2002**, *500*, 656-677.

(34) Liu, K. S.; Jiang, L. *Nano Today*, *6*, 155-175.

(35) Jiang, L.; Zhao, Y.; Zhai, J. *Angewandte Chemie-International Edition* **2004**, *43*, 4338-4341.

(36) Zhang, G. M.; Zhang, J.; Xie, G. Y.; Liu, Z. F.; Shao, H. B. *Small* **2006**, *2*, 1440-1443.

(37) Beckett, P. M.; Armstrong, W.; Justin, S.; Armstrong, J. *New Phytologist* **1988**, *110*, 463-468.

(38) Gao, X. F.; Jiang, L. *Nature* **2004**, *432*, 36-36.

(39) Gao, X. F.; Yan, X.; Yao, X.; Xu, L.; Zhang, K.; Zhang, J. H.; Yang, B.; Jiang, L. *Advanced Materials* **2007**, *19*, 2213-2217.

(40) Feng, L.; Li, S. H.; Li, Y. S.; Li, H. J.; Zhang, L. J.; Zhai, J.; Song, Y. L.; Liu, B. Q.; Jiang, L.; Zhu, D. B. *Advanced Materials* **2002**, *14*, 1857-1860.

(41) Yu, J. G.; Yu, J. C.; Ho, W. K.; Jiang, Z. T. *New Journal of Chemistry* **2002**, *26*, 607-613.

(42) Jin, M. H.; Wang, J.; Yao, X.; Liao, M. Y.; Zhao, Y.; Jiang, L. *Advanced Materials* **2011**, *23*, 2861-2864.

(43) Li, Y.; Sasaki, T.; Shimizu, Y.; Koshizaki, N. *Journal of the American Chemical Society* **2008**, *130*, 14755-14762.

(44) Tang, K. J.; Yu, J. H.; Zhao, Y. Y.; Liu, Y.; Wang, X. F.; Xu, R. R. *Journal of Materials Chemistry* **2006**, *16*, 1741-1745.

(45) Feng, X. J.; Feng, L.; Jin, M. H.; Zhai, J.; Jiang, L.; Zhu, D. B. *Journal of the American Chemical Society* **2004**, *126*, 62-63.

(46) Cordier, P.; Tournilhac, F.; Soulie-Ziakovic, C.; Leibler, L. *Nature* **2008**, *451*, 977-980.

(47) Gu, Z. Z.; Uetsuka, H.; Takahashi, K.; Nakajima, R.; Onishi, H.; Fujishima, A.; Sato, O. *Angewandte Chemie-International Edition* **2003**, *42*, 894-897.

(48) Hiller, J.; Mendelsohn, J. D.; Rubner, M. F. *Nature Materials* **2002**, *1*, 59-63.

(49) Mowery, C. L.; Crosby, A. J.; Ahn, D.; Shull, K. R. *Langmuir* **1997**, *13*, 6101-6107.

(50) Arico, A. S.; Bruce, P.; Scrosati, B.; Tarascon, J. M.; Van Schalkwijk, W. *Nature Materials* **2005**, *4*, 366-377.

(51) Khudhair, A. M.; Farid, M. M. *Energy Conversion and Management* **2004**, *45*, 263-275.

(52) Sun, T. L.; Feng, L.; Gao, X. F.; Jiang, L. *Accounts of Chemical Research* **2005**, *38*, 644-652.

(53) Gao, X.; Yan, X.; Yao, X.; Xu, L.; Zhang, K.; Zhang, J.; Yang, B.; Jiang, L. *Advanced Materials* **2007**, *19*, 2213-2217.

(54) Gao, H. J.; Wang, X.; Yao, H. M.; Gorb, S.; Arzt, E. *Mechanics of Materials* **2005**, *37*, 275-285.

(55) Kinoshita, S.; Yoshioka, S.; Miyazaki, J. *Reports on Progress in Physics* **2008**, *71*, 30.

(56) Bhushan, B.; Jung, Y. C.; Koch, K. *Philosophical Transactions of the Royal Society A: Mathematical, Physical and Engineering Sciences* **2009**, *367*, 1631-1672.

(57) Rodwell, A. *Science* **1968**, *160*, 1350-1351.

(58) Bunker, B. C.; Rieke, P. C.; Tarasevich, B. J.; Campbell, A. A.; Fryxell, G. E.; Graff, G. L.; Song, L.; Liu, J.; Virden, J. W.; McVay, G. L. *Science* **1994**, *264*, 48-55.

(59) Breslow, R. *Accounts of Chemical Research* **1980**, *13*, 170-177.

(60) Schreiber, F. *Progress in Surface Science* **2000**, *65*, 151-256.

(61) Brammer, L. *Chemical Society Reviews* **2004**, *33*, 476-489.

(62) Sellinger, A.; Weiss, P. M.; Nguyen, A.; Lu, Y. F.; Assink, R. A.; Gong, W. L.; Brinker, C. J. *Nature* **1998**, *394*, 256-260.

(63) Whitesides, G. M.; Mathias, J. P.; Seto, C. T. *Science* **1991**, *254*, 1312-1319.

(64) Zhang, S. G. *Nature Biotechnology* **2003**, *21*, 1171-1178.

(65) Elemans, J.; Rowan, A. E.; Nolte, R. J. M. *Journal of Materials Chemistry* **2003**, *13*, 2661-2670.

(66) Bhushan, B.; Koch, K.; Jung, Y. C. *Soft Matter* **2008**, *4*, 1799-1804.

(67) Bhushan, B.; Jung, Y. C.; Niemietz, A.; Koch, K. *Langmuir* **2009**, *25*, 1659-1666.

(68) Koch, K.; Bhushan, B.; Jung, Y. C.; Barthlott, W. *Soft Matter* **2009**, *5*, 1386-1393.

(69) Bhushan, B.; Jung, Y. C. *Progress in Materials Science* **2011**, *56*, 1-108.

(70) Förster, S.; Plantenberg, T. *Angewandte Chemie International Edition* **2002**, *41*, 688-714.

(71) Shimomura, M.; Sawadaishi, T. *Current Opinion in Colloid & Interface Science* **2001**, *6*, 11-16.

(72) S. Klymchenko, A.; Furukawa, S.; Auweraer, M. V. d.; Müllen, K.; De Feyter, S. *Nano Letters* **2008**, *8*, 1163-1168.

(73) Denisov, I. G.; Grinkova, Y. V.; Lazarides, A. A.; Sligar, S. G. *Journal of the American Chemical Society* **2004**, *126*, 3477-3487.

(74) Simonsen, J. B.; Westerlund, F.; Breiby, D. W.; Harrit, N.; Laursen, B. W. *Langmuir* **2011**, *27*, 792-799.

(75) Altman, M.; Shukla, A. D.; Zubkov, T.; Evmenenko, G.; Dutta, P.; van der Boom, M. E. *Journal of the American Chemical Society* **2006**, *128*, 7374-7382.

(76) Mai, Y.; Eisenberg, A. *Chemical Society Reviews* **2012**, *41*, 5969-5985.

(77) Cameron, N. S.; Corbierre, M. K.; Eisenberg, A. *Canadian Journal of Chemistry-Revue Canadienne De Chimie* **1999**, *77*, 1311-1326.

(78) Zhang, L. F.; Eisenberg, A. *Journal of the American Chemical Society* **1996**, *118*, 3168-3181.

(79) Chen, D. Y.; Jiang, M. *Accounts of Chemical Research* **2005**, *38*, 494-502.

(80) Duan, H. W.; Chen, D. Y.; Jiang, M.; Gan, W. J.; Li, S. J.; Wang, M.; Gong, J. *Journal of the American Chemical Society* **2001**, *123*, 12097-12098.

(81) Wang, J.; Jiang, M. *Journal of the American Chemical Society* **2006**, *128*, 3703-3708.

(82) Nie, L.; Liu, S.; Shen, W.; Chen, D.; Jiang, M. *Angewandte Chemie International Edition* **2007**, *46*, 6321-6324.

(83) Yu, S. Y.; Hu, J. H.; Pan, X. Y.; Yao, P.; Jiang, M. *Langmuir* **2006**, *22*, 2754-2759.

(84) Harvey, J. A. *Mechanical Engineers' Handbook: Materials and Mechanical Design, Volume 1, Third Edition.*; John Wiley & Sons, Inc., 2006; Vol. CHAPTER 11 SMART MATERIALS.

(85) Mackerle, J. *Modelling and Simulation in Materials Science and Engineering* **1998**, *6*, 293-334.

(86) Mackerle, J. *Modelling and Simulation in Materials Science and Engineering* **2003**, *11*, 707-744.

(87) Tzou, H. S.; Lee, H. J.; Arnold, S. M. *Mechanics of Advanced Materials and Structures* **2004**, *11*, 367-393.

(88) Chen, J. R.; Miao, Y. Q.; He, N. Y.; Wu, X. H.; Li, S. J. *Biotechnology Advances* **2004**, *22*, 505-518.

(89) Brahim, S.; Narinesingh, D.; Guiseppi-Elie, A. *Biosensors & Bioelectronics* **2002**, *17*, 973-981.

(90) Housner, G. W.; Bergman, L. A.; Caughey, T. K.; Chassiakos, A. G.; Claus, R. O.; Masri, S. F.; Skelton, R. E.; Soong, T. T.; Spencer, B. F.; Yao, J. T. P. *Journal of Engineering Mechanics-Asce* **1997**, *123*, 897-971.

(91) Rossiter, J.; Yap, B.; Conn, A. *Bioinspiration & Biomimetics*, *7*, 10.

(92) Ko, H. C.; Stoykovich, M. P.; Song, J.; Malyarchuk, V.; Choi, W. M.; Yu, C.-J.; Geddes Iii, J. B.; Xiao, J.; Wang, S.; Huang, Y.; Rogers, J. A. *Nature* **2008**, *454*, 748-753.

(93) Craelius, W. *Science* **2002**, *295*, 1018-1021.

(94) Galaev, I. Y.; Mattiasson, B. *Trends in Biotechnology* **1999**, *17*, 335-340.

(95) Kumar, A.; Srivastava, A.; Galaev, I. Y.; Mattiasson, B. *Progress in Polymer Science* **2007**, *32*, 1205-1237.

(96) Mano, J. F. *Advanced Engineering Materials* **2008**, *10*, 515-527.

(97) Aguilar, M. R. E., C.; Gallardo, A. *Smart polymers and their applications as biomaterials*; University of Oulu; Finland, 2007; Vol. 3.

(98) Schild, H. G. *Progress in Polymer Science* **1992**, *17*, 163-249.

(99) Elliott, J. E.; Macdonald, M.; Nie, J.; Bowman, C. N. *Polymer* **2004**, *45*, 1503-1510.

(100) Godbey, W. T.; Wu, K. K.; Mikos, A. G. *Journal of Controlled Release* **1999**, *60*, 149-160.

(101) Schild, H. G. *Progress in Polymer Science* **1992**, *17*, 163-249.

(102) Zheng, P. J.; Hu, X.; Zhao, X. Y.; Li, L.; Tam, K. C.; Gan, L. H. *Macromolecular Rapid Communications* **2004**, *25*, 678-682.

(103) Kagatani, S.; Shinoda, T.; Konno, Y.; Fukui, M.; Ohmura, T.; Osada, Y. *Journal of Pharmaceutical Sciences* **1997**, *86*, 1273-1277.

(104) Miyajima, D.; Tashiro, K.; Araoka, F.; Takezoe, H.; Kim, J.; Kato, K.; Takata, M.; Aida, T. *Journal of the American Chemical Society* **2008**, *131*, 44-45.

(105) Stoeva, S. I.; Huo, F. W.; Lee, J. S.; Mirkin, C. A. *Journal of the American Chemical Society* **2005**, *127*, 15362-15363.

(106) You, L.-C.; Lu, F.-Z.; Li, Z.-C.; Zhang, W.; Li, F.-M. *Macromolecules* **2002**, *36*, 1-4.

(107) Waldeck, D. H. *Chemical Reviews* **1991**, *91*, 415-436.

(108) Kumar, G. S.; Neckers, D. C. *Chemical Reviews* **1989**, *89*, 1915-1925.

(109) Krysanov, S. A.; Alfimov, M. V. *Chemical Physics Letters* **1982**, *91*, 77-80.

(110) Yokoyama, Y. *Chemical Reviews* **2000**, *100*, 1717-1740.

(111) Irie, M.; Kunwatchakun, D. *Macromolecules* **1986**, *19*, 2476-2480.

(112) Hammond, G. S.; Stout, C. A.; Lamola, A. A. *Journal of the American Chemical Society* **1964**, *86*, 3103-3106.

(113) Nabeshima, Y.; Shishido, A.; Kanazawa, A.; Shiono, T.; Ikeda, T.; Hiyama, T. *Chemistry of Materials* **1997**, *9*, 1480-1487.

(114) Higuchi, M.; Minoura, N.; Kinoshita, T. *Colloid and Polymer Science* **1995**, *273*, 1022-1027.

(115) Akiyama, H.; Tamaoki, N. *Macromolecules* **2007**, *40*, 5129-5132.

(116) Tong, X.; Wang, G.; Soldera, A.; Zhao, Y. *The Journal of Physical Chemistry B* **2005**, *109*, 20281-20287.

(117) Gil, E. S.; Hudson, S. M. *Progress in Polymer Science* **2004**, *29*, 1173-1222.

(118) Schmaljohann, D. *Advanced Drug Delivery Reviews* **2006**, *58*, 1655-1670.

(119) Galaev, I. Y. *Russian Chemical Reviews* **1995**, *64*, 471-489

(120) Matsumoto, A.; Yoshida, R.; Kataoka, K. *Biomacromolecules* **2004**, *5*, 1038-1045.

(121) Ercole, F.; Davis, T. P.; Evans, R. A. *Polymer Chemistry*, *1*, 37-54.

(122) Minkin, V. I. *Chemical Reviews* **2004**, *104*, 2751-2776.

(123) Berkovic, G.; Krongauz, V.; Weiss, V. *Chemical Reviews* **2000**, *100*, 1741-1753.

(124) Irie, M. *Chemical Reviews* **2000**, *100*, 1685-1716.

(125) Yokoyama, Y. *Chemical Reviews* **2000**, *100*, 1717-1739.

(126) Irie, M. *Chemical Reviews* **2000**, *100*, 1683-1683.

(127) Yager, K. G.; Barrett, C. J. *Journal of Photochemistry and Photobiology A: Chemistry* **2006**, *182*, 250-261.

(128) Yu, Y. L.; Nakano, M.; Ikeda, T. *Nature* **2003**, *425*, 145-145.

(129) Yu, Y. L.; Ikeda, T. *Angewandte Chemie-International Edition* **2006**, *45*, 5416-5418.

(130) Ikeda, T.; Tsutsumi, O. *Science* **1995**, *268*, 1873-1875.

(131) Tiago, M. L.; Ismail-Beigi, S.; Louie, S. G. *Journal of Chemical Physics* **2005**, *122*, 7.

(132) Fuss, W.; Kosmidis, C.; Schmid, W. E.; Trushin, S. A. *Angewandte Chemie-International Edition* **2004**, *43*, 4178-4182.

(133) Bullock, D. J. W.; Cumper, C. W. N.; Vogel, A. I. *Journal of the Chemical Society (Resumed)* **1965**, 5316-5323.

(134) Barrett, C.; Natansohn, A.; Rochon, P. *Chemistry of Materials* **1995**, *7*, 899-903.

(135) Irie, M.; Hirano, Y.; Hashimoto, S.; Hayashi, K. *Macromolecules* **1981**, *14*, 262-267.

(136) Boissiere, O.; Han, D. H.; Tremblay, L.; Zhao, Y. *Soft Matter*, *7*, 9410-9415.

(137) Han, D. H.; Tong, X.; Zhao, Y.; Galstian, T. *Macromolecules*, *43*, 3664-3671.

(138) Zhao, X. Y.; Hu, X.; Gan, L. H. *Polymers for Advanced Technologies* **2005**, *16*, 370-377.

(139) Zhao, X. Y.; Hu, X.; Zheng, P. J.; Gan, L. H.; Lee, C. K. P. *Thin Solid Films* **2005**, *477*, 88-94.

(140) Wang, G.; Tong, X.; Zhao, Y. *Macromolecules* **2004**, *37*, 8911-8917.

(141) Rau, H. In *Photochemistry and Photophysics*; Rabek, J. F., Ed.; Taylor & Francis: Boca Raton, Florida, USA, 1989; Vol. 2 p119-141.

(142) Paik, C. S.; Morawetz, H. *Macromolecules* **1972**, *5*, 171-177.

(143) Barrett, C.; Natansohn, A.; Rochon, P. *Macromolecules* **1994**, *27*, 4781-4786.

(144) Ho, M. S.; Natansohn, A.; Barrett, C.; Rochon, P. *Canadian Journal of Chemistry-Revue Canadienne De Chimie* **1995**, *73*, 1773-1778.

(145) Chu, O. Y.; Shuangjun, C. J.; Bo, C.; Gi, X. *Colloids and Surfaces a-Physicochemical and Engineering Aspects* **2007**, *301*, 346-351.

(146) Li, M. H.; Keller, P.; Li, B.; Wang, X.; Brunet, M. *Advanced Materials* **2003**, *15*, 569-572.

(147) Liao, X. J.; Chen, G. S.; Liu, X. X.; Chen, W. X.; Chen, F.; Jiang, M. *Angewandte Chemie-International Edition*, *49*, 4409-4413.

(148) Zhao, Y. *Macromolecules* **2012**, *45*, 3647-3657.

(149) Hu, X.; Zhao, X. Y.; Gan, L. H.; Xia, X. L. *Journal of Applied Polymer Science* **2002**, *83*, 1061-1068.

(150) Zhao, X. Y.; Hu, X.; Yue, C. Y.; Xia, X. L.; Gan, L. H. *Thin Solid Films* **2002**, *417*, 95-100.

(151) Hu, X.; Zheng, P. J.; Zhao, X. Y.; Li, L.; Tam, K. C.; Gan, L. H. *Polymer* **2004**, *45*, 6219-6225.

(152) Ravi, P.; Sin, S. L.; Gan, L. H.; Gan, Y. Y.; Tam, K. C.; Xia, X. L.; Hu, X. *Polymer* **2005**, *46*, 137-146.

(153) Ren, L.; Li, G. Y.; Hu, X.; Xia, X. L.; Shen, J. R.; Jia, D. M. *Tetrahedron Letters* **2005**, *46*, 1511-1513.

(154) Sin, S. L.; Gan, L. H.; Hu, X.; Tam, K. C.; Gan, Y. Y. *Macromolecules* **2005**, *38*, 3943-3948.

(155) Zhao, X. Y.; Niu, Y. H.; Hu, X. *Journal of Polymer Science Part B-Polymer Physics* **2005**, *43*, 1421-1432.

(156) Zheng, P. J.; Wang, C.; Hu, X.; Tam, K. C.; Li, L. *Macromolecules* **2005**, *38*, 2859-2864.

(157) Que, W. X.; Hu, X.; Xia, X. L.; Zhao, L. *Optics Express* **2007**, *15*, 480-485.

(158) Sun, M.; Que, W. X.; Hu, X. *Journal of Sol-Gel Science and Technology* **2009**, *50*, 415-420.

(159) Hu, J. H.; Yu, H.; Gan, L. H.; Hu, X. *Soft Matter* **2011**, *7*, 11345-11350.

(160) del Barrio, J.; Oriol, L.; Alcala, R.; Sanchez, C. *Macromolecules* **2009**, *42*, 5752-5760.

(161) Jankova, K.; Chen, X.; Kops, J.; Batsberg, W. *Macromolecules* **1998**, *31*, 538-541.

(162) Yu, H.; Gan, L. H.; Hu, X.; Gan, Y. Y. *Polymer* **2007**, *48*, 2312-2321.

(163) Fischer, E. *The Journal of Physical Chemistry* **1967**, *71*, 3704-3706.

(164) Victor, J. G.; Torkelson, J. M. *Macromolecules* **1987**, *20*, 2241-2250.

(165) Morishima, Y.; Tsuji, M.; Kamachi, M.; Hatada, K. *Macromolecules* **2002**, *25*, 4406-4410.

(166) Dhont, J. K. G. *An Introduction to Dynamics of Colloids*; Elsevier Science, 1996.

(167) Zemb, T.; Lindner, P. *Neutrons, X-rays and light: scattering methods applied to soft condensed matter*; Elsevier, 2002.

(168) Berret, J. F.; Cristobal, G.; Herv; xe; P.; Oberdisse, J.; Grillo, I. *Eur. Phys. J. E* **2002**, *9*, 301.

(169) Brown, W. *Dynamic light scattering: the method and some applications*; Clarendon Press, 1993.

(170) Cristobal, G.; Berret, J.-F.; Chevallier, C.; Talingting-Pabalan, R.; Joanicot, M.; Grillo, I. *Macromolecules* **2008**, *41*, 1872-1880.

(171) Ahir, S. V.; Terentjev, E. M. *Nature Materials* **2005**, *4*, 491-495.

(172) Wang, G. J.; Wang, X. G. *Polymer Bulletin* **2002**, *49*, 1-8.

(173) Wang, Y. P.; Ma, N.; Wang, Z. Q.; Zhang, X. *Angewandte Chemie-International Edition* **2007**, *46*, 2823-2826.

(174) Liu, X. K.; Jiang, M. *Angewandte Chemie-International Edition* **2006**, *45*, 3846-3850.

(175) Mabrouk, E.; Cuvelier, D.; Brochard-Wyart, F.; Nassoy, P.; Li, M. H. *Proceedings of the National Academy of Sciences of the United States of America* **2009**, *106*, 7294-7298.

(176) Zou, J.; Tao, F.; Jiang, M. *Langmuir* **2007**, *23*, 12791-12794.

(177) Su, W.; Han, K.; Luo, Y. H.; Wang, Z.; Li, Y. M.; Zhang, Q. J. *Macromolecular Chemistry and Physics* **2007**, *208*, 955-963.

(178) Bédard, M.; Skirtach, A. G.; Sukhorukov, G. B. *Macromolecular Rapid Communications* **2007**, *28*, 1517-1521.

(179) Han, K.; Su, W.; Zhong, M.; Yan, Q.; Luo, Y.; Zhang, Q.; Li, Y. *Macromolecular Rapid Communications* **2008**, *29*, 1866-1870.

(180) Shin, D. M.; Schanze, K. S.; Whitten, D. G. *Journal of the American Chemical Society* **2002**, *111*, 8494-8501.

(181) Reichardt, C. *Chemical Reviews* **1994**, *94*, 2319-2358.

(182) Mori, T.; Yuyama, K.; Narita, K.; Minagawa, K.; Haraguchi, M.; Tanaka, M. *Journal of Applied Polymer Science* **2006**, *100*, 3913-3918.

(183) Jung, B. D.; Hong, J. D.; Voigt, A.; Leporatti, S.; Dahne, L.; Donath, E.; Mohwald, H. In *9th International Conference on Organized Molecular Films (LB9)*; Elsevier Science Bv: Potsdam, Germany, 2000, p 483-489.

(184) Song, X.; Perlstein, J.; Whitten, D. G. *Journal of the American Chemical Society* **1997**, *119*, 9144-9159.

(185) Kuiper, J. M.; Engberts, J. *Langmuir* **2004**, *20*, 1152-1160.

(186) Dautel, O. J.; Wantz, G.; Almairac, R.; Flot, D.; Hirsch, L.; Lere-Porte, J. P.; Parneix, J. P.; Serein-Spirau, F.; Vignau, L.; Moreau, J. J. E. *Journal of the American Chemical Society* **2006**, *128*, 4892-4901.

(187) Tian, F.; Yu, Y.; Wang, C.; Yang, S. *Macromolecules* **2008**, *41*, 3385-3388.

(188) Kühlbrandt, W. *Nature* **2000**, *406*, 569-570.

(189) Peng, H. S.; Chen, D. Y.; Jiang, M. *Langmuir* **2003**, *19*, 10989-10992.

(190) Stuart, J.; Bilto, Y. Y.; Player, M.; Stone, P. C. W.; Chalder, S. M. *Journal Des Maladies Vasculaires* **1991**, *16*, 46-48.

(191) Hu, J. H.; Yu, S. Y.; Yao, P. *Langmuir* **2007**, *23*, 6358-6364.

(192) Luo, L.; Eisenberg, A. *Journal of the American Chemical Society* **2001**, *123*, 1012-1013.

(193) Bhushan, B. *Philosophical Transactions of the Royal Society a-Mathematical Physical and Engineering Sciences* **2009**, *367*, 1445-1486.

(194) Rodwell, A. *Science* **1968**, *160*, 1350-1351.

(195) Cohen, B. E.; Bangham, A. D. *Nature* **1972**, *236*, 173-174.

(196) Lawrence, M. B.; Springer, T. A. *Cell* **1991**, *65*, 859-873.

(197) Sunamoto, J.; Sato, T.; Taguchi, T.; Hamazaki, H. *Macromolecules* **1992**, *25*, 5665-5670.

(198) Lian, T.; Ho, R. J. Y. *Journal of Pharmaceutical Sciences* **2001**, *90*, 667-680.

(199) Cans, A. S.; Wittenberg, N.; Karlsson, R.; Sombers, L.; Karlsson, M.; Orwar, O.; Ewing, A. *Proceedings of the National Academy of Sciences of the United States of America* **2003**, *100*, 400-404.

(200) Murata, K.; Mitsuoka, K.; Hirai, T.; Walz, T.; Agre, P.; Heymann, J. B.; Engel, A.; Fujiyoshi, Y. *Nature* **2000**, *407*, 599-605.

(201) Kumar, M.; Grzelakowski, M.; Zilles, J.; Clark, M.; Meier, W. *Proceedings of the National Academy of Sciences of the United States of America* **2007**, *104*, 20719-20724.

(202) Zhao, Y.; Qiu, C.; Li, X.; Vararattanavech, A.; Shen, W.; Torres, J.; Hélix-Nielsen, C.; Wang, R.; Hu, X.; Fane, A. G.; Tang, C. Y. *Journal of Membrane Science*.

(203) Betz, H. *Neuron* **1990**, *5*, 383-392.

(204) Morris, C. E. *Journal of Membrane Biology* **1990**, *113*, 93-107.

(205) Catterall, W. A. *Annual Review of Biochemistry* **1995**, *64*, 493-531.

(206) Kaupp, U. B.; Seifert, R. *Physiological Reviews* **2002**, *82*, 769-824.

(207) Verkman, A. S. *Journal of Cell Science* **2005**, *118*, 3225-3232.

(208) Storrie, B. *Working with Molecular Cell Biology, Fourth Edition: A Study Companion*; Freeman, 2000.

(209) Delaire, J. A.; Nakatani, K. *Chemical Reviews* **2000**, *100*, 1817-1845.

(210) Lougheed, T.; Borisenko, V.; Hennig, T.; Ruck-Braun, K.; Woolley, G. A. *Organic & Biomolecular Chemistry* **2004**, *2*, 2798-2801.

(211) Kocer, A.; Walko, M.; Meijberg, W.; Feringa, B. L. *Science* **2005**, *309*, 755-758.

(212) Gorostiza, P.; Isacoff, E. *Molecular BioSystems* **2007**, *3*, 686-704.

(213) Banghart, M. R.; Mourot, A.; Fortin, D. L.; Yao, J. Z.; Kramer, R. H.; Trauner, D. *Angewandte Chemie International Edition* **2009**, *48*, 9097-9101.

(214) van Hest, J. C. M. *Nature* **2009**, *461*, 45-47.

(215) Zhang, W.; Aida, T. *Science* **2012**, *337*, 1462-1463.

(216) Sebai, S. C.; Cribier, S.; Karimi, A.; Massotte, D.; Tribett, C. *Langmuir*, *26*, 14135-14141.

(217) Shimomura, M.; Kunitake, T. *Journal of the American Chemical Society* **1987**, *109*, 5175-5183.

(218) Kang, E. H.; Liu, X. K.; Sun, J. Q.; Shen, J. C. *Langmuir* **2006**, *22*, 7894-7901.

(219) Ahmed, R.; Priimagi, A.; Faul, C. F. J.; Manners, I. *Advanced Materials*, *24*, 926-931.

(220) Weh, K.; Noack, M.; Hoffmann, K.; Schroder, K. P.; Caro, J. *Microporous and Mesoporous Materials* **2002**, *54*, 15-26.

(221) Okahata, Y.; Fujita, S.; Iizuka, N. *Angewandte Chemie-International Edition in English* **1986**, *25*, 751-752.

(222) Fujiwara, H.; Yonezawa, Y. *Nature* **1991**, *351*, 724-726.

(223) Lei, Y.; Hurst, J. K. *Langmuir* **1999**, *15*, 3424-3429.

(224) Park, C.; Lim, J.; Yun, M.; Kim, C. *Angewandte Chemie-International Edition* **2008**, *47*, 2959-2963.

(225) Liu, N. G.; Dunphy, D. R.; Atanassov, P.; Bunge, S. D.; Chen, Z.; Lopez, G. P.; Boyle, T. J.; Brinker, C. J. *Nano Letters* **2004**, *4*, 551-554.

(226) Houga, C.; Giermanska, J.; Lecommandoux, S.; Borsali, R.; Taton, D.; Gnanou, Y.; Le Meins, J. F. *Biomacromolecules* **2009**, *10*, 32-40.

(227) Yu, H.; Gan, L. H.; Hu, X.; Venkatraman, S. S.; Tam, K. C.; Gang, Y. Y. *Macromolecules* **2005**, *38*, 9889-9893.

(228) Yingchun, Z.; Masahiro, F. *Angewandte Chemie International Edition* **2007**, *46*, 2241-2244.

(229) Higashihara, T.; Hayashi, M.; Hirao, A. *Progress in Polymer Science*, *36*, 323-375.

(230) Walter, M. V.; Malkoch, M. *Chemical Society Reviews*, *41*, 4593-4609.

(231) Laurent, B. A.; Grayson, S. M. *Chemical Society Reviews* **2009**, *38*, 2202-2213.

(232) Wang, Y.; Grayson, S. M. *Advanced Drug Delivery Reviews*, *64*, 852-865.

(233) Riess, G. *Progress in Polymer Science* **2003**, *28*, 1107-1170.

(234) Bauer, B. J.; Fetters, L. J. *Rubber Chemistry and Technology* **1978**, *51*, 406-436.

(235) Bywater, S. In *Physical Chemistry*; Springer Berlin Heidelberg: 1979; Vol. 30, p 89-116.

(236) Grest, G. S.; Fetters, L. J.; Huang, J. S.; Richter, D. In *Advances in Chemical Physics*; John Wiley & Sons, Inc.: 2007, p 67-163.

(237) He, E.; Yue, C. Y.; Tam, K. C. *Langmuir* **2009**, *25*, 4892-4899.

(238) Stepanek, M.; Uchman, M.; Prochazka, K. *Polymer* **2009**, *50*, 3638-3644.

(239) Szejtli, J. *Chemical Reviews* **1998**, *98*, 1743-1753.

(240) Liu, J. H.; Chen, G. S.; Jiang, M. *Macromolecules* **2011**, *44*, 7682-7691.

(241) Liu, Z.; Jiang, M. *Journal of Materials Chemistry* **2007**, *17*, 4249-4254.

(242) Matthews, J. R.; Tuncel, D.; Jacobs, R. M. J.; Bain, C. D.; Anderson, H. L. *Journal of the American Chemical Society* **2003**, *125*, 6428-6433.

(243) Sun, T.; Wang, G.; Feng, L.; Liu, B.; Ma, Y.; Jiang, L.; Zhu, D. *Angewandte Chemie International Edition* **2004**, *43*, 357-360.

(244) Wang, S.; Song, Y.; Jiang, L. *Journal of Photochemistry and Photobiology C: Photochemistry Reviews* **2007**, *8*, 18-29.

(245) Jiang, W. H.; Wang, G. J.; He, Y. N.; Wang, X. G.; An, Y. L.; Song, Y. L.; Jiang, L. *Chemical Communications* **2005**, 3550-3552.

(246) Feng, C. L.; Zhang, Y. J.; Jin, J.; Song, Y. L.; Xie, L. Y.; Qu, G. R.; Jiang, L.; Zhu, D. B. *Langmuir* **2001**, *17*, 4593-4597.

(247) Zhai, L.; Cebeci, F. Ç.; Cohen, R. E.; Rubner, M. F. *Nano Letters* **2004**, *4*, 1349-1353.

(248) Lim, H. S.; Han, J. T.; Kwak, D.; Jin, M. H.; Cho, K. *Journal of the American Chemical Society* **2006**, *128*, 14458-14459.

(249) Vogler, E. A. *Advances in Colloid and Interface Science* **1998**, *74*, 69-117.

(250) K.L. Osborne III, *Temperature-Dependence of the Contact Angle of Water on Graphite, Silicon, and Gold*, **2009**.

(251) Siewierski, L. M.; Brittain, W. J.; Petrash, S.; Foster, M. D. *Langmuir* **1996**, *12*, 5838-5844.